THE UNIVERSITY
of EDINBURGH

Energy Efficient Transmitter Design with Compact Antenna for Future Wireless Communication Systems

Lin Zhou

A thesis submitted for the degree of Doctor of Philosophy.

School of Engineering
The University of Edinburgh

July, 2018

Abstract

This thesis explores a novel technique for transceiver design in future wireless systems, which is cloud radio access networks (CRANs) with single radio frequency (RF) chain antennas at each remote radio head (RRH).

This thesis seeks to make three contributions.

Firstly, it proposes a novel algorithm to solve the oscillatory/unstable behaviour of electronically steerable parasitic array radiators (ESPAR) when it provides multi-antenna functionality with a single RF chain. This thesis formulates an optimization problem and derives closed-form expressions when calculating the configuration of an ESPAR antenna (EA) for arbitrary signals transmission. This results in simplified processing at the transmitter. The results illustrate that the EA transmitter, when utilizing novel closed-form expressions, shows significant improvement over the performance of the EA transmitter without any pre-processing. It performs at nearly the same symbol error rate (SER) as standard multiple antenna systems.

Secondly, this thesis illustrates how a practical peak power constraint can be put into an EA transceiver design. In an EA, all the antenna elements are fed centrally by a single power amplifier. This makes it more probable that during use, the power amplifier reaches maximum power during transmission. Considering limited power availability, this thesis proposes a new algorithm to achieve stable signal transmission.

Thirdly, this thesis shows that an energy efficiency (EE) optimization problem can be formulated and solved in CRANs that deploy single RF chain antennas at RRHs. The closed-form expressions of the precoder and power allocation schemes to transmit desired signals are obtained to maximise EE for both single-user and multi-user systems. The results show that the CRANs with single RF chain antennas provide superior EE performance compared to the standard multiple antenna based systems.

Lay Summary

Due to an ever-increasing number of customers and data-hungry mobile applications, the capacity demands in cellular networks are constantly rising. To meet such high requirements, this thesis focuses on an original and promising transmission technique: cloud radio access networks (CRANs) with single RF chain antennas at remote radio heads (RRHs).

The next generation of wireless cellular networks attempt to satisfy the continually increasing demand for higher data rates and mobility. CRANs have the potential to meet these ambitious objectives. In CRANs, a large number of low-cost remote radio heads (RRHs) are deployed and connected to the base band unit (BBU) pool through optical links. However, from the hardware perspective, cost and size constraints could affect the wide application of CRANs.

To overcome these present problems, this thesis explores approaches that enable an EA to provide multi-antenna functionality and the application of single RF chain antennas into CRANs. Firstly, while considering the oscillatory behaviour of an EA to transmit signals, this thesis proposes a novel algorithm to guarantee stable EA transmission. Furthermore, considering the power limitations for EA transmissions, it proposes a practical and new transmission scheme that enables EA to provide stable multi-antenna functionality. It then considers energy-efficient CRANs in which single-RF antennas are employed at the RRHs. By considering EE in both single-user and multi-user CRANs, this thesis introduces new techniques that can deliver better EE when compared to standard multiple antenna systems.

Declaration of originality

I hereby declare that the research recorded in this thesis and the thesis itself was composed and originated entirely by myself in the Department of Electronics and Electrical Engineering at The University of Edinburgh.

Lin Zhou

Acknowledgements

First of all, I would like to express my deepest and sincere gratitude to my supervisor Prof John Thompson, for his insightful comments, useful guidance, considerable encouragements and continuous support on this thesis and for his patience, motivation, enthusiasm and immense knowledge. His guidance helped me in all the time of research and doing the corrections of this thesis. I am proud of being one of his students, and his charm of personality will influence all my life. The valuable experience I gained during this period will be extremely significant for my future life and career.

I would also like to express my appreciation to my second supervisor Dr Timothy Stratford, without whose support this thesis would have been very difficult to come to a completion stage. I thank the financial support from the Seventh Framework Programme for Research of the European Commission under project grant number HARP-318489, and sincerely hope that my efforts will repay its expectations. I thank all my colleagues at the HARP project and IDCOM.

I would like to thank some special people during my PhD, Dr Fahd Ahmed Khan, Dr Garrey Rice and Dr John O'Sullivan, for many useful discussions on research and practical LTE systems. I wish to extend my thanks to Ms Elizabeth Tudhope, Ms Sheila McBain and Ms Angharad Jenkins, who provided me a lot of advices and help during my PhD.

Finally, I also present my most sincere respect to my family, who have always provided me solid support in China. I can honestly say that it was only their determination and constant encouragement that ultimately made it possible for me to see this project through to the end. I would like to give special thanks to my son, Lingyun Xiao, for his company and all his support while in the UK. It is your smiling face and company that help me carry on my research despite many difficulties. Thank you, Xiao Xiao, for accepting all my ups and downs during these years and providing emotional and financial support. I thank our parents, my brother Liang Zhou, my sister Xiaoling Zhou and other family members. The most valuable treasure I have is your love and support.

Contents

List of figures

List of tables

Acronyms and abbreviations

1G	1st Generation
2G	2nd Generation
2D	Two-Dimensional
3G	3rd Generation
4G	4th Generation
5G	5th Generation
ADC	Analog-to-Digital Converter
ADMM	Alternating direction method of multipliers
AOA	Anlge-of-arrival
AOD	Anlge-of-departure
AWGN	Additive white Gaussian noise
aDOF	aerial Degree of Freedom
BBU	Baseband unit
BC	Broadcast channel
BS	Base Station
CCI	Co-channel interference
CDF	Cumulative Density Function
CPU	Central processing unit
CRANs	Cloud radio access networks
CSI	Channel Statement Information
CSIT	Channel Statement Information at the Transmitter
DAC	Digital-to-Analogue Converter
DL	Downlink
DoF	Degrees of Freedom
DPCs	Distributed Processing Centers
DU	Data Unit
EA	ESPAR Antenna

EA-P	EA with Preprocessing
EE	Energy Efficiency
EMF	Induced Electromotive Force
ESPAR	Electronically Steerable Parasitic Array Radiator
E/O and O/E	Electrical-to-Optical and Optical-to-Electrical
eDOF	efficient Degree of Freedom
FD	FULL-Duplex
FDD	Frequency-Division Duplexing
FDTD	Finite-difference time-domain
FFT	Fast Fourier Transform
HARP	High capacity network Architecture with Remote radio heads and Parasitic antenna arrays
HD	Half-Duplex
IQ	In-phase and quadrature
i.i.d.	independent and identically distributed
ISI	Intersymbol interference
KKT	Karush-Kuhn-Tucker
LMA	Load Modulated Arrays
LOS	Line-of-Sight
LS	Least Square
LTE	Long-Term Evolution
LTE-A	LTE-Advanced
MAC	Media Access Control
MC	Mutual Coupling
MCM	Mutual Coupling Matrix
MIMO	Multiple-Input-Multiple-Output
MISO	Multiple-Input Single-Output
MMSE	Minimum Mean Square Error
MoM	Method of Moments
MRT	Maximum Ratio Transmission
MSE	Mean Squared Error

NFC	Near Field Communication
NGS	Nonlinear Gauss-Seidel
UL	Uplink
ULA	Uniform Linear Array
OFDM	Orthogonal Frequency-Division Multiplexing
PDF	Probability Density Function
PHY	Physical Layer
PSK	Phase-Shift-Keying
QCQP	Quadratically Constrained Quadratic Programming
RAN	Radio Access Network
RF	Radio Frequency
RoF	Radio-over-Fibre
RRU	Remote Radio Unit
RRH	Remote Radio Head
Rx	Receiver
SE	Spectral Efficiency
SER	Symbol Error Rate
SINR	Signal-to-Interference-plus-Noise Ratio
SISO	Single-Input Single-Output
SMA	Standard MIMO Antenna with multiple RF chains
SRFA	Single RF chain MIMO Antennas
SNR	Signal-to-Noise Ratio
SOCP	Second-Order Cone Programming
STBC	Space-Time Block Codes
TDD	Time-Division Duplexing
Tx	Transmitter
ULA	Uniform linear array
ZF	Zero-forcing

Nomenclature

$\mathbf{A}_r$	Steering matrix at the transmitter
$\mathbf{A}_t$	Steering matrix at the receiver
$\mathbf{H_b}$	The matrix whose elements are complex path gains
$\mathbf{a}_t(\theta_m) \in \mathbb{C}^{N_r}$	Steering vectors at the transmitter
$\mathbf{a}_r(\phi_m) \in \mathbb{C}^{N_t}$	Steering vectors at the receiver
B_c	Coherence bandwidth
B_s	Signal bandwidth
B_{max}	Doppler spread
$\mathbf{c}_j^{UL} \in \mathbb{C}^{M_j^{UL}}$	Transmitter distortion at the j-th UL user
d_0	Reference distance and is setting to 1km
d_{tr}	Distance between the transmitter and the receiver
d	Antenna spacing
d_R	Antenna spacing at the receiver
d_T	Antenna spacing at the transmitter
$\mathbf{D}_{rad}$	Radiation pattern
$\mathbf{e}_k^{DL} \in \mathbb{C}^{N_k^{DL}}$	Receiver distortion at the k-th DL user
η_{ee}	Energy efficiency
g_{k,t_m}	Small scale fading from the $(m+1)$-th antenna element at the t-th RRH to the k-th user's antenna
$\mathbf{F}$	Precoding matrix
$\mathbf{h}$	Channel model from the EA transmitter to the single-antenna receiver
h_{k,t_m}	Channel from the $(m+1)$-th antenna element at the t-th RRH to the k-th user's antenna
$\mathbf{h}_{k,t} \in \mathbb{C}^{M_t}$	Channel model from all RRHs to the single-antenna user k
$\mathbf{h}_k \in \mathbb{C}^{M_{tot}}$	Channel model from the t-th RRH to the single-antenna user k

$\mathbf{H} \in \mathbb{C}^{N_r \times N_t}$	Channel model from the transmitter to the receiver
$\hat{\mathbf{H}}$	Non-coherent contribution in the channel $\mathbf{H}$
$\overline{\mathbf{H}}$	Coherent components in the channel $\mathbf{H}$
$\mathbf{H}_k^{DL} \in \mathbb{C}^{N_k^{DL} \times M_0^{BS}}$	The k-th DL channel
i	Current in the circuit
i_m	Current at the $(m+1)$-th antenna element
i_{t_j}	Current of the j-th antenna element at the t-th RRH
$\mathbf{i} \in \mathbb{C}^M$	Current vector at the M-element antenna
$\hat{\mathbf{i}} \in \mathbb{C}^M$	Desired current vector corresponding to ideal signals that is required to be transmitted by th EA
$\mathbf{i}_t \in \mathbb{C}^M$	Desired transmitted current vector at the t-th RRH
$\mathbf{I}_N \in \mathbb{R}^{N \times N}$	N by N identity matrix
$\mathbf{i}_R$	Current vector at the receiver
J	Number of users for uplink transmission
l_{k,t_m}	Large scale fading from the $(m+1)$-th antenna element at the t-th RRH to the k-th user's antenna
M	Number of antenna elements
M_t	Number of antenna elements at the t-th RRH
M_{tot}	Total number of transmitted antenna elements
N_t	Number of the transmitting antenna elements
N_r	Number of the receiving antenna elements
N_s	Number of the scatters
N_b	Number of basis beam patterns
N_0	The noise power
N_k^{DL}	Number of antenna elements at the k-th DL user
N	Number of RRHs in network
$N_{RF}^{(t)}$	Number of RF circuits at the t-th RRH
$\mathbf{n} \in \mathbb{C}^{N_r}$	Noise vector
$\mathbf{n}_k \in \mathbb{C}^{N_k^{DL}}$	AWGN vector at the k-th DL user
P_h	Dissipated power
P_{in}	Input power

P_E	Power delivered to an EA at the active element
P_{LOS}	Distance-dependent path model with LOS path
P_S	Total power supplied by source at the active element with considering matching
P_k^U	Allocated power to the k-th user
P_t^{RRH}	Allocated power to the t-th RRHs
P_{tot}	Total power consumption for the downlink transmission
$P_{k,t}$	Power from t-th RRH to the k-th user
P_{bbu}	Power consumption of baseband signal-processing at BBU
P_{fiber}	Traffic-dependent power consumption of fiber transmission between all RRHs to the BBU
P_{op}	Power consumption per unit-bit of optical modules connected to the fiber line
P_{rrh}	Power consumption for all RRHs
P_{user}^{DL}	Received power consumption of a DL users
P_t^c	RF circuit power consumption at the t-th RRH
P_T	Transmitting power
P_{max}	Maximal transmitting power
P_{min}	Minimal transmitting power
$\mathbf{p}^{RRH} \in \mathbb{R}^N$	Allocated power vector to all RRHs
$\mathbf{p}^U \in \mathbb{R}^K$	Allocated power vector to users
$\mathbf{P}_0 \in \mathbb{R}^{M_0^{DL} \times M_0^{DL}}$	Diagonal matrices denoting the per-antenna maximum power constraints at the BS
$\mathbf{Q}_A$	Its columns are eigenvectors of matrix $\mathbf{A}$
$\mathbf{Q}_B$	Its columns are eigenvectors of matrix $\mathbf{B}$
R	Achievable rate from all RRHs to all users
R_i	Resistance of the i-th antenna element
R_{in}	Input resistance
R_{ij}	Mutual resistance between the i-th and j-th antenna element
R_{in}^R	Radiation resistance
R_{in}^L	Antenna loss resistance
R_s	Resistance of the generator
$R_{in}^{(t)}$	Input resistance at the t-th RRH
r_k	Achievable rate over bandwidth Ω Hz for the k-th user

s_i	Transmitted symbol to the i-th antenna elements
s_k^{DL}	Transmitted symbol to the k-th user with a single data stream
$\mathbf{s}^{DL} \in \mathbb{C}^{K\times 1}$	Transmitted symbols to all the DL users for a single data stream per user
$\mathbf{s}_k^{DL} \in \mathbb{C}^{d_j^{DL}}$	Source symbols for the k-th DL user
T_c	Coherence time
$\mathbf{S}_+^n$	Set of symmetric positive semidefinite
$\mathbf{U}_j^{UL} \in \mathbb{C}^{N_0^{BS}\times d_j^{UL}}$	Received linear decoders at the BS
$\mathbf{U}_k^{DL} \in \mathbb{C}^{N_k^{DL}\times d_j^{DL}}$	Received linear decoders at the k-th DL user
v_{t_0}	Voltage feeding at the active element at the t-th RRH
v_0	Voltage of the generator
$\mathbf{v} \in \mathbb{C}^M$	Vector of source voltage for M-element antenna
$\mathbf{v}_t \in \mathbb{C}_t^M$	Voltage vector at the t-th RRH with for M_t-element antenna
$\mathbf{v}_{RL}$	Voltage vector at the receiver
$\mathbf{V}_j^{UL} \in \mathbb{C}^{M_j^{UL}\times d_j^{UL}}$	Precoders for the data streams of the j-th UL
$\mathbf{V}_k^{DL} \in \mathbb{C}^{M_0^{BS}\times d_j^{DL}}$	Precoders for the data streams of the k-th DL user
$\mathbf{V}\,(\mathbf{U})$	Set of all precoding (receiving) matrices
$\mathbf{w}$	Its elements w_{2m+1} and w_{2m+2} denote the real part and the imaginary part of i
$\hat{\mathbf{w}}$	Its elements are the practical real part and the imaginary part of $\hat{i}_m$
$\mathbf{w}$	Its elements are the ideal real part and the imaginary part of i_m
$\mathbf{w}_k \in \mathbb{C}^{M_{tot}}$	Precoder for the user k for a single data stream per user
$\mathbf{w}_{k,t} \in \mathbb{C}^{M_t}$	Precoder at the t-th RRH for the user k for a single data stream per user
$\mathbf{W}_t^{RRH} \in \mathbb{C}^{M_t\times K}$	Precoder for the t-th RRH for a single data stream per user
X_i	Reactance of the i-th antenna element
$\mathbf{x}_0 \in \mathbb{C}^{M_0^{BS}}$	Transmitted signal vector for the FD BS
$\mathbf{x}_{bs} \in \mathbb{C}^{N_b}$	Transmit signal vector at the beamspace domain
$\mathbf{x}_j^{UL} \in \mathbb{C}^{M_j^{UL}}$	Transmitted signal vector for the j-th UL user
X_{ij}	Mutual reactance between the i-th and j-th antenna element
$\mathbf{y} \in \mathbb{C}^{N_r}$	Received signal vector
$\mathbf{y}_0 \in \mathbb{C}^{N_0^{BS}}$	Signal received by the FD BS
$\mathbf{y}_k^{DL} \in \mathbb{C}^{N_k^{DL}}$	Signal received by the k-th DL user
z_0	Source impedance at the active element of EA

z_m	Impedance at the m-th parasitic elements
z_{t_j}	Impedance of the j-th antenna element at the t-th RRH
Z_{00}	Self impedance of active element of the EA
Z_{in}	Input impedance of an EA
$Z_{in}^{(t)}$	Input impedance of an EA at the t-th RRH
$Z_{t_{ij}}$	Mutual coupling impedance between the i-th and j-th antenna element at the t-th RRH
Z_{ij}	Mutual coupling impedance between the i-th and j-th antenna element
$\mathbf{Z}_{RT}$	Trans-impedance matrix between the transmitter and the receiver
$\mathbf{Z} \in \mathbb{C}^{M \times M}$	Mutual coupling matrix for a M-element antenna
$\mathbf{Z}_t \in \mathbb{C}^{M_t \times M_t}$	Mutual coupling matrix at the t-th RRH with a M_t-element antenna
$\mathbf{Z}_L \in \mathbb{C}^{M \times M}$	Source impedance matrix for a M-element antenna
$\mathbf{Z}_{Lt} \in \mathbb{C}^{M_t \times M_t}$	Loading matrix of the antenna at the t-th RRH with a M_t-element antenna
$\mathbf{Z}_{RR}$	Mutual coupling matrix at the receiver
$\mathbb{I}_{P\xi}$	Set for current vectors which yield input resistance greater than ξ
$\mathbb{I}_{N\xi}$	Set for current vectors which yield input resistance less than ξ
κ	The ratio of the energy in the specular path to the energy in the scattered paths
α	Attenuation of the path
δ_B	Lagrange multiplier
$\mathbb{C}$	Complex number
ζ	Fraction of downlink transmission
η	Power amplifier efficiency at the RRHs
η_1	The free space impedance
ρ_k	Received SINR of the k-th user
ϕ_{rn}	Angle-of-arrival (AOA) at the receiver
θ_{tm}	Angle-of-departure (AOD) at the transmitter
λ	Free space wavelength
$\mathbf{\Lambda}_A$	Its elements are eigenvalues of $\mathbf{A}$
Ω	Bandwidth
$\mathcal{P}$	Probability
ζ_1 ζ_3	Eigenvalues of $\mathbf{B}$
τ_{max}	Delay spread

$\mathbf{0}_{N\times M}$	N by M zero matrix
$\succcurlyeq \mathbf{0}$	Positive semi-definite
$\mathbb{C}^{m\times n}$	$m \times n$ complex matrix
$\mathbb{C}^{m\times n}$	$m \times n$ complex matrix
$(\cdot)'$	Derivative operation
$(\cdot)^H$	Conjugation transpose
$(\cdot)^T$	Transpose
$\overline{(\cdot)}$	Conjugation
$(\cdot)^\perp$	Orthogonal vector or space
$\|\cdot\|$	2-norm or Euclidean norm
$\|\cdot\|_F$	Frobenius Norm
$\mathbf{\Sigma}_j^{UL} \in \mathbb{C}^{N_0^{BS}\times N_0^{BS}}$	Covariance matrix of the aggregate interference-plus-noise terms at the j-th UL
$\mathbf{\Sigma}_k^{DL} \in \mathbb{C}^{N_k^{DL}\times N_k^{DL}}$	Covariance matrix of the aggregate interference-plus-noise terms at the k-th DL user
$\Re\{.\}$	Real part
$\Im\{.\}$	Imaginary part
λ_m	The m-th eigenvalue of a matrix
$F_{R_{in}}$	Cumulative distribution function (CDF) of R_{in}
tr$\{\cdot\}$	Trace
diag $(\mathbf{A})$	Diagonal matrix with the same diagonal elements as $\mathbf{A}$
$\mathbf{0}_{m,n}$	A $m \times n$ zero matrix
$\mathbf{0}_m$	A $m \times 1$ zero vector
∇	Gradient of a function

Chapter 1
Introduction

This thesis explores a novel technique for transceiver design in 5th generation (5G) and beyond wireless communication systems, which is cloud radio access networks (CRANs) with single-RF antennas. In this chapter, Section 1.1 introduces the challenges of modern wireless networks that motivate this work. Section 1.2 describes the contributions this thesis makes. Finally, Section 1.3 outlines how the remaining chapters are organised.

1.1 Motivations

The next generation of wireless cellular networks attempt to satisfy the continually increasing demand for higher data rates and mobility. Recently, CRANs have been used as a new approach. Through this method, a large number of low-cost remote radio heads (RRHs) are deployed and connected to the base band unit (BBU) pool through optical links. Through this new network perspective, since the baseband processing is centralised at the BBU pool, the cooperative techniques can reduce interference. Moreover, by moving RRHs closer to the users, higher system capacity and lower power consumption can be achieved, as the signals do not need to be transmitted long distance to reach the users.

However, from the hardware perspective, cost and size are two main factors that could affect the wide application of this approach. More specifically, the benefits of multiple antenna transmission increase as the number of antennas increases. Each additional antenna element requires an additional radio frequency (RF) chain, resulting in increased cost and complexity. In addition, to maximise the benefits offered by multiple antenna elements, the antennas need to be placed far enough apart to minimise coupling. This results in an increase in the size of the device and reduces mobility [12]. Therefore, the *High capacity network Architecture with Remote radio head and Parasitic antenna arrays (HARP)* project proposes that single-RF antennas can provide multiple antenna functionality to overcome hardware issues [13, 14].

As an attempt to make a single-RF antenna, electronically steerable parasitic array radiator (ESPAR) was proposed by [15]. The authors in [16] provided the design conditions that an ESPAR antenna (EA) must satisfy to support an arbitrary precoding scheme. For some signals, varying the parasitic loads might lead to oscillatory/unstable behaviour. Thus, these signals cannot be transmitted by EAs. The main design condition considered in [16] stated that the real part of the input impedance, also labelled *input resistance* [17], should be positive. Satisfying this condition is essential, because negative input resistance results in a positive reflection coefficient (dB). This implies that the EA is reflecting power back and exhibiting an oscillatory/unstable behaviour [18]. In the case of an EA system, the value of the input resistance depends on the currents at the antenna elements (which depend on the signal to be transmitted) and the mutual coupling (MC) matrix (which depends on different parameters, including inter-element spacing, antenna element pattern, array geometry, relative positioning of the antenna elements in the array, operational frequency and near field scatterers [40, 41].). If the MC matrix (MCM) is fixed, which is typically the case for an EA, a change in the antenna signal or current vectors can result in negative input resistance. This implies that for such signals or current vectors, the EA will reflect power back and exhibit unstable behaviour. To transmit such signals, a new MCM, and by extension a new EA, need to be designed. This approach is proposed in [16]. The authors designed an EA with a suitable MCM by increasing the self-resistance of the EA. However, one issue with the approach in [16] is that once an EA is designed, there are still some signals for which the EA will be unstable, as such signals resulting in negative input resistance. Chapter 3 adopts a new approach to overcome this issue.

Unlike standard multiple antenna systems, where each antenna element has its own power amplifier, in an EA, all the antenna elements are fed centrally by a single power amplifier. This makes it more probable that an EAs power amplifier might reach maximum power during transmission. This highlights the importance of enforcing a peak power constraint for the power amplifier. Such considerations have led to the research that is the focal point of Chapter 4. This chapter examines a more realistic scenario, with a peak power constraint at the element feeding the EA.

When applying single-RF antennas to CRANs, the main difference for single-RF antenna

transmitters compared with standard multiple antenna systems is the configuration of the antennas at the RRHs. In CRANs, the configuration of the antennas at each RRH is calculated at the BBU and is then transmitted to the RRH by optical links. For standard multiple antennas, the configuration is a set of voltage feedings for all the antenna elements. When a single-RF antenna is brought into CRANs, the antenna configuration might be another configuration. For example, the configuration for an EA is a voltage feeding at the active element and a set of loadings at the parasitic elements [16, 19]. Moreover, energy consumption is one of the most urgent and critical challenges in the design of the next generation of mobile networks. This is due to increased data rates, economic reasons, and environmental concerns relating to sustainable growth. Therefore, in Chapter 5, energy efficiency (EE) is utilised as a metric to find optimal precoding and power allocation schemes at the RRHs in CRANs.

1.2 Contributions

The main work for this thesis has followed the purposes of the EU 7th framework project, High capacity network Architecture with Remote radio head and Parasitic antenna arrays (HARP), which are to enable single-RF antenna to provides multi-antenna-like functionality and to bring distributed multi-antenna wireless access to reality.

The main contributions this thesis seeks to make are as follows:

- A new approach is adopted to solve the oscillatory/unstable behaviour of an EA when it realises arbitrary signal transmission. Instead of trying to transmit the actual/ideal signals, which produce a negative input resistance at the EA, signals closely approximating the actual/ideal signals that do not lead to a negative input resistance are transmitted. In this way, the EA does not need to be redesigned. In order to obtain the approximate signal, an optimisation problem is proposed to minimise the MSE between the ideal and approximate signals. This proposal takes into consideration the implementation constraint of the EA. The optimisation problem is solved analytically, and novel closed-form expressions are derived to easily calculate the approximate current signals for the EA system. Our simulation results, conducted for various communica-

tion scenarios, show that the EA transmitter utilising the novel closed-form expressions generates a significant improvement over the performance of the EA transmitter that does not contain any pre-processing. It performs nearly the same as standard multiple antenna systems.

- Considering the power limitations for EA transmission, we propose a practical new transmission scheme that enables an EA to provide stable multi-antenna functionality. This problem is formulated as a non-convex optimisation problem. It is solved analytically via coordination transformation and geometric analysis. Closed-form expressions are obtained for optimal approximate transmission signals. Our analytical results show that the increasing self-impedance of an EA to achieve stability, as shown in [16], is highly power inefficient.

- An EE maximisation problem is formulated to obtain optimal precoding and power allocation schemes when multiple RRHs transmit signals to one user. The closed-form expressions for precoding and power allocation among different RRHs maximise the EE in the system. These results are not only applicable for single-RF antennas, but also for other types of antennas. The EE problem is extended into multi-user CRANs. An optimisation problem is formulated by introducing zero-forcing (ZF) constraints for multi-user interference cancellation. To maximise EE, closed-form expressions for the precoders and power allocation are obtained among different users. Additionally, we compare the EE performance of standard multiple antenna systems and single-RF antenna systems. The results show that the EE of single-RF antenna based systems outperform the standard multiple antenna systems.

1.3 Thesis Layout

Chapter 2 provides some background information. It starts with the introduction of wireless propagation channels; it then looks at MIMO systems, followed by a brief introduction to CRANs. Next, it illustrates the background of mutual coupling and its impact on MIMO antennas. The end of this chapter presents the fundamental models and development of front-end feeding architectures for antenna arrays, with a special focus on the EA transmitter.

Chapter 3 analyses the stability of the ESPAR transmitter when it is used to provide multi-antenna-like functionality. For signal transmission by an EA, the input resistance becomes negative for some signals. A negative input resistance would lead to the oscillatory/unstable behaviour of an EA as it transmits signals. This problem is solved by obtaining approximate signals for transmission that are close to the ideal signals in terms of MSE. Closed-form expressions that calculate the approximate signal vector from the ideal signal vector are obtained, resulting in simplified processing at the transmitter. In the last section of the chapter, the performance of the proposed algorithms is compared with that of an EA transmitter that does not have any pre-processing, and with standard multiple antenna systems for various communication scenarios.

Chapter 4 considers the impact of limited power on EA transmission. We propose a new practical transmission scheme that enables an EA to provide stable multi-antenna functionality by taking into account instantaneous total power requirements. This problem is formulated as a non-convex optimisation problem, and it is solved analytically using coordination transformation and geometric analysis. Closed-form expressions for optimal approximate transmission signals are derived from this problem.

Chapter 5 considers the generic loaded modulated antennas with single-RF chain and studies the EE of loaded modulated antennas equipped CRANs consisting of multiple RRHs. An EE optimisation problem is formulated to derive closed-form expressions for precoding and power allocation schemes at each RRH for single-user systems. The analysis then extends to multi-user scenarios and derives closed-form expressions for precoding and power allocation schemes for multi-user systems.

Finally, Chapter 6 provides some conclusions on the work carried out in the main chapters, and discusses possible research directions for the future.

Chapter 2
Background

This thesis is devoted to a novel technique about cloud radio access networks (CRANs) with single-RF antennas. This chapter offers its background, starting with the properties of wireless channels. MIMO systems are introduced, followed by a brief introduction of CRANs. After that, it presents basic antenna theory including antenna parameters, the background to mutual coupling and its impact on MIMO antennas. Finally, the fundamental systems of front-end feeding architectures for antenna arrays and CRANs with single RF antennas at RRHs systems are briefly presented in the end.

2.1 Wireless Channel Modelling

This thesis explores novel techniques for transceiver design with single-RF antennas. The performances of proposed algorithms are compared with that of the standard multiple antenna transmitter with multi-RF antennas through wireless communication channel. The channel is the medium of signal propagation between the transmitter and receiver. It can be referred to as the variation of electromagnetic propagation. Roughly, the variations can be divided into two types: large-scale fading and small-scale fading.

2.1.1 Large-scale Fading

The received signal is affected by large-scale fading consisting of path loss, which is a deterministic function of distance, and shadowing, which is modelled as a random attenuation to cover signal loss caused by obstacles such as buildings and hills [20].

2.1.1.1 Path Loss

Path loss is the mean power attenuation of the transmitted signal in terms of the distance between the transmitter and the receiver. It can be represented by a path loss exponent, which depends on the terrain and foliage [20]. Several empirically based path loss models have been developed for different frequency [22–24, 87, 105]. An example of distance-dependent path loss model for an outdoor RRH model with LOS path when carrier frequency is 2GHz in [87] is $P_{LOS} = 103.8 + 20.9 \log_{10} \frac{d_{tr}}{d_0}$, which $d_0 = 1$km and P_{LOS} is expressed in dB.

2.1.1.2 Shadowing

The shadowing effect is the variation of mean path loss caused by large objects. It is found in [25] that the impact of shadowing on the received power is approximately log-normally distributed .

2.1.2 Small-scale Fading

Due to the constructive and destructive interference of the multiple signal paths between the transmitter and receiver, small-scale fading leads to rapid fluctuations in signal amplitude and phase. More specifically, multipath is the arrival of the transmitted signal at an intended receiver through differing angles and/or differing time delays and/or differing frequency shifts. This is due to the scattering of electromagnetic waves in the environment. Consequently, the received signal power fluctuates in space (due to angle spread) and/or frequency (due to delay spread) and/or time (due to Doppler spread) through the impacts from multipath components [26].

Small fading can be modelled as Rayleigh fading when there are a large number of statistically independent reflected and scattered paths and no line-of-sight (LOS) signal component. In this case, as the distance between devices are much larger than the wavelength of the carrier frequency, the phases of different paths can be assumed to be independent and the phase for each path can be assumed to be uniformly distributed [20]. Moreover, based on the central limit theorem, the channel impulse response can be modelled as a Gaussian process

irrespective of the distribution of wave components. Assuming Gaussian probability density, the magnitude has a Rayleigh density function [27]. When the signal arrives at the receiver through several different paths, and the LOS signal is much stronger than the others, the amplitude gain is characterised by a Rician distribution.

2.1.2.1 Time Delay of the Signal

If a narrow impulse signal is transmitted in a multipath propagation environment, several delayed and scaled versions of it will arrive at the receiver. Thus, the received signal is composed of various impulse signals which have different time delays. The delay spread is the time difference between the last and first arriving resolvable delay signals, which are denoted as τ_{max} [28]. The coherence bandwidth, B_c, which describes the impact of a multipath propagation environment, is defined as

$$B_c \propto \frac{1}{\tau_{max}}. \tag{2.1}$$

- **Frequency-selective fading:** If the signal bandwidth, B_s, is greater than B_c, multipath components arrive go beyond the symbol duration and some of the signal components fall outside the coherence bandwidth. In other words, transmitted signals are influenced by the channel differently. Thus, the symbols are overlapped by each other. Finally, intersymbol interference (ISI) occurs, which results in so-called frequency-selective fading.

- **Flat fading:** If the signal bandwidth B_s is smaller than B_c, it means all the multipath components arrive within the symbol duration. In other words, the frequency components undergo the same attenuation and phase-shift in transmission through the channel, which is called a flat fading channel. The channel-induced ISI distortion does not happen in a flat fading channel, however, because of the loss in signal-to-noise ratio (SNR) whenever the signal experiences fading, the performance degradation still exists [6].

2.1.2.2 Time Variance of the Signal

The time-varying property of the channel is another important parameter of small-scale fading. This time variance of the signal is normally caused by relative motion between the transmitter and receiver, or the movement of scatterers within the channel [6]. The two important relevant parameters are the Doppler spread and the coherence time [20]. When the receiver is moving, the received signal frequency changes from that of the original transmitted signal and this additional frequency shift is known as Doppler frequency shift. In a multipath channel, the largest difference between the Doppler shifts for different multipath components is known as the Doppler spread [20]. Assuming B_{max} to be the Doppler spread, the coherence time, T_c, is typically defined in [29] as

$$T_c \propto \frac{1}{B_{max}}. \tag{2.2}$$

In wireless communication systems, with respect to the time-varying property, channels are often categorised as fast fading or slow fading [20]. This depends, not only on the environment, but also on the delay requirement of different applications.

- **Fast fading:** Fast fading occurs when the channel coherence time T_c is much shorter than the packet duration of the application [20]. In this case, the fading characteristic of the channel changes several times while a data packet is propagating, which induces distortion of the baseband signal [29]. If the channel remains approximately constant for one packet duration, it is called a block fading model.

- **Slow fading:** If the coherence time T_c is longer than one packet duration, then the amplitude and phase variation imposed by the channel can be considered roughly constant over the period of use [20]. This is known as slow fading. In this case, the channel stays invariant during the time in which a data packet is transmitted.

2.2 MIMO Systems

The quality of radio communication can be severely affected by the fluctuation in signal level from the wireless channel. Additionally, it is challenging to design communication systems with high reliability and high data rates under the constraints of limited bandwidth frequency channels and limited power. In order to meet the challenges caused by the impairments in wireless channels and resource constraints, MIMO technology constitutes a breakthrough in wireless communication system design [26]. Generally speaking, in MIMO systems both transmitters and receivers are equipped with multiple antenna elements to improve the overall performance. MIMO systems can obtain significant performance gains, such as array gain, spatial diversity gain, spatial multiplexing gain and interference reduction [26]. Note that it might not be possible to exploit simultaneously all the benefits due to conflicting demands, and improved performance can be achieved by using some combination of the performance gains [26]. An example of combining two performance gains is the shown in the excellent groundbreaking paper [21] that both diversity and multiplexing gains can be simultaneously obtained, but there is a tradeoff between how much of each type of gain any MIMO scheme can extract.

2.2.1 MIMO Channel

As shown in Figure 2.1, we consider a $N_r \times N_t$ MIMO system with a linear array at each link end, in which, N_t and N_r is the number of the transmitting and receiving antenna elements, respectively. The antenna spacing at the transmitter and receiver are d_T and d_R, respectively. Note that, hereinafter, our analysis focuses on two-dimensional (2D) space only. Furthermore, the channel focused on is for a sample realisation, i.e. the channel is deterministic and time-independent.

2.2.1.1 Physical Channel Model

As shown in Figure 2.1(a), it is assumed that there are N_s scatters between the transmitter and receiver. Therefore the transmitter and receiver are coupled via a finite number of scattering paths. This is called a finite scatterer representation [30–32]. The 2D physical channel of

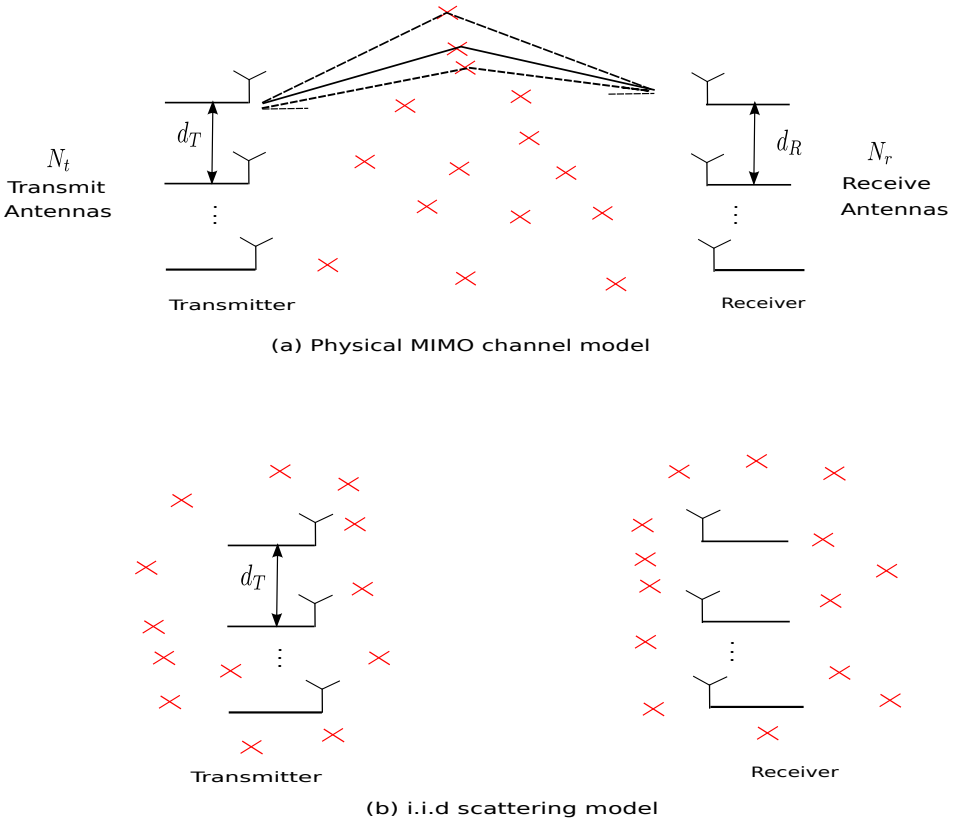

Figure 2.1: MIMO channel models [6]

MIMO systems can be constructed as [32, 33]

$$\mathbf{H} = \mathbf{A}_r \mathbf{H}_b \mathbf{A}_t^T, \tag{2.3}$$

where the columns of $\mathbf{A}_r \in \mathbb{C}^{N_r \times N_s}$ and $\mathbf{A}_t \in \mathbb{C}^{N_t \times N_s}$ are the steering vectors related to the directions of each path observed at the receiver and the transmitter, respectively, and $\mathbf{H_b}$ represent the $N_s \times N_s$ matrices whose elements are the complex path gains. The matrices $\mathbf{A}_r$ and $\mathbf{A}_t$ can be expressed as

$$\begin{aligned} \mathbf{A}_r &= [\mathbf{a}_r(\phi_1), \mathbf{a}_r(\phi_2), \ldots, \mathbf{a}_r(\phi_{N_s})], \\ \mathbf{A}_t &= [\mathbf{a}_t(\theta_1), \mathbf{a}_t(\theta_2), \ldots, \mathbf{a}_t(\theta_{N_s})], \end{aligned} \tag{2.4}$$

in which $\mathbf{a}_r(\phi_m)$ and $\mathbf{a}_t(\theta_m)$ are steering vectors. For uniform linear arrays (ULA) oriented to the link axis, they are given by

$$\begin{aligned} \mathbf{a}_r(\phi_n) &= \left[1, e^{-j\phi_n}, e^{-j2\phi_n}, \ldots, e^{-jN_r\phi_n}\right]^T, \\ \mathbf{a}_t(\theta_m) &= \left[1, e^{-j\theta_m}, e^{-j2\theta_m}, \ldots, e^{-jN_t\theta_m}\right]^T, \end{aligned} \tag{2.5}$$

where

$$\begin{aligned} \phi_n &= \frac{2\pi d_R}{\lambda} \cos\left(\phi_{rn}\right), \\ \theta_m &= \frac{2\pi d_T}{\lambda} \cos\left(\theta_{tm}\right). \end{aligned} \tag{2.6}$$

Here, ϕ_{rn} and θ_{tm} are angle-of-arrival (AOA) and angle-of-departure (AOD), respectively. They are referenced with respect to the link axis [32, Page 43], and λ is the wavelength in air.

2.2.1.2 Analytical MIMO channel

While physical models reproduce the properties of the MIMO channel by specifying the locations of obstacles and the array configuration, analytical models provide a mathematical representation of the channel matrix [32]. In this subsection, analytical representations are discussed.

Classical Independent and Identically Distributed (i.i.d.) Rayleigh Fading MIMO Channel Model In a richly scattered environment, a significant number of scatterers are evenly distributed around both transmitter and receiver. As shown in Figure 2.1(b), the energy of multipaths is equally spread out, and the antenna elements are sparsely spaced [6]. In this environment, $h_{i,j}$ is the entry in the i-th row and j-th column of $\mathbf{H}$ and $h_{i,j} \sim \mathbb{CN}(0,1)$. This MIMO fading model is named as Rayleigh fading model. It is normally used in MIMO communication schemes due to its analytical tractability [20].

Rician Fading Channels In mobile cellular networks, there may exist a strong coherent component, which does not experience any fading over time, for example, a line-of-sight field, or one or several specular contributions. This leads to a Rician distribution of the received field amplitude [20, 32]. In this case, the channel $\mathbf{H}$ can be written as

$$\mathbf{H} = \sqrt{\frac{\kappa}{1+\kappa}}\overline{\mathbf{H}} + \sqrt{\frac{1}{1+\kappa}}\hat{\mathbf{H}}, \tag{2.7}$$

where $\hat{\mathbf{H}}$ is the non-coherent contribution, κ is the ratio of the energy in the specular path to the energy in the scattered paths, and $\overline{\mathbf{H}}$ corresponding to the coherent components has fixed amplitude entries with different phase shifts [32].

2.2.2 Single-user MIMO Systems

As this work focuses on the downlink transmission, considering a system with N_t transmitting antenna elements and N_r receiving antenna elements, as discussed in Section 2.2.1, the received signal $\mathbf{y}$ at the user can be written as

$$\mathbf{y} = \mathbf{H}\mathbf{s} + \mathbf{n}, \tag{2.8}$$

where $N_r \times 1$ vector $\mathbf{s}$ is the transmitted vector and $\mathbf{n}$ is the noise at the receiver.

2.2.3 Multi-user MIMO Systems

Multi-user MIMO systems are more complex than single-user MIMO systems, since there is co-channel interference among the different users. As this work focuses on the MIMO broadcast channel (BC) system, this thesis considers the BC transmission from base station (BS) with N_t transmitting antenna elements to K users with N_r antenna elements for each. The received signal of the k-th user is

$$\mathbf{y}_k = \mathbf{H}_k^{DL}\mathbf{s}_k + \sum_{i=1, i\neq k}^{K} \mathbf{H}_k^{DL}\mathbf{s}_i + \mathbf{n}_k, \tag{2.9}$$

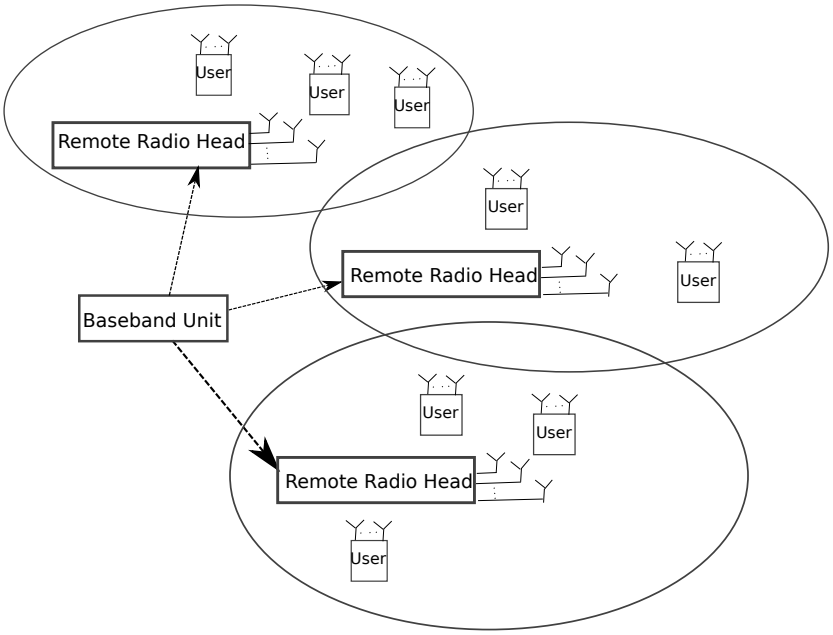

Figure 2.2: CRANs architecture [7].

where $\mathbf{s}_k$ is the transmitted signal to the k-th user and $\mathbf{n}_k$ is noise at the k-th user.

2.3 Radio Access Network

This section provides a description of the evolution of base stations and the basic benefits of the CRANs. Currently, CRANs have attracted intense research interest from both academia and industry (such as China Mobile, Huawei, Alcatel-Lucent and Qualcomm) [35]. In CRANs, a large number of low-cost remote radio heads (RRHs) are deployed and connected to the baseband unit (BBU) pool through optical links, as shown in Figure 2.2. CRANs have several advantages. Firstly, because the signals do not need to propagate a long distance to reach the users, by moving RRHs closer to the users it is possible to achieve higher system capacity and lower power consumption. Secondly, cooperative techniques can reduce the interference, as the baseband processing is centralised at the BBU pool [7]. Last, but not least, CRANs are much more efficient in both energy and cost aspects as they exploit resource pooling and sharing.

2.3.1 Traditional All-in-one Architecture

In the 1st generation (1G) and 2nd generation (2G) mobile networks, base stations usually have an all-in-one architecture design with integration of the radio and baseband processing functionality. In this design, the base station cabinet is placed in a few metres from the radio module with all necessary supporting facilitates. The radio frequency (RF) signal is generated by the base station RF unit and travels through pairs of RF cables up to the antennas on mounting points [7].

2.3.2 Base Station with Remote Radio Heads and a Baseband Unit

A distributed base station architecture is introduced for 3rd generation (3G) networks. The base station is separated into a radio unit and a signal processing unit. The radio unit is called an RRH or remote radio unit (RRU), and the baseband signal processing part is a baseband unit (BBU) or data unit (DU) [36]. RRHs are connected to the BBU by optical links and provide the function of digital processing, digital to analogue conversion, filtering and analogue-to-digital conversion [37]. In the traditional all-in-one radio access network (RAN) architecture, a BBU needs to be placed close to the antenna and the RF signals travel through a cable from BS to the antenna at the top of tower. RRHs are statically assigned to BBUs [37].

2.3.3 Cloud Radio Access Networks

The concept of CRANs is first introduced in [38] and is explained in [39]. In CRANs, a BBU pool is a virtualized cluster to improve the utilisation of BBU between heavily and lightly loaded BS. A BBU pool consists of general purpose processors to perform baseband processing. In a virtualized BBU pool, baseband processing is shared among sites, which means that it is able to utilise the resources more efficiently. Because of the fact that fewer BBUs are needed in CRANs when compared to traditional architecture, CRANs also have the potential to decrease the cost of a network operation and reduce energy consumption. The scalability and maintenance of the network are improved when compared with traditional

RAN architecture. Moreover, different operators are able to share a virtualized BBU pool.

2.4 Antenna Parameters

The definitions of various parameters are necessary in order to describe the performance of an antenna. This section offers a brief introduction of antenna input impedance, followed by the impact of negative input resistance. After that, antenna matching is introduced. Finally, it presents the background to mutual coupling.

2.4.1 Input Impedance

Input impedance is the impedance presented by an antenna at its terminals and it can be defined as the ratio of the voltage to current at a pair of terminals as in [17]. Let Z_{in} denote the impedance of the antenna, it can be written as

$$Z_{in} = R_{in} + \Im\{Z_{in}\}, \tag{2.10}$$

in which, R_{in} is the antenna resistance (ohms) and $\Im\{Z_{in}\}$ is the antenna reactance at the terminals (ohms).

The resistive part, R_{in}, can be further divided into two components as

$$R_{in} = R_{in}^{R} + R_{in}^{L}, \tag{2.11}$$

where R_{in}^{R} is radiation resistance and R_{in}^{L} is antenna loss resistance. The amount of power delivered for radiation is through R_{in}^{R} and the amount dissipated in R_{in}^{L} as heat.

2.4.2 Negative Input Resistance

The radiated power comes from a generator/source connected via a feed network to the antenna terminals. If the antenna is attached to a generator, the internal impedance of the generator

is

$$Z_s = R_s + \Im\{Z_s\}, \tag{2.12}$$

in which, R_s and $\Im\{Z_s\}$ are the resistance and reactance of the generator, respectively. The amount of power delivered to the antenna can be written as

$$P_{in} = \mid i \mid^2 \Re\{Z_{in}\}, \tag{2.13}$$

where i is the current developed within the circuit and it can be obtained by Ohm's law as

$$i = \frac{v_0}{Z_s + Z_{in}}. \tag{2.14}$$

Here, v_0 is the average voltage generated by the generator. By substituting (2.14) into (2.13), the amount of power delivered to the antenna can be rewritten as

$$P_{in} = \mid v_0 \mid^2 \frac{R_{in}}{(R_{in} + R_s)^2 + (\Im\{Z_{in}\} + \Im\{Z_s\})^2}. \tag{2.15}$$

It is noted that input resistance should be positive to guarantee that there is power delivered to the antenna. As shown in [18], a system structure is unstable if the input port impedance has a negative real part. A negative input resistance implies that the antenna would work as a generator. Thus, the antenna is reflecting power back and exhibiting oscillatory/unstable behaviour [18, 55].

2.4.3 Antenna Matching

Part of power provided by the generator is the input power to the antenna as shown in (2.15), while the rest is dissipated as heat on the generator and it is given by

$$P_h = \mid v_0 \mid^2 \frac{R_s}{(R_{in} + R_s)^2 + (\Im\{Z_{in}\} + \Im\{Z_s\})^2}. \tag{2.16}$$

Thus, for maximum power transfer, the generator/source impedance needs to be conjugate

matched to the input impedance [17]; that is

$$\begin{aligned} R_{in} &= R_s, \\ \Im\{Z_{in}\} &= -\Im\{Z_s\}. \end{aligned} \tag{2.17}$$

By substituting (2.17) into (2.15) and (2.16) , we have

$$\begin{aligned} P_{in} &= \frac{|\, v_0 \,|^2}{4R_{in}}, \\ P_h &= \frac{|\, v_0 \,|^2}{4R_s}. \end{aligned} \tag{2.18}$$

Thus, the power supplied by the generator during conjugate matching is

$$P_S = \frac{|\, v_0 \,|^2}{2R_{in}}. \tag{2.19}$$

It is noted that half of the power provided by the generator is delivered to the antenna when we have conjugate matching. For the power delivered to the antenna, as $R_{in} = R_{in}^R + R_{in}^L$ in (2.11), part is radiated through the antenna according to the radiation resistance and the other is dissipated as heat [17].

2.4.4 Mutual Coupling

2.4.4.1 Mutual Coupling Definition

The electromagnetic interaction between the antenna elements is called mutual coupling [17]. In general, mutual coupling between antenna elements depends on different parameters, including inter-element spacing, antenna element pattern, array geometry, relative positioning of the antenna elements in the array, operational frequency and near field scatterers [40, 41]. Most of these parameters can be measured or estimated, except near field scatterers. It is shown in many studies that mutual coupling between closely spaced antenna elements has undesired effects on the performance of compact MIMO systems, such as signal correlation, diversity gain, radiation efficiency [42], received power [43, 44], and capacity [43, 45].

2.4.4.2 Mutual Coupling in the Transmitting Mode

In this section, we model the mutual coupling effect using the mutual impedance. Take a transmitting antenna with two elements as an example in Figure. 2.3, the two coupled antennas can be modelled as two equivalent circuits. The antenna elements are separated by a distance of d and the excitation voltage sources are v_{s1} and v_{s2}. When the mutual coupling effect is taken into account, there are two additional excitation sources as the controlled voltage sources, v_{12} and v_{21}. These controlled voltage sources are the coupled voltages induced by the currents on the other antennas. For an N element array, the circuit can be modeled in [33] as

$$\mathbf{v} = \mathbf{Z}\mathbf{i}, \tag{2.20}$$

where $\mathbf{v}$ is a vector of voltages across the element ports and $\mathbf{i}$ is a vector of the element port input currents. The impedance matrix $\mathbf{Z}$ describes the inherent structure of the antenna array and does not depend on the signals that are fed to the different antenna elements [33]. The form of the mutual impedance matrix would be

$$\mathbf{Z} = \begin{bmatrix} Z_{00} & Z_{01} & \cdots & Z_{0(M-1)} \\ Z_{10} & Z_{11} & \cdots & Z_{1(M-1)} \\ \vdots & \vdots & \ddots & \vdots \\ Z_{(M-1)0} & Z_{(M-1)2} & \cdots & Z_{(M-1)(M-1)} \end{bmatrix}. \tag{2.21}$$

As already noted, mutual coupling has been traditionally considered as an undesired effect, mainly due to the fact that coupled power is fed back the circuit as a reflected wave, decreasing the efficiency of the design. This effect becomes more severe as the antenna elements are placed closer together. The mutual impedance can be either theoretically calculated or obtained by antenna design tools.

2.4.4.3 Methods for Mutual Coupling Analysis

Mutual coupling is always analysed during antenna design using the numerical methods in computational electromagnetics. Three methods are prominent, namely, induced electromo-

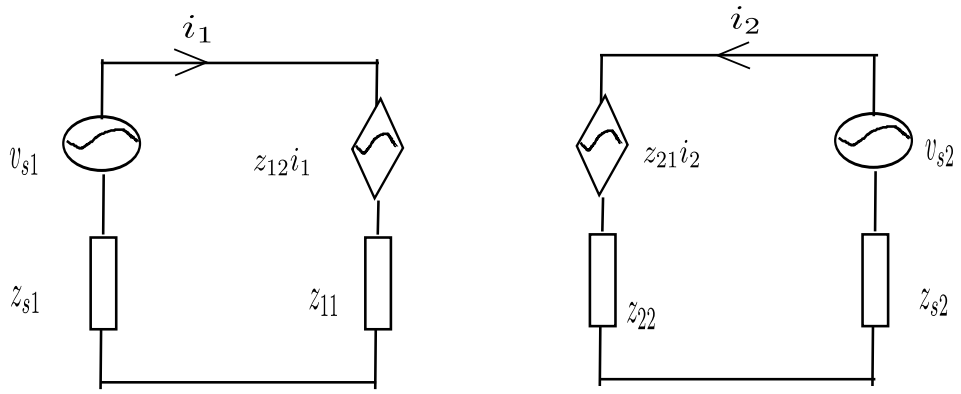

Figure 2.3: Equivalent circuit of an array of two antennas

tive force (EMF), method of moments (MoM) and finite-difference time-domain (FDTD) [6]. The EMF method will be used to get the mutual coupling matrix in the simulation parts of this thesis.

The classical EMF method is applied for straight, parallel and linear arrays [17]. Figure. 2.3 illustrates a linear array of two identical thin wire dipoles with length l placed in a side-by-side configuration and separated by a distance of d. Due to reciprocity theorem, $z_{12} = z_{21}$. Let $\eta_1 = 120\pi$ denotes the free space impedance and $k = \frac{2\pi}{\lambda}$ denotes the wave number. The mutual impedance, z_{12}, can be expressed as

$$z_{12} = R_{12} + jX_{12}, \tag{2.22}$$

and its real and imaginary parts are given by

$$\begin{aligned} X_{12} &= -\frac{\eta_1}{4\pi}\left[2SI(\mu_0) - SI(\mu_1) - SI(\mu_2)\right], \\ R_{12} &= \frac{\eta_1}{4\pi}\left[2CI(\mu_0) - CI(\mu_1) - CI(\mu_2)\right], \end{aligned} \tag{2.23}$$

where

$$\begin{aligned} &\mu_0 = kd, \\ &mu_1 = k\left(\sqrt{d^2 + l^2} + l\right), \\ &\mu_2 = k\left(\sqrt{d^2 + l^2} - l\right), \end{aligned} \tag{2.24}$$

$SI(\mu)$ and $CI(\mu)$ are the cosine and sine integrals and can be written as

$$\begin{aligned} CI(x) &= \int_{\infty}^{x} \frac{\cos x}{x} \mathrm{d}_x, \\ SI(x) &= \int_{\infty}^{x} \frac{\sin x}{x} \mathrm{d}_x. \end{aligned} \tag{2.25}$$

2.5 Front-end Feeding Architectures for Antenna Arrays

For standard multiple antenna array with multiple RF chains, the RF-related costs grow linearly with the number of antennas. As every RF chain in the current state of MIMO transmitters includes a linear power amplifier, a mixer, and a digital-to-analogue converter (DAC) [8], each additional antenna element requires an additional RF chain resulting in increased cost and complexity. In addition, in order to maximise the benefits offered by multiple antenna elements, the antenna elements need to be placed at least half a wavelength apart from each other to minimise the coupling. This results in an increase in the size of the device and reduced mobility. Single RF MIMO transmitters are proposed to alleviate the aforementioned issues with reduced RF cost. They are explored to control or cancel the mutual coupling effect by allowing for compact arrays with fewer RF chains. This section provides an overview of the front-end feeding architectures for antenna arrays as [8].

2.5.1 Standard Multiple Antenna Array with Multiple RF Chains

The circuit diagram of the standard MIMO implementation is illustrated in Figure. 2.4 (a), where the arrays are considered in the transmitting mode. For standard multiple antenna, each element is connected to its dedicated RF chain. When considering compact array, there is mutual coupling among the antenna elements when they are closely spaced, which is shown as the mutual coupling block $\mathbf{Z}$ in Figure. 2.4 (a). In order to avoid the harmful effects of mutual coupling, the antennas are usually spaced about half a wavelength apart, which is shown in Figs. 2.4 (b). This reduces the mutual coupling effect. In this case, the impedance matrix of the antenna array is approximately diagonal. The main drawback of the approaches

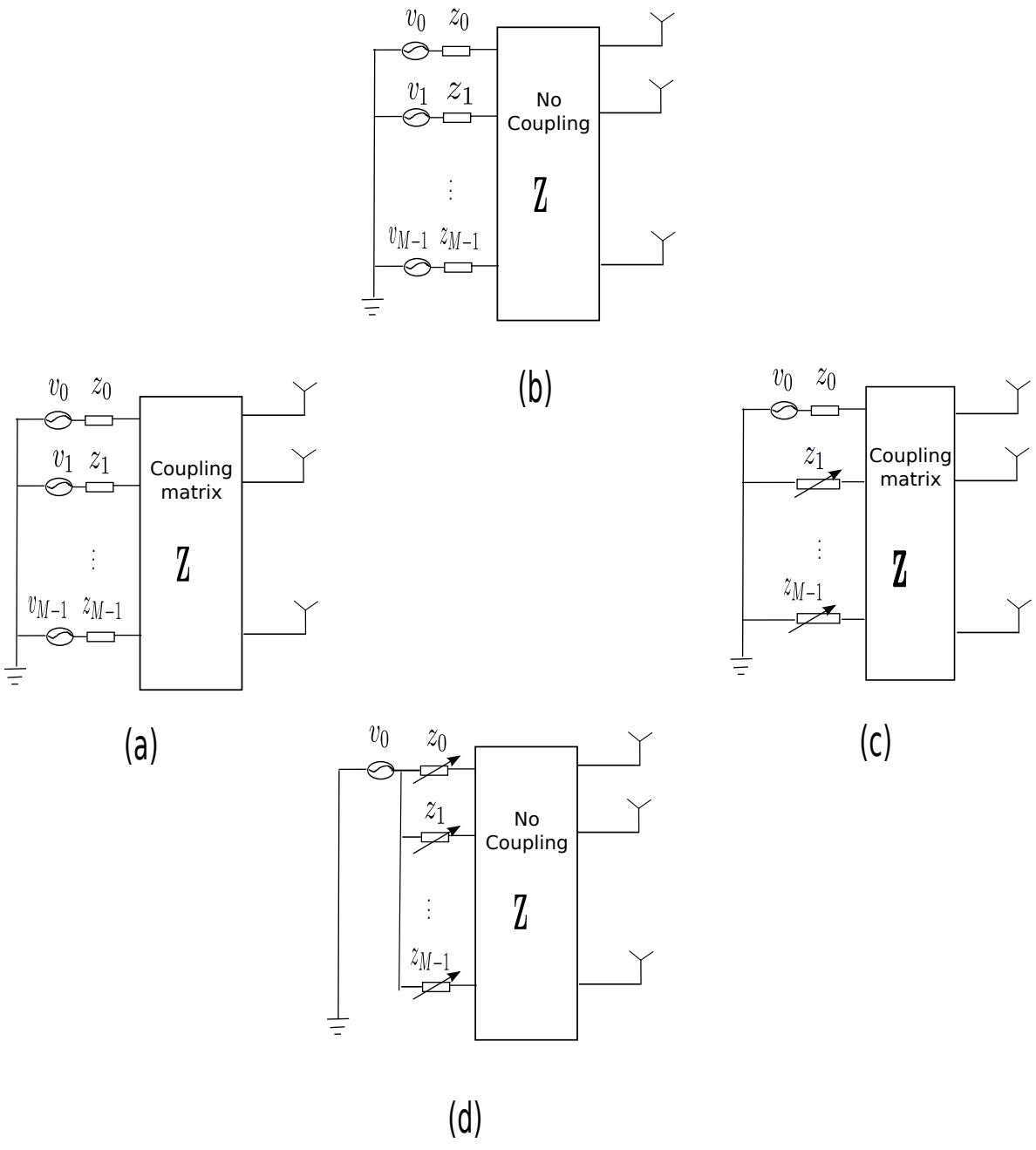

Figure 2.4: Different front-end circuit feeding architectures for antenna arrays [8].

in Figs. 2.4 (a) and 2.4 (b) is the cost of the RF chains. The number of antenna elements grows linearly with the number of RF chains. Each additional antenna element requires an additional RF chain resulting in increased cost. In other words, the antennas with M elements would require M power amplifiers, M mixers, and M DACs. Due to this disadvantage, single-RF MIMO arrays are proposed to provide more efficient implementation. This scheme is illustrated in Figures. 2.4 (c) and 2.4 (d), and is analysed in more detail in the following subsections.

2.5.2 Electronically Steerable Parasitic Array Radiator

An attempt to alleviate aforementioned issues can be made through use of the ESPAR transmitter, as shown in Figure. 2.4 (c). An M-element ESPAR consists of a single active element with an RF unit and $(M-1)$ parasitic elements without any RF units. On the other hand, the standard multiple antenna consists of M elements, each connected to an RF chain. ESPAR alleviates the implementation issues of conventional MIMO systems by employing only a single-RF chain for all the antenna elements. Due to using a single-RF chain, the cost and the circuit energy consumption of the equipment is reduced. In addition, the ESPAR design is based on mutual coupling among various antenna elements; therefore, lower spacing between antenna elements is favourable. It means that the antenna elements can be placed closer to each other resulting in a smaller device size.

EA was initially proposed for low-cost analogue beamforming in [15,50]. Then multiplexing two symbols over the air from lower order phase-shift keying (PSK) modulation formats were explored in the beamspace MIMO model with EA in [12,14,51,52]. An experiment for PSK modulation was presented to validate the functionality of ESPAR MIMO transmitters in [53]. However, several weaknesses of the beamspace MIMO model were discussed [54]. For example, the receiver cannot guarantee the orthogonality of basic beam patterns, and arbitrary channel-dependent precoding cannot be realised for an arbitrary antenna array. Therefore, an alternate model based on the currents at the ports of the transmit antenna is introduced in [55]. As shown in Figure. 2.4, in the standard multiple antenna system, the currents are driven by the RF voltage supply of each antenna element through fixed impedances [45,56]. In the case of the EA systems, the currents at the elements are varied by varying the input voltage at the

active element and the loads at the parasitic elements. When feeding the active element, the currents are induced on the parasitic elements due to the mutual coupling between antenna elements. The overall radiation pattern is shaped by controlling the sole feeding at the active element and the impedance of the parasitics [57]. The development of the ESPAR MIMO transmitter will be discussed in details in the next section.

2.5.3 Load Modulated Array Architecture

Figure. 2.4 (d) illustrates a newly alternative solution. This is called load modulated array architecture and is proposed in [58]. In this approach, all antenna elements are connected to a common carrier source by two-port loading networks, and these networks are passive and lossless. These loads are tuned to control the input currents to all radiating elements, thereby implementing a desired signal constellation in the analogue domain [8]. This scheme is favorable in the application of the massive MIMO systems with large numbers of antennas as explained in [8]. The antenna in our work, however, focuses on EA. For more details about load modulated array, please refer to [8, 58–60].

2.6 ESPAR MIMO Transmitter

As discussed in Section 2.5.2, the ESPAR MIMO transmitter was first explored through the beamspace MIMO model in [12,14,51,52]. A proof-of-concept experiment was implemented to validate the functionality of single-RF beamspace MIMO transmitters in [53]. After that, an alternate and more general model based on the currents at the ports of the transmit antenna elements were introduced in [55]. In this section, the beamspace MIMO model with EA is discussed. This is followed by a more general system model based on the currents at the transmitting antenna elements.

2.6.1 ESPAR Antenna Design

In order to validate the functionality of EA, several EAs have been designed using the IE3D antenna software in literature previously [55, 72]. IE3D is a full-wave, method-of-moments based electromagnetic simulator that solves the current distribution on 3D and multilayer structures of general shape and is provided by Mentor Graphics [55].

In [72] , an EA has been designed to verify the proposed smart loading scheme which can enable EA to provide the multiplexing of two 16-QAM signals. Its coupling matrix is given by

$$\mathbf{Z}^{(1)} = \begin{bmatrix} 45.12 - 16.60i & 42.39 - 29.51i \\ 42.39 - 29.51i & 21.12 - 29.64i \end{bmatrix} \Omega. \tag{2.26}$$

In [16], in order to demonstrate the stability conditions of EA, an EA has been designed using the IE3D antenna software and its coupling matrix is

$$\mathbf{Z}^{(2)} = \begin{bmatrix} 52.81 - 11.09i & 40.27 - 20.75i \\ 40.27 - 20.75i & 52.81 - 11.09i \end{bmatrix} \Omega. \tag{2.27}$$

It is shown that this EA cannot support arbitrary precoding. To avoid such a situation, a new EA has been designed to implement the Alamouti space-time precoding scheme with a QAM signaling constellation. The coupling matrix of this new array is

$$\mathbf{Z}^{(3)} = \begin{bmatrix} 465.4 - 659.5i & -24.06 + 34.93i \\ -24.06 + 34.93i & 21.12 - 157.2i \end{bmatrix} \Omega. \tag{2.28}$$

These three mutual coupling matrices will be used in the simulations to show the performance of practical EAs in the remainder of this thesis.

2.6.2 Beamspace MIMO Systems with ESPAR Transmitter

The system with M-element EA at the transmitter and a traditional uniform linear array (ULA) at the receiver is shown in Figure 2.5. It is noted that the number of the transmit-

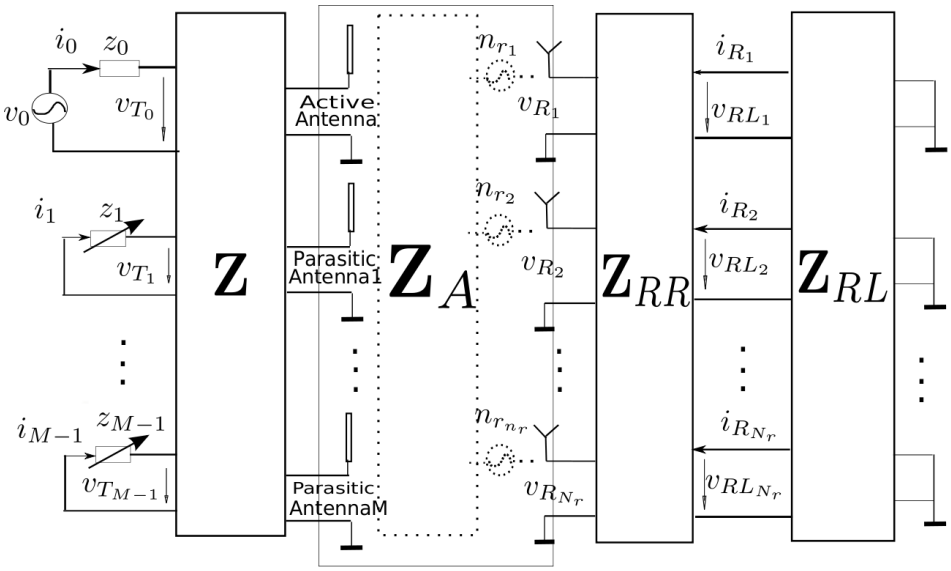

Figure 2.5: MIMO systems with EA at the transmitter and ULA at the receiver

ting antenna elements $N_t = M$ in this case. At the transmitter, $\mathbf{v} = [v_0, 0, \ldots, 0]^T$ denotes the source voltage vector. $\mathbf{Z}_L = \text{diag}(z_0, z_1, z_2, \ldots, z_{M-1})$ are the load values. $\mathbf{v}_T = [v_{T_0}, v_{T_1}, \ldots, v_{T_{M-1}}]^T$, $\mathbf{i} = [i_0, i_1, \ldots, i_{M-1}]^T$ and $\mathbf{Z} \in \mathbb{C}^{M \times M}$ are voltages, currents and mutual coupling matrix at the transmitter, respectively. Similarly, $\mathbf{v}_{RL} = [v_{RL_1}, v_{RL_2}, \ldots, v_{RL_{N_r}}]^T$, $\mathbf{i}_R = [i_{R_1}, i_{R_2}, \ldots, i_{R_{N_r}}]^T$ and $\mathbf{Z}_{RR} \in \mathbb{C}^{N_r \times N_r}$ are corresponding voltages, currents and mutual coupling matrix at the receiver, respectively. $\mathbf{Z}_{RT} \in \mathbb{C}^{N_r \times M}$ is the trans-impedance matrix between the transmitter and the receiver [45, 61]. The noise impact on the voltages at the transmitter and receiver is denoted by $\mathbf{n}_T$ and $\mathbf{n}_R$, respectively.

Based on this circuit, the transfer function between the receiver and the transmitter can be expressed as

$$\begin{bmatrix} \mathbf{v}_T \\ \mathbf{v}_{RL} \end{bmatrix} = \begin{bmatrix} \mathbf{Z} & \mathbf{Z}_{TR} \\ \mathbf{Z}_{RT} & \mathbf{Z}_{RR} \end{bmatrix} \begin{bmatrix} \mathbf{i} \\ \mathbf{i}_R \end{bmatrix} + \begin{bmatrix} \mathbf{n}_T \\ \mathbf{n}_R \end{bmatrix}. \tag{2.29}$$

As the transmitter is not affected by the current conditions at the receiver, we have $\mathbf{Z}_{TR} = \mathbf{0}_{M,N_r}$ [45]. Similarly, since the noise has no impact on the transmitting voltages, then $\mathbf{n}_T = \mathbf{0}_M$. By substituting $\mathbf{Z}_{TR} = \mathbf{0}_{M,N_r}$ and $\mathbf{n}_T = \mathbf{0}_M$ into (2.29), it can be simplified as

$$\begin{bmatrix} \mathbf{v}_T \\ \mathbf{v}_{RL} \end{bmatrix} = \begin{bmatrix} \mathbf{Z} & \mathbf{0}_{M,N_r} \\ \mathbf{Z}_{RT} & \mathbf{Z}_{RR} \end{bmatrix} \begin{bmatrix} \mathbf{i} \\ \mathbf{i}_R \end{bmatrix} + \begin{bmatrix} \mathbf{0}_M \\ \mathbf{n}_R \end{bmatrix}. \tag{2.30}$$

According to Ohm's law, the transmitting voltages are

$$\mathbf{v}_T = \mathbf{Z}\left(\mathbf{Z} + \mathbf{Z}_L\right)^{-1}\mathbf{v}_S. \tag{2.31}$$

At the receiver, $\mathbf{v}_{RL}$ is

$$\mathbf{v}_{RL} = -\mathbf{Z}_L\mathbf{i}_R. \tag{2.32}$$

By substituting them into (2.30), and after some algebraic manipulations, the receiving voltage vector $\mathbf{v}_{RL}$ can be rewritten as

$$\mathbf{v}_{RL} = \mathbf{Z}_L\left(\mathbf{Z}_{RR} + \mathbf{Z}_L\right)^{-1}\left(\mathbf{Z}_{RT}\left(\mathbf{Z} + \mathbf{Z}_L\right)^{-1}\mathbf{v}_S + \mathbf{n}_R\right). \tag{2.33}$$

As we focus on the ESPAR transmitter, the spacing among receiver antenna elements is assumed to be large enough; therefore there is no coupling at the receiver. Thus, $\mathbf{v}_R$ can be written as

$$\mathbf{v}_R = \left(\mathbf{Z}_{RR} + \mathbf{Z}_L\right)\mathbf{Z}_L^{-1}\mathbf{v}_{RL}. \tag{2.34}$$

Substituting (2.33) into (2.34), $\mathbf{v}_R$ is

$$\begin{aligned}\mathbf{v}_R &= \mathbf{Z}_{RT}\left(\mathbf{Z} + \mathbf{Z}_L\right)^{-1}\mathbf{v}_S + \mathbf{n}_R \\ &= \mathbf{Z}_{RT}\mathbf{i} + \mathbf{n}_R.\end{aligned} \tag{2.35}$$

As in [45], $\mathbf{y}$ is denoted as receive signals and $\mathbf{n}$ as receive noise signals. $\mathbf{Z}_{RT}$ reflects the impact of the transmitter on the receiver and can be expressed as $\mathbf{Z}_{RT} = \mathbf{H}$, where $\mathbf{H}$ is the channel model between the transmitter and the receiver. Then (2.35) can be rewritten as

$$\begin{aligned}\mathbf{y} &= \mathbf{H}\left(\mathbf{Z} + \mathbf{Z}_L\right)^{-1}\mathbf{v}_S + \mathbf{n} \\ &= \mathbf{H}\mathbf{i} + \mathbf{n}.\end{aligned} \tag{2.36}$$

When the number of scatters is assumed to be N_s, the physical channel model can be represented as $\mathbf{H} = \mathbf{A}_r\mathbf{H}_b\mathbf{A}_t^T$ [12,32]. This has been described in Section 2.2.1.1. By substituting

it into (2.36), it can be presented as

$$\mathbf{y} = \mathbf{A}_r \mathbf{H}_b \mathbf{A}_t^T \mathbf{i} + \mathbf{n}, \tag{2.37}$$

where $\mathbf{A}_r$ is a traditional ULA steering matrix at the receiver and $\mathbf{A}_t \in \mathbb{C}^{M \times N_s}$ is the steering matrix at the transmitter. $\mathbf{A}_t$ can be expressed as

$$\mathbf{A}_t = \left[\mathbf{a}_t(\theta_1), \mathbf{a}_t(\theta_2), \ldots, \mathbf{a}_t(\theta_{N_s})\right], \tag{2.38}$$

in which $\mathbf{a}_t(\theta_m) \in \mathbb{C}^{M \times 1}$ is the m-th column of $\mathbf{A}_t$ and θ_m is AOD for the EA transmitter [15]. The system model in (2.37) can be further rewritten as

$$\mathbf{y} = \mathbf{A}_r \mathbf{H}_b \left[\mathbf{a}_t(\theta_1), \mathbf{a}_t(\theta_2), \ldots, \mathbf{a}_t(\theta_{N_s})\right]^T \mathbf{i} + \mathbf{n}. \tag{2.39}$$

As shown in [15], the radiation pattern for an EA ,$\mathbf{D}_{rad}$, is

$$\mathbf{D}_{rad} = \mathbf{A}_t^T \mathbf{i} = \left[\mathbf{a}_t(\theta_1), \mathbf{a}_t(\theta_2), \ldots, \mathbf{a}_t(\theta_{N_s})\right]^T \mathbf{i}. \tag{2.40}$$

By substituting (2.40) into (2.37), we have

$$\mathbf{y} = \mathbf{A}_r \mathbf{H}_b \mathbf{D}_{rad} + \mathbf{n}. \tag{2.41}$$

The radiation pattern can be further decomposed as

$$\mathbf{D}_{rad} = \left[\mathbf{b}_0, \mathbf{b}_1, \ldots, \mathbf{b}_{N_b}\right] \mathbf{x}_{bs}, \tag{2.42}$$

where N_b is the number of basis beam patterns, the $N_s \times 1$ vector $\mathbf{b}_m$ is the basis beam pattern, and $\mathbf{x}_{bs}$ is a $N_b \times 1$ transmit signal vector at the beamspace domain.

By substituting (2.42) into (2.41), the receive signals are given by

$$\mathbf{y} = \mathbf{A}_r \mathbf{H}_b \left[\mathbf{b}_0, \mathbf{b}_1, \ldots, \mathbf{b}_{N_b}\right] \mathbf{x}_{bs} + \mathbf{n}. \tag{2.43}$$

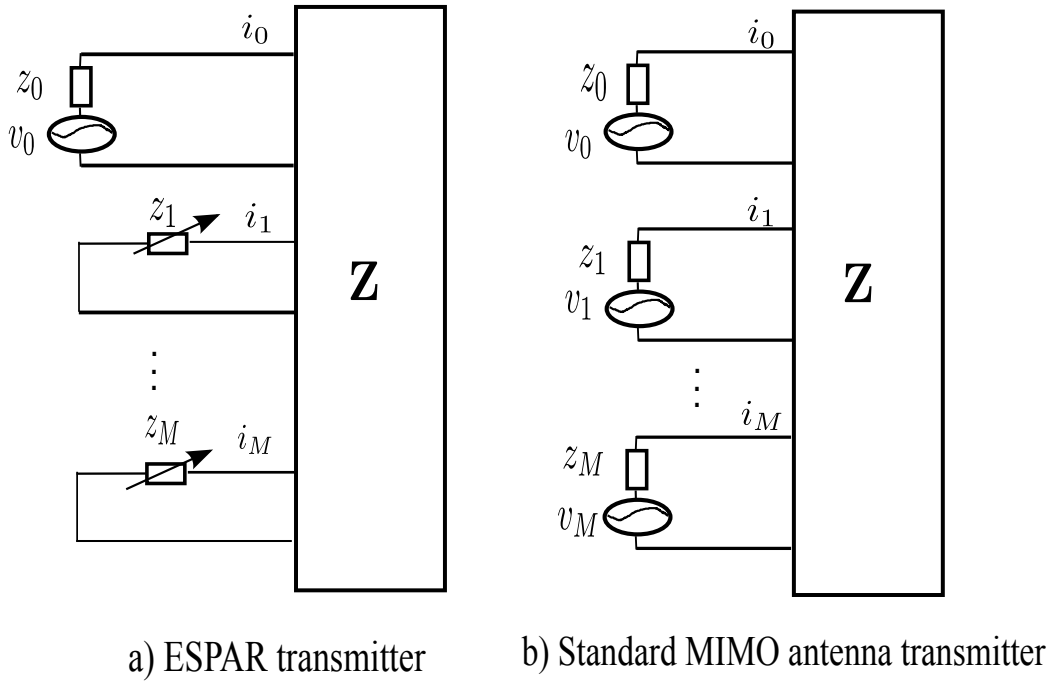

Figure 2.6: Circuit comparison of a) the EA transmitter and b) a standard multiple antenna transmitter

In beamspace MIMO systems, transmitting signals $\mathbf{x}_{bs}$ are mapped onto different basis beams, $\mathbf{b}_0, \mathbf{b}_1, \ldots, \mathbf{b}_{n_b}$, rather than transmit antenna elements. The basic beam patterns are derived from the decomposition of $\mathbf{D}_{rad}$. For example, two orthonormal basis beam patterns using 3-elements EA are proposed in [51]. In general, the authors in [13] provided a general approach to obtaining basis patterns and introduced aerial degree of freedoms (aDOFs) and efficient degree of freedoms (eDOFs) which are equal to the number of basis beam patterns.

2.6.3 General System Model with ESPAR Transmitter

As discussed in Section 2.5.2, several weaknesses are discussed in the beamspace MIMO model [54]. Therefore, an alternate model based on the currents at the ports of the transmit antenna is introduced in [55]. The circuit diagrams of an M-element EA and a standard multiple antenna with multiple RF units are shown in Figure. 2.6 [62]. The EA consists of a single active element with an RF unit and $M-1$ parasitic elements without any RF unit. On the other hand, the standard multiple antenna consists of M elements each connected to an

RF chain.

As depicted in Figure. 2.6, $\mathbf{i} = [i_0, i_1, \ldots, i_{M-1}]^T$ is the vector of currents at the antenna elements, where T denotes the transpose operation. The matrix $\mathbf{Z} \in \mathbb{C}^{M \times M}$ denotes the MCM and it depends on the antenna geometry [63]. $\mathbf{Z}_L = \mathrm{diag}(z_0, z_1, z_2, \ldots, z_{M-1})$ is the source impedance matrix where z_0 is the source resistance [17] and $z_1, z_2, \ldots, z_{M-1}$ are the loads at the parasitic elements.

For the standard multiple antenna system, the vector of source voltages $\mathbf{v}$ is $[v_0, v_1, \ldots, v_{M-1}]^T$. The currents are driven by the RF voltage supply of each antenna element through fixed impedances $z_0, z_1, z_2, \ldots, z_{M-1}$ [45, 56]. In the case of the EA system, $\mathbf{v}$ is $[v_0, 0, \ldots, 0]^T$. The currents at the elements are varied by varying the input voltage v_0 at the active element and the loads $z_1, z_2, \ldots, z_{M-1}$ at the parasitic elements. When feeding the active element, the currents are induced on the parasitic elements due to the mutual coupling between antenna elements. The MCM $\mathbf{Z}$ is given as

$$\mathbf{Z} = \begin{bmatrix} Z_{00} & Z_{01} & \ldots & Z_{0(M-1)} \\ Z_{10} & Z_{11} & \ldots & Z_{1(M-1)} \\ \vdots & \vdots & \ddots & \vdots \\ Z_{(M-1)0} & Z_{(M-1)2} & \ldots & Z_{(M-1)(M-1)} \end{bmatrix}. \tag{2.44}$$

According to Ohm's law, the port current vectors for both circuits can be expressed as

$$\mathbf{i} = (\mathbf{Z} + \mathbf{Z}_L)^{-1} \mathbf{v}. \tag{2.45}$$

If the current vector $\mathbf{i}$, which is the function of $\mathbf{Z}$ and $\mathbf{Z}_L$ in (2.45), flows through the antenna elements, then the input impedance, Z_{in}, is given by [16]

$$Z_{in} = Z_{00} + \frac{\sum_{m=1}^{M-1} Z_{0m} i_m}{i_0}. \tag{2.46}$$

Note that Z_{in} is a function of $\mathbf{Z}$ and current vector $\mathbf{i}$ as shown in (2.46), and the current vector

$\mathbf{i}$ varies with voltage feeding and loads value $\mathbf{Z}_L$ in (2.45). Therfore, Z_{in} depends on the MCM $\mathbf{Z}$ as well as the loads $\mathbf{Z}_L$. After transmission from an EA, the received signal at the receiver, with N_r antennas, is given as [55, 64, 65]

$$\mathbf{y} = \mathbf{H}\mathbf{i} + \mathbf{n}, \tag{2.47}$$

where $\mathbf{H} \in \mathbb{C}^{N_r \times M}$ is the channel matrix as the number of the transmitting antenna elements is $N_t = M$ for the EA transmitter and $\mathbf{n} \in C^{N_r \times 1}$ denotes the noise vector at the receiver. The receiver is assumed to be a standard multiple antenna receiver.

2.6.4 Impedance Matching for ESPAR Transmitter

As discussed in section 2.4.3 in this chapter, for maximum power transfer, impedance matching is necessary. The generator/source impedance needs to be matched to the overall input impedance of the EA. In [16], a dynamic impedance matching circuit is proposed to compensate the impedance mismatch between the source and input impedance of the EA. After matching the impedance, one only needs to reconsider the new feeding voltage [16]. As shown in Figure. 2.7, the input voltage to ESPAR is v_0. As the matching impedance is $Z_{dm} = \Re\{Z_{in}\} - \Im\{Z_{in}\}$, the new feeding voltage can be calculated as $v_s = 2v_0$ and then $\mathbf{v}$ is $[\frac{v_s}{2}, v_1, \ldots, v_{M-1}]^T$. The loads and feeding can be calculated from the current vectors based on dynamic matching [16] as

$$v_s = 2(z_0 i_0 + \sum_{j=0}^{M-1} Z_{0j} i_j), \tag{2.48a}$$

$$z_m = -\frac{\sum_{j=0}^{M-1} Z_{mj} i_j}{i_m},\ m = 1, 2, \ldots, M-1. \tag{2.48b}$$

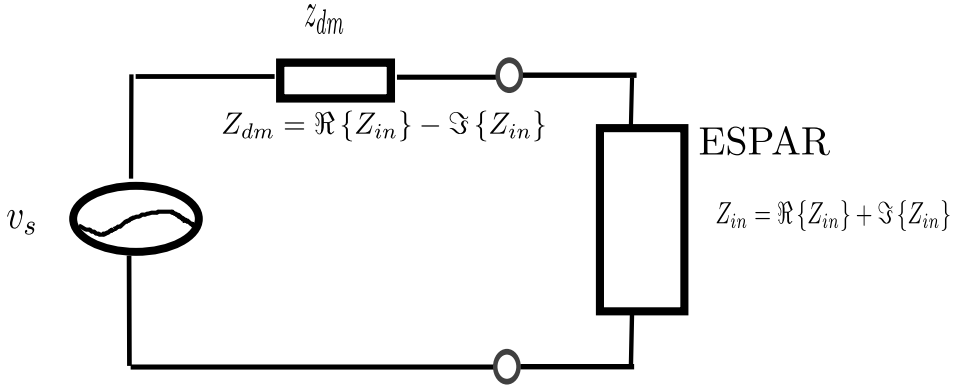

Figure 2.7: Antenna matching

2.7 Remote Radio Head with single-RF Antenna Transmitter

As part of our work focuses on RRHs with single-RF antenna transmitter, we consider downlink transmission from N RRHs with M_t-element antennas at the t-th RRH to K users with a single antenna element for each in this section. The signal received by the k-th user is given by

$$y_k = \underbrace{\sum_{t=1}^{N} \mathbf{h}_{k,t}^H \mathbf{w}_{k,t} s_k^{DL}}_{\text{desired signal}} + \underbrace{\sum_{t=1}^{N} \left(\sum_{j=1, j\neq k}^{K} \mathbf{h}_{k,t}^H \mathbf{w}_{j,t} s_j^{DL} \right)}_{\text{interference}} + \underbrace{n_k}_{\text{noise}}, \tag{2.49}$$

where n_k is the additive white Gaussian noise (AWGN), $\mathbf{h}_{k,t} = [h_{k,t_0}, h_{k,t_1}, \ldots, h_{k,t_{M_t-1}}]^H$ is channel from the t-th RRH to k-th user and $h_{k,t_m} = l_{k,t_m} g_{k.t_m}, m \in \{0, 1, \ldots, (M_t - 1)\}$, where l_{k,t_m} and g_{k,t_m} denote the large scale fading and the small scale fading from the $(m+1)$-th antenna element at the t-th RRH to the k-th user's antenna, respectively. $\mathbf{w}_{k,t} \in \mathbb{C}^{M_t \times 1}$ is a precoder from the t-th RRH to the k-th user. s_k^{DL} denotes the transmitted signal to k-th user. Each user is assumed to have only one data stream and $\mathbf{s}^{DL} = \left[s_1^{DL}, s_2^{DL}, \ldots, s_K^{DL}\right]^T$ is the transmit data vector from the BBU to all users through RRHs, and are assumed to be independent and identically distributed (i.i.d.) with unit power.

Let $\mathbf{h}_k$ and $\mathbf{w}_k$ denote the global channel and precoder for the k-th user, respectively. Then, we have $\mathbf{h}_k = \left[\mathbf{h}_{k,1}^H, \mathbf{h}_{k,2}^H, \ldots, \mathbf{h}_{k,N}^H\right]^H \in \mathbb{C}^{M_{tot} \times 1}$ and $\mathbf{w}_k = \left[\mathbf{w}_{k,1}^H, \mathbf{w}_{k,2}^H, \ldots, \mathbf{w}_{k,N}^H\right]^H \in \mathbb{C}^{M_{tot} \times 1}$, where $M_{tot} = \sum_{t=1}^{N} M_t$. Similarly, the global precoder for the t-th RRH is denoted

as $\mathbf{W}_t^{RRH}$, and it can be expressed as $\mathbf{W}_t^{RRH} = [\mathbf{w}_{1,t}, \mathbf{w}_{2,t}, \ldots, \mathbf{w}_{K,t}] \in \mathbb{C}^{M_t \times K}$. Then, (2.49) can be rewritten as

$$y_k = \mathbf{h}_k^H \mathbf{w}_k s_k^{DL} + \sum_{j=1, j\neq k}^{K} \mathbf{h}_k^H \mathbf{w}_j s_j^{DL} + n_k. \tag{2.50}$$

It is assumed that the RRHs power allocation is directly controlled by BBU. The total number of users is assumed to be less than the total number of transmit antenna elements at all RRHs. Let $P_{k,t}$ denotes the power from t-th RRH to the k-th user and $\mathbf{p}^U = [P_1^U, P_2^U, \ldots, P_K^U]^T$ denotes the allocated power vector to users, whose elements P_k^U denote the transmitted power allocated to the k-th user. Then, we have

$$\begin{aligned} P_k^U &= \mathbb{E}\left\{\text{tr}\left\{\mathbf{w}_k s_k^{DL} \left(\mathbf{w}_k s_k^{DL}\right)^H\right\}\right\} = \text{tr}\left\{\mathbf{w}_k \mathbf{w}_k^H\right\} \\ &= \text{tr}\left\{\mathbf{w}_k^H \mathbf{w}_k\right\} = \sum_{t=1}^{N} \mathbf{w}_{k,t}^H \mathbf{w}_{k,t} = \sum_{t=1}^{N} P_{k,t}. \end{aligned}$$

Similarly, $\mathbf{p}^{RRH} = [P_1^{RRH}, P_2^{RRH}, \ldots, P_N^{RRH}]^T$ denotes the allocated transmitted power vector to RRHs, whose element P_t^{RRH} is the total power allocated to the t-th RRH and

$$P_t^{RRH} = \mathbb{E}\left\{\text{tr}\left\{\left(\mathbf{W}_t^{RRH} \mathbf{s}^{DL}\right)\left(\mathbf{W}_t^{RRH} \mathbf{s}^{DL}\right)^H\right\}\right\} = \sum_{k=1}^{K} \mathbf{w}_{k,t}^H \mathbf{w}_{k,t} = \sum_{k=1}^{K} P_{k,t}.$$

2.7.1 Realistic Power Model for Distributed RRHs

In a realistic RRH setting, the total power consumption for the downlink transmission, P_{tot}, can be divided into four parts [10, 84] as

$$P_{tot} = P_{bbu} + P_{fibre} + P_{rrh} + K P_{user}^{DL}, \tag{2.51}$$

where P_{bbu} is the power consumption of signal-processing at BBU, which depends on baseband processing including DAC, synthesizer, filters, and mixer. $P_{fibre} = N P_{op} R$ is the traffic-dependent power consumption of fibre transmission from the BBU to all RRHs, P_{op} is the power consumption per unit-bit of optical modules connected to the fibre line, which includes possibly modulator driver, optical amplifier, laser, and electrical-to-optical and optical-to-

electrical (E/O and O/E) converters. R is the achievable rate of the system. P_{rrh} is the power consumption of all RRHs. KP_{user}^{DL} is the power consumption of all users.

The power consumption for all RRHs [11] is

$$P_{rrh} = \sum_{t=1}^{N} \left(P_t^{RRH} \frac{1}{\eta} + N_{RF}^{(t)} P_t^c \right), \tag{2.52}$$

where P_t^c is RF circuit power consumption at the t-th RRH, η is power amplifier efficiency at the RRHs, $N_{RF}^{(t)}$ is the number of RF circuits at t-th RRH. For standard multiple antenna, $N_{RF}^{(t)}$ is equal to the number of antenna elements M_t. In the case of a single-RF antenna, $N_{RF}^{(t)}$ equals to 1.

2.7.2 Energy Efficiency

It is assumed that $\mathbf{H}$ is known at both the transmitter and the receiver. Thus, all RRH ports and the users possess perfect CSI. The received SINR of the k-th user is

$$\begin{aligned} \rho_k &= \frac{\mathbb{E}\left| \left(\sum_{t=1}^{N} \mathbf{h}_{k,t}^H \mathbf{w}_{k,t} \right) s_k^{DL} \right|^2}{\sum_{j=1, j\neq k}^{K} \left(\mathbb{E}\left| \sum_{t=1}^{N} \mathbf{h}_{k,t}^H \mathbf{w}_{j,t} s_j^{DL} \right|^2 \right) + \sigma_n^2} \\ &= \frac{\left| \mathbf{h}_k^H \mathbf{w}_k \right|^2}{\sum_{j=1, j\neq k}^{K} \left| \mathbf{h}_k^H \mathbf{w}_j \right|^2 + \sigma_n^2}. \end{aligned} \tag{2.53}$$

As in [10], when the input signal is Gaussian, the achievable rate over bandwidth Ω Hz for the k-th user is

$$r_k = \Omega \log_2 \left(1 + \frac{\left| \mathbf{h}_k^H \mathbf{w}_k \right|^2}{\sum_{j=1, j\neq k}^{K} \left| \mathbf{h}_k^H \mathbf{w}_j \right|^2 + \sigma_n^2} \right), \tag{2.54}$$

The system achievable downlink sum-rate is $R = \sum_{k=1}^{K} r_k$.

The EE, η_{ee}, is the ratio of data transmission rate (in bit/second) and total power consumption

(in Watt = Joule/second) [85] and it is given by

$$\eta_{ee} = \frac{R}{P_{tot}} = \frac{\Omega \sum_{k=1}^{K} \log_2 \left(1 + \frac{\left|\mathbf{h}_k^H \mathbf{w}_k\right|^2}{\sum_{j=1, j\neq k}^{K} \left|\mathbf{h}_k^H \mathbf{w}_j\right|^2 + \sigma_n^2}\right)}{P_{bbu} + P_{fibre} + P_{rrh} + K P_{user}^{DL}}. \tag{2.55}$$

2.8 Summary

This chapter has reviewed the characteristics and classification of wireless propagation channels. MIMO systems are introduced with various channel modelling and radio access networks are discussed. After that, basic antenna theory including antenna parameters, the background to mutual coupling and its impact on MIMO antennas have been discussed. The fundamental systems of front-end feeding architectures for antenna arrays and CRANs with single RF antennas at RRHs systems are briefly presented in the end. This chapter has covered all the background and will provide a good understanding of the remainder of this thesis.

Chapter 3
Achieving Arbitrary Signals Transmission Using an ESPAR antenna

3.1 Introduction

The spatial multiplexing and diversity benefits from MIMO communication systems increase as the number of antennas increases. However, each additional antenna element requires an additional radio frequency (RF) chain resulting in increased cost and complexity. In addition, in order to maximize the benefits offered by multiple antennas, the antennas need to be placed sufficiently apart to minimize the coupling. Electronically steerable parasitic array radiator (ESPAR) has been proposed to reduce the cost of multiple antenna devices. For ESPAR antenna (EA), the antenna elements in EA are placed close together, resulting in strong coupling among antenna elements. This coupling is exploited to control the currents at the antenna elements and the overall radiation pattern is shaped by varying the feeding voltage at the active element and adjusting the impedance of the parasitic elements. Therefore, ESPAR gives multi-antenna functionality utilizing a single RF chain and alleviates the complexity and implementation issues associated with standard multiple antenna systems.

As described in Chapter 2, a system model based on the currents at the ports of the transmit antenna was introduced in [8, 55]. The authors in [16] provided the design conditions that an EA has to satisfy in order to support an arbitrary precoding scheme. The main design condition considered in [16] is that input resistance should be positive. Satisfying this condition is essential because a negative input resistance results in a positive reflection coefficient (dB), which implies that the EA is reflecting power back and exhibiting oscillatory/unstable behaviour [18].

The approach in [16] was to design a new EA by increasing its self-resistance. However, in the case of the EA system, the value of the input resistance depends on the currents at the

antenna elements which depend on the signal to be transmitted, and on the mutual coupling matrix (MCM) which depends on different parameters, including inter-element spacing, antenna element pattern, array geometry, relative positioning of the antenna elements in the array, operational frequency and near field scatterers [40, 41]. If the MCM is fixed, which is typically the case for an EA, a change in the antenna signal/current vectors can result in a negative input resistance. This implies that for such signals/current vectors, the EA will reflect back power and exhibit unstable behaviour. In order to transmit such signals, a new MCM, implying a new EA, needs to be designed. Therefore, one issue with the approach in [16] is that, once an EA is designed, there are still some signals for which the EA will be unstable, as such signals result in a negative input resistance. In order to transmit such signals, a new EA needs to be designed.

In this chapter, a new approach is adopted, i.e. instead of trying to transmit the actual/ideal signals, which give a negative input resistance at the EA; we transmit signals closely approximating the actual/ideal signals which do not lead to a negative input resistance. In this way, the EA does not need to be redesigned. To the authors best knowledge, this approach is new and has not been proposed in literature previously. In order to obtain the approximate signal, an optimisation problem is proposed to minimise the mean square error (MSE) between the ideal and approximate signals considering the implementation constraint of the EA. The underlying problem is originally not convex. We recast it to convex form via equivalent reformulation and Lagrange duality. Finally, as practical transmitters require real-time operation, the optimisation problem is solved analytically and novel closed-form expressions are derived to easily calculate the approximate current signals for the EA system.

Moreover, we denote the EA utilising the proposed algorithm in this chapter as EA with preprocessing (EA-P). For the EA without any preprocessing, no signal is stably transmitted when the input resistance is negative, we denote this case as the standard EA (EA-S). The performance of a standard transmitter system with one RF chain per antenna element is also provided as a benchmark and we denote this case as SMA. The performances of EA-P are compared with the performances of the EA-S and the standard multiple antenna transmitter in various communication scenarios. Specifically, when the transmitter does not possess the channel state information (CSI), the spatial multiplexing scenario and space-time block

precoding are considered. Whereas, when the transmitter possesses the CSI, the performances of EA-P, EA-S and standard multiple antenna with maximum ratio transmission (MRT) are compared. The performance metric compared is the system error rate (SER). Our results show that the EA-P performs significantly better compared with the EA-S and gives almost the same performance as the standard multiple antenna transmitter. However, replacing the ideal signal with approximate signal leads to some performance loss. If in addition, when one takes into account the cost and complexity of the EA, the EA-P scheme is well performing and practical.

The rest of the chapter is organised as follows. The system model along with the working of an EA is explained in Section 3.2. The processing required for the EA-P is derived by solving an optimisation problem in Section 3.3. The performance of the EA-P is compared with the performance of the EA-S and standard multiple antenna transmitters, in different communication scenarios, in Section 3.4. Finally, the main results are summarized in the concluding Section 3.5.

3.2 System Model for ESPAR MIMO

3.2.1 ESPAR Transmitter

As described in Chapter 2, after transmission from an EA, the signal at the receiver, with N_r antennas, is given in current form as [55, 64, 65]

$$\mathbf{y} = \mathbf{H}\mathbf{i} + \mathbf{n}, \tag{3.1}$$

where $\mathbf{H} \in \mathbb{C}^{N_r \times N_t}$ is channel matrix and $\mathbf{n} \in C^{N_r \times 1}$ denotes the noise vector at the receiver. The receiver is assumed to be a standard multiple antenna receiver. It is noted that $N_t = M$ when using a M-element EA at the transmitter.

3.2.2 Signal Transmission Using an EA Transmitter

In order to radiate the signal, the currents at the antenna element need to be varied based on the transmission signals. In the case of the standard multiple antenna systems, the currents are varied by varying the input voltage at each antenna element. However, in the case of an EA, the loads at the parasitic elements and the voltage feeding at the active element needs to be varied. As discussed previously, for a certain transmission signal, it is possible that the voltage and loadings are such that they lead to a negative input resistance and result in an unstable EA. Let $\hat{\mathbf{i}} = [\hat{i}_0, \hat{i}_1, \ldots, \hat{i}_{M-1}]^T$ denotes desired current vector corresponding to ideal signals, which can be transmitted by a multiple RF chain antenna array and are required to be transmitted by EAs. Utilising (2.46), the input impedance, Z_{in}, can be calculated for $\hat{\mathbf{i}}$ as

$$Z_{in} = Z_{00} + \frac{\sum_{m=1}^{M-1} Z_{0m}\hat{i}_m}{\hat{i}_0}. \tag{3.2}$$

If for some signals, $\hat{\mathbf{i}}$, the input resistance becomes negative, we propose that instead of transmitting the ideal signal, a signal closely approximating the ideal signal, which does not lead to a negative input resistance, is transmitted. In this way, the EA system does not need to be redesigned based on the transmission signal. As mentioned previously, we denote this EA with pre-processing as EA-P.

3.3 Signal Processing for an ESPAR Antenna with Preprocessing

In this section, we obtain the current vector approximating the ideal current vector that lead to a positive input resistance. One can easily obtain the corresponding values of the voltage and the loads for an EA-P by using the approximate currents.

3.3.1 Problem Formulation

As discussed in Chapter 2, the voltage feeding at the active element v_s is $2v_0$ with dynamic matching. The problem to obtain the configuration for the EA-P, i.e. obtaining the values of the voltage and the loads, for each transmission signal can be formulated as an optimisation problem to minimise the MSE between the currents corresponding to the ideal and approximate transmission signals, under the practical consideration of positive input resistance, and is given as

$$\min_{v_s, z_1, z_2, \ldots, z_{M-1}} \quad \left\| \hat{\mathbf{i}} - \mathbf{i} \right\|_2^2, \tag{3.3a}$$

$$\text{st.} \quad \Re \left\{ Z_{00} + \frac{\sum_{m=1}^{M-1} Z_{0m} i_m}{i_0} \right\} \geq \xi, \tag{3.3b}$$

$$\mathbf{i} = \left(\mathbf{Z} + \mathbf{Z}_L \right)^{-1} \mathbf{v}, \tag{3.3c}$$

where $\mathbf{i}$ denotes the approximate current vectors. The objective of this optimisation problem is to find the voltage v_s and the loads $z_1, z_2, \ldots, z_{M-1}$ to minimise MSE between the ideal and approximate current vectors. As input resistance is required to be positive, a positive variable, ξ, is introduced in constraint (3.3b) to make sure that the input resistance is positive. The work in this chapter focuses on the stable operation of an EA transmitter and no limit on the power of an EA is assumed. Thus, choosing $\xi > 0$ ensures the stability of the EA. The impact of the value of ξ on SER performances will be discussed in Subsection 3.4.3. In addition, the positivity constraint on ξ would affect the instantaneous input power requirement. A detailed discussion of this important issue is provided in Chapter 4. In Chapter 4, a new transmission scheme has been designed to enable an EA to provide stable multiple antenna functionality taking into account the instantaneous total power requirement. As the configuration variables $\mathbf{Z}_L$ and $\mathbf{v}$ only appear in the (3.3c), the optimisation problem in (3.3) can be solved in two steps. The first step is to obtain the approximate currents, $\mathbf{i}$, which can be obtained by solving the optimisation problem with only constraint (3.3b). Once $\mathbf{i}$ is obtained, the loads and the voltage feeding can be calculated using (3.3c).

If for a certain ideal current vector $\hat{\mathbf{i}}$, the corresponding input resistance is greater than ξ,

$\mathbf{i} = \hat{\mathbf{i}}$ and no optimisation is required. The set for current vectors which yield input resistance greater than ξ can be represented as

$$\mathbb{I}_{P\xi} = \left\{ \hat{\mathbf{i}} \middle| \Re \left(Z_{00} + \frac{\sum_{m=1}^{M-1} Z_{0m} \hat{i}_m}{\hat{i}_0} \right) \geq \xi \right\}. \tag{3.4}$$

Similarly, the unsupported set $\mathbb{I}_{N\xi}$ is the complement of $\mathbb{I}_{P\xi}$.

3.3.2 Alternate Representation for the Input Resistance Constraint

In order to simplify the constraint (3.3b), we reformulate variables from the complex domain into the real domain by separating their real and imaginary parts. let R_m and X_m denote the real part and the imaginary part of Z_{0m}, respectively. $\hat{w}_{2m+1}$ and $\hat{w}_{2m+2}$ denote the real part and the imaginary part of $\hat{i}_m$, respectively. Similarly, w_{2m+1} and w_{2m+2} are the real part and the imaginary part of i_m, respectively. Then the ideal current vectors can be written as new vectors

$$\hat{\mathbf{w}} = [\hat{w}_1, \hat{w}_2, \hat{w}_3, \hat{w}_4, \ldots, \hat{w}_{2M-1}, \hat{w}_{2M}]^T$$

and the approximate current vectors is

$$\mathbf{w} = [w_1, w_2, w_3, w_4, \ldots, w_{2M-1}, w_{2M}]^T.$$

Proposition 1 *The input resistance at the active element of an EA can be expressed as*

$$\Re \left\{ Z_{00} + \frac{\sum_{m=1}^{M-1} Z_{0m} i_m}{i_0} \right\} = \frac{\mathbf{w}^T \mathbf{A} \mathbf{w}}{w_1^2 + w_2^2}, \tag{3.5}$$

where Z_{0m}, for $m = 1, 2, \ldots, m-1$ *is the mutual coupling impedance between the active*

and the m-th parasitic element of the EA, the matrix $\mathbf{A}$ is

$$\mathbf{A} = \begin{bmatrix} R_0 & 0 & \frac{R_1}{2} & -\frac{X_1}{2} & \dots & \frac{R_{M-1}}{2} & -\frac{X_{M-1}}{2} \\ 0 & R_0 & \frac{X_1}{2} & \frac{R_1}{2} & \dots & \frac{X_{M-1}}{2} & \frac{R_{M-1}}{2} \\ \frac{R_1}{2} & \frac{X_1}{2} & 0 & 0 & \dots & 0 & 0 \\ -\frac{X_1}{2} & \frac{R_1}{2} & 0 & 0 & \dots & 0 & 0 \\ \vdots & \vdots & \vdots & \vdots & \ddots & \vdots & \vdots \\ \frac{R_{M-1}}{2} & \frac{X_{M-1}}{2} & 0 & 0 & \dots & 0 & 0 \\ -\frac{X_{M-1}}{2} & \frac{R_{M-1}}{2} & 0 & 0 & \dots & 0 & 0 \end{bmatrix}. \tag{3.6}$$

and

$$\mathbf{w} = \left[w_1, w_2, w_3, w_4, \dots, w_{2M-1}, w_{2M}\right]^T,$$

in which, w_{2m+1} and w_{2m+2} denote the real part and the imaginary part of i_m,respectively.

Proof: See Appendix A.

As ξ is positive, by substituting (3.5) into (3.3b), we get

$$\mathbf{w}^T\mathbf{A}\mathbf{w} \geq \xi\left(w_1^2 + w_2^2\right) = \xi\left(\mathbf{w}^T\mathbf{G}\mathbf{w}\right), \tag{3.7}$$

where $\mathbf{G} = \mathrm{diag}(1, 1, 0, \dots, 0)$. The constraint (3.3b) can be expressed as

$$\mathbf{w}^T\mathbf{B}\mathbf{w} \geq 0, \tag{3.8}$$

where $\mathbf{B}$ is

$$\mathbf{B} = \mathbf{A} - \xi\mathbf{G}. \tag{3.9}$$

The optimisation problem to obtain the approximate current vectors can be then reformulated as

$$\min_{\mathbf{w}} \quad \|\hat{\mathbf{w}} - \mathbf{w}\|_2^2, \tag{3.10a}$$

$$\text{st.} \quad \mathbf{w}^T\mathbf{B}\mathbf{w} \geq 0. \tag{3.10b}$$

The convexity of (3.10) depends on the matrix $\mathbf{B}$ as the objective function (3.10a) is convex.

Proposition 2 *The optimisation problem in* (3.10) *is nonconvex as* $\mathbf{B}$ *is an indefinite matrix. The eigenvalues of* $\mathbf{B}$ *are given by*

$$\begin{cases} \zeta_1 = \zeta_2 = (R_0 - \xi) - \sqrt{(R_0 - \xi)^2 + \sum_{m=1}^{M-1} (R_m^2 + X_m^2)} < 0 \\ \zeta_3 = \zeta_4 = (R_0 - \xi) + \sqrt{(R_0 - \xi)^2 + \sum_{m=1}^{M-1} (R_m^2 + X_m^2)} > 0 \\ \zeta_n = 0 \quad \textit{for } n = 5, 6, \ldots, 2M \end{cases} . \tag{3.11}$$

where $\zeta_n, \quad$ *for* $n = 1, 2, \ldots, 2M$ *are the eigenvalues of the* $2M \times 2M$ *matrix* $\mathbf{B}$.

Proof: See Appendix B.

3.3.3 Reformulation of the Nonconvex-Constrained Optimisation Problem

For the problem in (3.10), the objective function is quadratic convex and the constraint is a quadratic nonconvex inequality. As strong duality holds for (3.10) [66], its solution can be obtained by solving its dual problem. The Lagrangian of this optimisation problem is

$$\begin{aligned} L(\mathbf{w}, \delta_B) &= \|\hat{\mathbf{w}} - \mathbf{w}\|_2^2 + \delta_B \left(-\mathbf{w}^T \mathbf{B} \mathbf{w}\right) \\ &= \mathbf{w}^T (\mathbf{I} - \delta_B \mathbf{B}) \mathbf{w} - 2\mathbf{w}^T \hat{\mathbf{w}} + \hat{\mathbf{w}}^T \hat{\mathbf{w}}, \end{aligned} \tag{3.12}$$

where δ_B is Lagrange multiplier, and $\mathbf{I}$ is an identity matrix of size $2M$. The stationarity condition is

$$\nabla_{\mathbf{w}} L(\mathbf{w}, \delta_B) = 2(\mathbf{I} - \delta_B \mathbf{B}) \mathbf{w} - 2\hat{\mathbf{w}} = 0. \tag{3.13}$$

As $\mathbf{B}$ is a square matix, the optimal value, $\mathbf{w}(\delta_B)$, which satisfies (3.13) is

$$\mathbf{w}^*(\delta_B) = (\mathbf{I} - \delta_B \mathbf{B})^{-1} \hat{\mathbf{w}}. \tag{3.14}$$

The dual function of (3.10) can be expressed using the Lagrangian as

$$g\left(\delta_B\right) = \inf_{\mathbf{w}} \left(\mathbf{w}^T \left(\mathbf{I} - \delta_B \mathbf{B}\right) \mathbf{w} - 2\hat{\mathbf{w}}^T \mathbf{w}\right) + \hat{\mathbf{w}}^T \hat{\mathbf{w}}. \tag{3.15}$$

After substituting (3.14) into (3.15), it can be noticed that $g\left(\delta_B\right) = -\infty$ if matrix $\left(\mathbf{I} - \delta_B \mathbf{B}\right)$ is not a positive semidefinite matrix or $\hat{\mathbf{w}}^T$ is not in the range of $\mathbf{I} - \delta_B \mathbf{B}$. Therefore, the dual problem can be expressed as

$$\max_{\delta_B} \quad -\hat{\mathbf{w}}^T \left(\mathbf{I} - \delta_B \mathbf{B}\right)^{-1} \hat{\mathbf{w}} + \hat{\mathbf{w}}^T \hat{\mathbf{w}}, \tag{3.16a}$$

$$\text{st.} \quad \mathbf{I} - \delta_B \mathbf{B} \in \mathbf{S}_+^{2M}, \tag{3.16b}$$

$$\hat{\mathbf{w}} \in \mathbb{R}\left(\mathbf{I} - \delta_B \mathbf{B}\right), \tag{3.16c}$$

$$\delta_B \geq 0, \tag{3.16d}$$

where $\mathbf{S}_+^n$ denotes the set of symmetric positive semidefinite $n \times n$ matrices, and $\mathbb{R}\left(\mathbf{I} - \delta_B \mathbf{B}\right)$ denotes the range of $\mathbf{I} - \delta_B \mathbf{B}$. This can be further reformulated to obtain the closed-form expression of the optimal value of δ_B.

Proposition 3 *The dual problem in* (3.16) *can be reformulated as*

$$\min_{\delta_B} \quad \frac{r_1}{1 - \delta_B \zeta_1} + \frac{r_2}{1 - \delta_B \zeta_3}, \tag{3.17a}$$

$$\textit{st.} \quad -\delta_B \leq 0, \tag{3.17b}$$

$$\delta_B \leq 1/\zeta_3, , \tag{3.17c}$$

where $r_1 = g_1^2 + g_2^2$ *and* $r_2 = g_{2M+1}^2 + g_{2M+2}^2$*, here* $\mathbf{g} = [g_1, g_2, \ldots, g_{2M+1}, g_{2M+2}]^T = \mathbf{Q}_B^T \hat{\mathbf{w}}$*,* ζ_1 *and* ζ_3 *are the eigenvalues of* $\mathbf{B}$*, and the columns of* $\mathbf{Q}_B$ *are eigenvectors of matrix* $\mathbf{B}$ *when the corresponding eigenvalues are in ascending order.*

Proof: See Appendix C

3.3.4 Solution of the Optimisation Problem

As the dual optimisation problem is convex, the Lagrangian of (3.17) is expressed as

$$L_{\delta_B}\left(\delta_B, \sigma_1, \sigma_2\right) = \frac{r_1}{1-\delta_B\zeta_1} + \frac{r_2}{1-\delta_B\zeta_3} - \sigma_1\delta_B + \sigma_2\left(\delta_B - \frac{1}{\zeta_3}\right), \tag{3.18}$$

where σ_1 and σ_2 are Lagrange multipliers associated with the two inequality constraints. The stationarity condition of the KKT conditions is given by

$$\nabla_{\delta_B} L_{\delta_B}\left(\delta_B, \sigma_1, \sigma_2\right) = \frac{\zeta_1 r_1}{\left(1-\delta_B\zeta_1\right)^2} + \frac{\zeta_3 r_2}{\left(1-\delta_B\zeta_3\right)^2} - \sigma_1 + \sigma_2 = 0. \tag{3.19}$$

The remaining Karush-Kuhn-Tucker (KKT) conditions with respect to the complementary slackness conditions are

$$\sigma_1 \geq 0, \sigma_2 \geq 0 \tag{3.20a}$$

$$\delta_B \geq 0, \tag{3.20b}$$

$$\delta_B - \frac{1}{\zeta_3} \leq 0, \tag{3.20c}$$

$$\sigma_1\delta_B = 0, \tag{3.20d}$$

$$\sigma_2\left(\delta_B - \frac{1}{\zeta_3}\right) = 0. \tag{3.20e}$$

Proposition 4 *After solving the optimisation problem in* (3.17) *based on* (3.19) *and* (3.20)*, the result of optimal value of* δ_B *is given as*

$$\delta_B^* = \begin{cases} 0 & \text{for } \hat{\mathbf{i}} \in \mathbb{I}_{P\xi} \\ \frac{\sqrt{-\zeta_1 r_1} - \sqrt{\zeta_3 r_2}}{\zeta_3\sqrt{-\zeta_1 r_1} - \zeta_1\sqrt{\zeta_3 r_2}} & \text{for } \hat{\mathbf{i}} \in \mathbb{I}_{N\xi} \end{cases}. \tag{3.21}$$

Proof: See Appendix D

Substituting (3.21) into (3.14), the value of approximate transmit current vectors is given in the following theorem.

Theorem 1 *The entry* $i_m,\ m = 0, 1, \ldots, M$ *of the approximate current vectors* $\mathbf{i} = (i_0, i_1, \ldots, i_M)$*, for an EA-P, can be obtained as* $i_m = w_{2m+1} + jw_{2m+2}$*, where* w_k *is the* k*-th entry of vector* $\mathbf{w}$*. The value of* $\mathbf{w}$ *is*

$$\begin{cases} \mathbf{w}^* = \hat{\mathbf{w}} & \text{for } \hat{\mathbf{i}} \in \mathbb{I}_{P\xi} \\ \mathbf{w}^* = \left(\mathbf{I} - \frac{\sqrt{-\zeta_1 r_1} - \sqrt{\zeta_3 r_2}}{\zeta_3\sqrt{-\zeta_1 r_1} - \zeta_1\sqrt{\zeta_3 r_2}}\mathbf{B}\right)^{-1} \hat{\mathbf{w}} & \text{for } \hat{\mathbf{i}} \in \mathbb{I}_{N\xi} \end{cases}, \tag{3.22}$$

where $\hat{\mathbf{w}}$ *is obtained by separating the real and imaginary parts of ideal current vectors* $\hat{\mathbf{i}} = \left(\hat{i}_0, \hat{i}_1, \ldots, \hat{i}_{M-1}\right)$*, and its* k*-th entry is*

$$\hat{w}_k^* = \begin{cases} \Re\left(\hat{i}_{\frac{k-1}{2}}\right) & k = 1, 3, ..., 2M+1 \\ \Im\left(\hat{i}_{\frac{k-2}{2}}\right) & k = 2, 4, ..., 2M+2 \end{cases}. \tag{3.23}$$

where $\Im\left(\hat{i}_{\frac{k-2}{2}}\right)$ *denotes the imaginary part of* $\hat{i}_{\frac{k-2}{2}}$*.*

Theorem 1 gives the expression to calculate the approximate current vectors. When the input resistance from the ideal current vectors is no less than ξ, the ideal current vectors can be realised by the EA-P without any optimisation operation. Otherwise, the EA-P transmits the approximate current vectors which are obtained from Theorem 1. The loads and feeding, for the EA-P, can be calculated from the approximate current vectors based on dynamic matching as discussed in Section 2.6.4,

$$v_s = 2v_0 = 2(z_0 i_0 + \sum_{j=0}^{M-1} Z_{0j} i_j), \tag{3.24a}$$

$$z_m = -\frac{\sum_{j=0}^{M-1} Z_{mj} i_j}{i_m},\ m = 1, 2, \ldots, M-1. \tag{3.24b}$$

From these expressions, it can be noted that the load values depends on the normalised current vectors and MCM, and the input power to the active element is controlled by the feeding. When the normalised current vectors are fixed, the load values are independent of the feeding circuit.

The steps to obtain the configuration for the EA-P for every transmitted signal are summarised in Algorithm 1.

Algorithm 1 The EA configuration for $\hat{\mathbf{i}}$

Input:

Required ideal current vectors $\hat{\mathbf{i}}$

Output:

EA-P loads and voltage feeding for $\hat{\mathbf{i}}$,

Step 1: if $\hat{\mathbf{i}} \in \mathbb{I}_{P\xi}$ {Goto Step 6. } else {Goto Step 2.}

Step 2: Obtain $\hat{\mathbf{w}}$ by separating real and imaginary parts of $\hat{\mathbf{i}}$. Calculate $\mathbf{B}$ from $\mathbf{B} = \mathbf{A} - \xi\mathbf{G}$ and (3.6).

Step 3: Calculate ζ_1, ζ_3, and $\mathbf{Q}$ from (3.11) and eigenvalue decomposition of $\mathbf{B}$.

Step 4: Calculate $\mathbf{g}$ by $\mathbf{g} = \mathbf{Q}^T\hat{\mathbf{w}}$.

Step 5: Calculate r_1 and r_2 by $r_1 = g_1^2 + g_2^2$ and $r_2 = g_{2M_{t-1}}^2 + g_{2M_t}^2$.

Step 6: Calculate $\mathbf{i}$ from (3.22).

Step 7: Calculate the corresponding loads $z_1, z_2, \ldots, z_{M-1}$ and feeding v_0 as (3.24).

3.3.5 Discussion

3.3.5.1 Complexity

For the computation of the approximate currents, the EA-P algorithm involves only matrix operations and no iteration is required. The eigenvalues and corresponding eigenvectors of the MCM need to be computed only once. In other words, steps 1 to 3 in Algorithm 1 need to be calculated only once and can be used for the subsequent signal transmissions. Thus, the complexity from step 1 to 3 is negligible. Steps 4 to 7 of Algorithm 1 are required to be performed for each signal transmission. Therefore, from the complexity perspective, step 4 involves a matrix multiplication, step 6 has a matrix multiplication and an inversion operation, and step 7 involves two inner products. The floating point (flop) operations required for these operations are [67] [69]

- Multiplication of a $n \times n$ matrix and a $n \times 1$ vector: $2n^2 - n$.

- Inversion of a $n \times n$ positive definite matrix: $n^3 + n^2 + n$.
- Inner products of two $n \times 1$ vector: $2n - 1$.

When the ideal signal cannot be supported by EA, it requires the total of $n^3 + 5n^2 + 3n - 2$ floating point (flop) operations. For example, when the ideal signal cannot be supported by EA, the required flops for 2, 3 and 5 element ESPAR are 154, 412, 1528, respectively.

3.3.5.2 Stability and implementation of Parasitic loads

After solving the optimisation problem, the loads z_1 to z_{M-1} might lead to a negative resistance value. A stable circuit for generating parasitic loads with a negative real part has been proposed in [70, 71]. The parasitic elements might require some gain to produce the required currents. As in [18], a system structure is unstable if the input port impedance has a negative real part. Thus, it is necessary to satisfy this condition of stability for an EA when the parasitic loads have a negative real part.From the expression (3.24), the loads z_1 to z_{M-1} might lead to a negative resistance value. If there exists a load value z_m at the m-th parasitic element, its real part is negative, $\Re(z_m) < 0$. From (3.24b), we have

$$\Re(z_m) = \Re\left(-\frac{\sum_{j=0}^{M} Z_{mj} i_j}{i_m}\right) = -\Re\left(\frac{\sum_{j=0}^{M} Z_{mj} i_j}{i_m}\right) < 0, \tag{3.25}$$

As this is an active load, the input impedance at the m-th parasitic element is

$$Z_{in}^{(m)} = \frac{V_{in}^{(m)}}{i_m} = \frac{\sum\limits_{j=0}^{M} Z_{mj} i_j}{i_m}, \tag{3.26}$$

and its real part is

$$\Re\left(Z_{in}^{(m)}\right) = \Re\left(\sum_{j=0}^{M} Z_{mj} i_j / i_m\right). \tag{3.27}$$

From (3.25), we have $\Re\left(Z_{in}^{(m)}\right) > 0$. Thus, this guarantee the stability of the system while z_1 to z_{M-1} might have negative real parts.

3.4 Application of the Algorithm in Various Communication Scenarios

As it is unfair to compare two systems if the one system (EA-S) cannot transmit all signals, we analyse and compare the performances of the EA-P, EA-S, and the standard multiple antenna transmitter (SMA) in various communication scenarios in this section.

3.4.1 Each Antenna Element Transmits the Same Signal

First, we consider the simplest scenario in which all the antenna elements transmit the same signal s, i.e. $\hat{i} = [s, s, \ldots, s]^T$. In this case, substituting $\hat{i}$ in (3.2), yields the input resistance, R_{in} as

$$R_{in} = \Re\left(Z_{00} + \frac{\sum_{m=1}^{M-1} Z_{0m}s}{s}\right) = R_0 + \sum_{m=1}^{M-1} R_m. \tag{3.28}$$

From (3.28), it can be noted that the input resistance is independent of the transmitted signal and only depends on the MCM. Therefore, any EA characterised by a MCM which satisfies the condition, $R_0 + \sum_{m=1}^{M-1} R_m > 0$, can be employed to transmit the same signal from every antenna element. If this condition is generally satisfied in a practical EA system, radiating the same signal is generally feasible. Thus, in this scenario, the EA-P gives the same performance as EA-S and the standard multiple antenna transmitter.

3.4.2 Spatial Multiplexing

Next we consider the scenario in which each antenna element, transmits a different signal. In this case, $\hat{i} = [s_0, s_1, \ldots, s_M]^T$ where s_m denotes the signal at the $(m+1)$-th antenna

element. The input resistance can be expressed as

$$R_{in} = \Re\left(Z_{00} + \frac{\sum_{m=1}^{M-1} Z_{0m} s_m}{s_0}\right). \tag{3.29}$$

From (3.29), it can be noted that unlike the previous scenario, whether a signal can be transmitted not only depends on the MCM but also on the transmission signal. The transmission signal depends on the modulation scheme employed. As an example, assume that the modulation scheme is N-PSK. The signal at the $(m+1)$-th element can be denoted as

$$s_m = \exp(j\phi_m),$$

where N is the order of the PSK signal constellation [51], and ϕ_m is the phase of the signal at the $(m+1)$-th antenna element which is given by

$$\phi_m = \frac{2\pi n_m}{N}, n_m \in \{0, 1, ..., (N-1)\}.$$

In this case, the input resistance can be expressed as

$$\begin{aligned} R_{in} &= \Re\left(Z_{00} + \sum_{m=1}^{M-1} Z_{0m} \exp\left(j\left(\phi_m - \phi_0\right)\right)\right) \\ &= R_0 + \sum_{m=1}^{M-1}\left(R_m \cos\frac{2\pi\left(n_m - n_0\right)}{N} - X_m \sin\frac{2\pi\left(n_m - n_0\right)}{N}\right). \end{aligned} \tag{3.30}$$

Therefore, in order to transmit different N-PSK signals for each antenna element, the MCM of the EA is required to satisfy

$$R_{in} > 0, \quad \text{for} \quad n_m, n_0 \in \{0, 1, \ldots, N-1\}. \tag{3.31}$$

In the special case of BPSK modulation, when the transmit signal set is $\{\exp(j0), \exp(j\pi)\}$,

the input resistance can be simply expressed as

$$R_{in} = R_0 + \sum_{m=1}^{M-1} a_m R_m, \tag{3.32}$$

where

$$a_m = \begin{cases} 1 & \text{for } \phi_m = \phi_0 \\ -1 & \text{for } \phi_m \neq \phi_0 \end{cases}. \tag{3.33}$$

Thus, the BPSK signal can be transmitted by the EA when it satisfies the condition

$$\begin{aligned} R_{in} = R_0 + \sum_{m=1}^{M-1} a_m R_m > 0, \\ \text{for} \quad a_m \in \{1, -1\}. \end{aligned} \tag{3.34}$$

These conditions, for BPSK and N-PSK modulation, might not be satisfied for some EAs, and therefore in such cases, EA-P can be employed to achieve transmission of those signals.

Simulation Results

As an example, in Figure. 3.1, we plot the input resistance against the phase of the transmission signal for an EA with two antenna elements. In the simulations, only the transmitter is assumed to be equipped with an EA and a standard multiple antenna receiver is considered. Without loss of generality, the number of antennas at the receiver, N_r, is assumed to be one and the channel is Rayleigh faded. The modulation scheme is 16-PSK. In Figure. 3.1, the green colored region denotes $R_{in} > 0$ and the red region denotes $R_{in} \leq 0$. The black points are all possible phase combinations of the two 16-PSK signals. Figure. 3.1(a) is for the EA with MCM given by $Z^{(1)}$, and Figure. 3.1(b) is for the EA with MCM given by $Z^{(2)}$ and $Z^{(3)}$. These three MCMs for 2-element ESPAR in the IE3D antenna software have been designed in [16, 72] and are given in Section 2.6.1.

It can be observed from the figure that some combinations of the 16-PSK signals cannot be supported using $\mathbf{Z}^{(1)}$. For this EA, by employing EA-P, the transmission of these signal

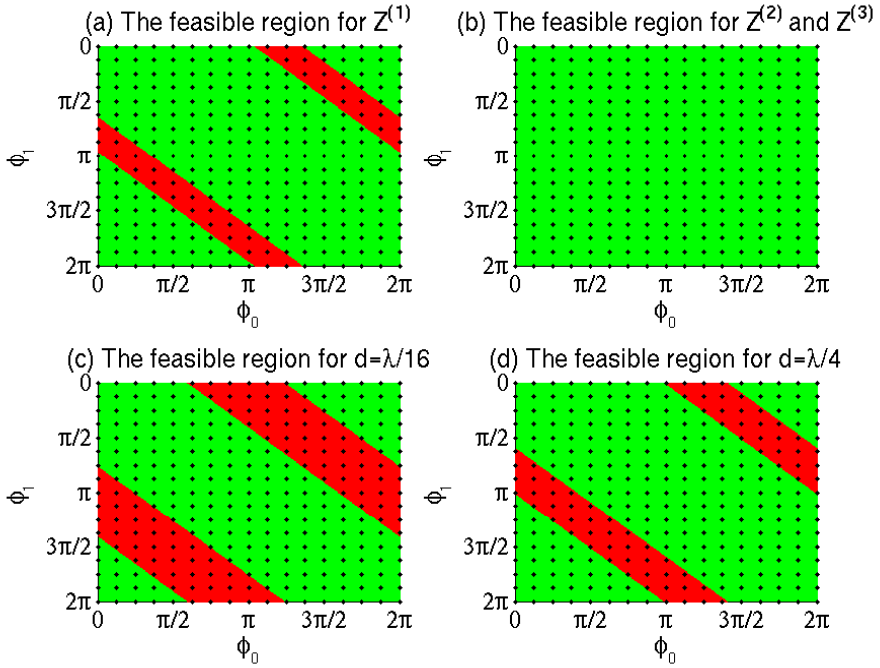

Figure 3.1: The feasible region for different EAs when 16-PSK is transmitted.

combinations is possible. Whereas, for the EA with $\mathbf{Z}^{(2)}$ and $\mathbf{Z}^{(3)}$, all possible signal combinations can be supported. Comparing $\mathbf{Z}^{(1)}$, $\mathbf{Z}^{(2)}$, and $\mathbf{Z}^{(3)}$, it can be noted that the EA, whose MCM has higher self impedance at the feeding element can support more signal combinations. In the Figure. 3.1(a) and Figure. 3.1(b), the MCM $Z^{(1)}$, $Z^{(2)}$, and $Z^{(3)}$ is obtained using the IE3D antenna design software. Furthermore, the feasible regions for linear EAs with different antenna spacing are shown the Figure. 3.1(c) and 3.1(d), respectively. The MCMs, in this case, are obtained using the IEFM for different antenna spacing [73]. The feasible region for two different antenna spacing $d = \frac{\lambda}{16}$ and $d = \frac{\lambda}{4}$ for linear EAs are shown in the Figure. 3.1(c) and Figure. 3.1(d), respectively. It can observed from Figure. 3.1(c) and Figure. 3.1(d), the proportion of supported signal combinations decreases as the antenna spacing is reduced. Therefore, in this scenario, for signal transmission, the EA-P algorithm becomes indispensable.

The SER performance of the system where the transmitter transmits different data streams from each antenna is shown in Figure. 3.2 and Figure. 3.3. For simplicity, we denote the results from standard multiple antenna as SMA in the simulation figures. The SER is plotted

against SNR. The modulation scheme considered in these figures is 16-PSK and 16-QAM, respectively. As any positive ξ can guarantee signal transmission using an EA, without loss of generality, ξ is set equal to one. Three EAs with MCMs, $\mathbf{Z}^{(1)}$, $\mathbf{Z}^{(2)}$, and $\mathbf{Z}^{(3)}$ respectively, are considered and the SER performances of EA-P, EA-S, and the standard multiple antenna transmitters are compared. In the case of the standard multiple antenna transmitter, $\hat{\mathbf{i}}$ is transmitted exactly. For the EA-P transmitter, the transmission policy is given in Theorem 1. For a fair comparison of SER with respect to transmit SNR, the transmitted signal $\mathbf{i}$ is normalised by $\frac{\hat{P}}{P}$, where $\hat{P}$ and P are power based on ideal signals and practical signals, respectively, and the normalisation factor is controlled by varying the voltage feeding. In the case of EA-S, no signal is stably transmitted when input resistance is negative and transmitted otherwise. It can be observed in Figure.3.2, that as the EA with MCM, $\mathbf{Z}^{(2)}$, and $\mathbf{Z}^{(3)}$, can support all signal combinations for 16-PSK modulation, and the performances of the EA-P, EA-S and standard multiple antenna transmitters are similar. However, for the EA with MCM, $\mathbf{Z}^{(1)}$, all possible signal combinations cannot be supported using the EA-S. Therefore, in this case, the SER performance of EA-S degrades significantly compared with the standard multiple antenna transmitter. However, it can be observed that by employing the proposed EA-P, performance similar to that of the standard multiple antenna transmitter can be achieved. In Figure. 3.3, the results are shown for 16-QAM modulation scheme. It can be observed that in this case, the EAs with both $\mathbf{Z}^{(1)}$ and $\mathbf{Z}^{(2)}$, do not support all possible signal combinations and the performance of EA-S transmitter is significantly degraded. However, nearly the same SER performance can be achieved as in the case of the standard multiple antenna transmitter by using the proposed EA-P.

This also highlights the usefulness of our scheme. All signal combinations could be transmitted by using the EA with MCM, $\mathbf{Z}^{(2)}$, for 16-PSK. But once the modulation scheme changed to 16-QAM, some signal combinations became infeasible. However, the same EA can be used to transmit signals with any modulation scheme by using the proposed EA-P.

3.4.3 Transmit Diversity

One of the main advantages of multiple antennas is that they provide diversity gain which results in significant performance improvement. There are different approaches to achieve

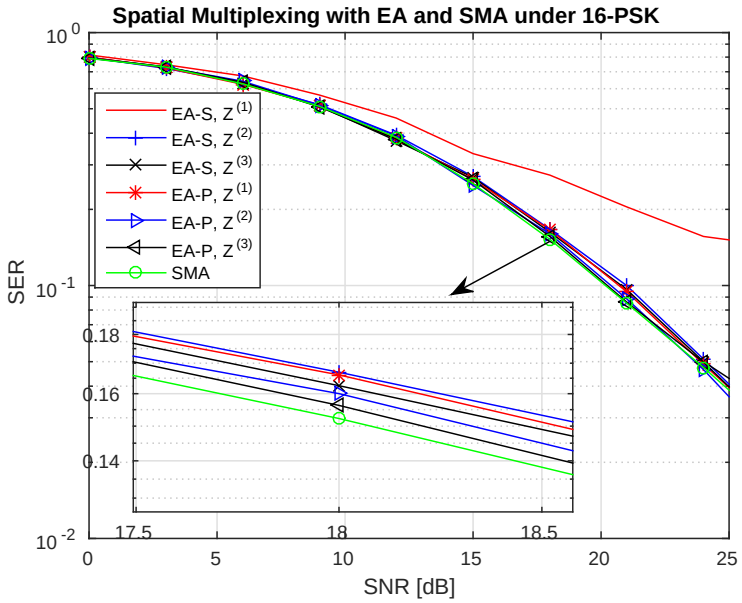

Figure 3.2: SER performance comparison of the EA transmitter and standard multiple antenna transmitter in the case of spatial multiplexing scheme under 16-PSK under the stability constraint.

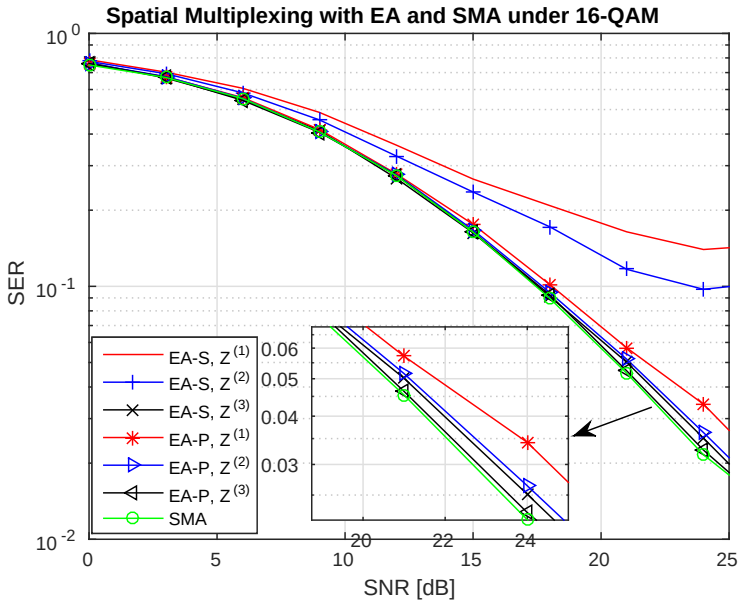

Figure 3.3: SER performance comparison of the EA transmitter and standard multiple antenna transmitter in the case of spatial multiplexing scheme under 16-QAM under the stability constraint.

transmit diversity gain depending on the CSI availability at the transmitter.

3.4.3.1 Transmitter without CSI

The proposed algorithm is a generic method and can be applied to different applications which enables the ESPRA antenna (single RF chain antenna) to provide multiple RF antenna functionality. There are different approaches to achieve transmit diversity gain depending on the CSI availability at the transmitter. When the transmitter does not possess CSI, the diversity gain can be achieved by using space-time block codes (STBC). One of the simplest STBC that gives diversity gain is the Alamouti code. In the case of a two elements EA, given a signal vector $[s_0, s_1]^T$, the ideal port current vectors is

$$\hat{\mathbf{i}} = \begin{bmatrix} s_0 & -\overline{s_1} \\ s_1 & \overline{s_0} \end{bmatrix}.$$

The corresponding input resistances for these two symbol periods are

$$\begin{aligned} R_{in}^{(1)} &= \Re\left(Z_{00} + \frac{Z_{01}s_1}{s_0}\right) = R_0 + \Re\left(\frac{Z_{01}s_1}{s_0}\right), \\ R_{in}^{(2)} &= \Re\left(Z_{00} + \frac{Z_{01}\overline{s_0}}{-\overline{s_1}}\right) = R_0 + \Re\left(\frac{Z_{01}\overline{s_0}}{-\overline{s_1}}\right). \end{aligned} \tag{3.35}$$

The supported signal vector set $[s_0, s_1]^T$, which can be exactly transmitted according to Alamouti code by an EA, is

$$\mathbb{S}_{P\xi} = \left\{ [s_0, s_1] \middle| R_{in}^{(1)} > 0, R_{in}^{(2)} > 0 \right\}. \tag{3.36}$$

Again, in this case, whether a signal can be supported depends on the MCM and also the transmission signals. In the case of N-PSK modulation, where the transmission symbols s_0 and s_1 have phases ϕ_0 and ϕ_1, respectively. The input resistances are

$$\begin{aligned} R_{in}^{(1)} &= R_0 + R_1\cos(\phi_1 - \phi_0) - X_1\sin(\phi_1 - \phi_0), \\ R_{in}^{(2)} &= R_0 - R_1\cos(\phi_1 - \phi_0) + X_1\sin(\phi_1 - \phi_0). \end{aligned} \tag{3.37}$$

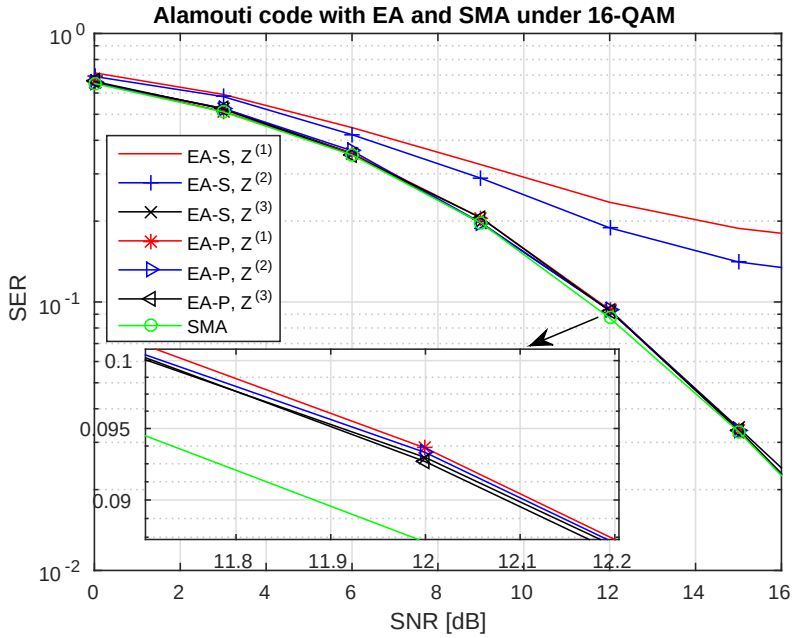

Figure 3.4: SER performance comparison of the EA transmitter and standard multiple antenna transmitter in the case of Alamouti scheme under 16-QAM under the stability constraint.

It can be noted that the input resistances vary with the MCM and the phases of transmitted signals. When the transmitter uses BPSK, then the MCM is required to satisfy that $R_{in} = R_0 \pm R_1 > 0$.

Simulation Results

The SER performance of the system where the transmitter employs Alamouti code is shown in Figure. 3.4. The modulation scheme is 16-QAM. Three EAs with MCMs, $\mathbf{Z}^{(1)}$, $\mathbf{Z}^{(2)}$, and $\mathbf{Z}^{(3)}$, respectively, are considered and the SER performances of EA-P, EA-S and the standard multiple antenna transmitters are compared. It can be observed that the performance for EA-S system with $\mathbf{Z}^{(1)}$ and $\mathbf{Z}^{(2)}$ degrades significantly as the EAs with MCMs, $\mathbf{Z}^{(1)}$ and $\mathbf{Z}^{(2)}$ do not support all possible signal combinations. However, again by using EA-P, the SER is improved and nearly the same performance as that of the standard multiple antenna transmitter can be achieved.

3.4.3.2 Transmitter with CSI

When the transmitter has CSI, transmit diversity can be achieved by precoding using the CSI. One such precoding scheme, called MRT, is considered here. Assuming that symbol s is to be transmitted, the ideal port current vectors for the transmitter is $\hat{\mathbf{i}} = \frac{\mathbf{h}}{\|\mathbf{h}\|}s$, where $\mathbf{h} = [h_0, h_1, \ldots, h_M]^H \in \mathbb{C}^{M\times 1}$ and h_m denotes the channel from the $(m+1)$-th element of EA transmitter to the signal antenna receiver [74].

The corresponding input impedance can be obtained as

$$\begin{aligned} Z_{in} &= Z_{00} + \frac{\sum_{m=1}^{M-1} Z_{0m}\hat{i}_m}{\hat{i}_0} \\ &= Z_{00} + \frac{\sum_{m=1}^{M-1} Z_{0m}h_j}{h_0}. \end{aligned} \tag{3.38}$$

From (3.38), it can be noted that the input impedance is the function of channel and the MCM only, and that it is independent of the data symbols. This implies that, for the EA-P, in the case of a block fading channel, in which the channel is constant over a block of symbols, the signal only needs to be preprocessed once in the beginning of the block. Moreover, from (3.38), it can be noted that the input resistance is random as the channel is random. Therefore, in this case, a measure of suitability of an EA can be the probability that

$$R_{in} > 0,$$

i.e.

$$\mathcal{P} = \Pr\left(R_{in} > 0\right).$$

An EA can be selected which has the highest probability $\mathcal{P}$. Note that

$$\mathcal{P} = \Pr(R_{in} > 0) = 1 - F_{R_{in}}(0), \tag{3.39}$$

where $F_{R_{in}}$ denotes the cumulative distribution function (CDF) of R_{in}.

As an example, the CDF of R_{in} is derived for a circular antenna array. As an example, a

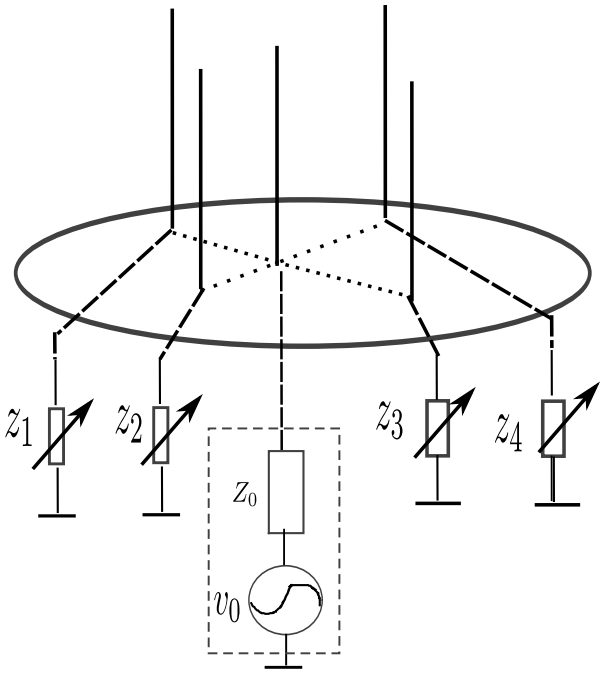

Figure 3.5: 5-element circular ESPAR antenna

5-element ESPAR is shown in Figure. 3.5. In the case of a circular antenna array [33], we have

$$Z_{0m} = Z_{01}, \text{for } m = 2, 3, \ldots, M.$$

We denote the real and imaginary part of Z_{01} by R_1 and X_1, respectively. Substituting R_1 and X_1 into (3.38), yields the input resistance as

$$\begin{aligned} R_{in} &= \Re\left(Z_{00} + Z_{01}\frac{\sum_{m=1}^{M-1} h_j}{h_0}\right) \\ &= R_0 + R_1\Re\left(\frac{\sum_{m=1}^{M-1} h_j}{h_0}\right) - X_1\Im\left(\frac{\sum_{m=1}^{M-1} h_j}{h_0}\right). \end{aligned} \tag{3.40}$$

Let

$$\kappa_t = \frac{\sum_{m=1}^{M-1} h_m}{h_0}.$$

Denoting the real and imaginary parts of κ by r_κ and x_κ, respectively, the input resistance can be expressed as

$$R_{in} = R_0 + R_1 r_\kappa - X_1 x_\kappa.$$

As r_κ and x_κ are the random variables, in order to obtain the CDF of R_{in}, the distributions of r_κ and x_κ are required. For a Rayleigh faded channel, $h_j \sim \mathbb{CN}(0, \sigma^2)$, for all $j \in \{0, 1, \ldots, M\}$, where $\mathbb{CN}$ denotes a complex Gaussian distribution. As h_m is a complex Gaussian, the sum of h_m also follows complex Gaussian distribtion, $\sum_{m=1}^{M-1} h_j \sim \mathbb{CN}(0, M\sigma^2)$. This implies that the random variable κ is a ratio of two independent complex Gaussian variables, and the joint PDF of the r_κ and x_κ can be given as [75]

$$f(r_\kappa, x_\kappa) = \frac{M}{\pi}\left(r_\kappa^2 + x_\kappa^2 + M\right)^{-2}. \tag{3.41}$$

The CDF for R_{in} can be obtained by solving

$$F_{R_{in}}(r_{in}) = \iint_{R_{in} \le r_{in}} f(r_\kappa, x_\kappa) \mathrm{d}r_\kappa \mathrm{d}x_\kappa. \tag{3.42}$$

Substituting R_{in} and (3.41) into (3.42), we have

$$F_{R_{in}}(r_{in}) = \iint_{R_0 + R_1 r_\kappa - X_1 x_\kappa \le r_{in}} \frac{M}{\pi}\left(r_\kappa^2 + x_\kappa^2 + M\right)^{-2} \mathrm{d}r_\kappa \mathrm{d}x_\kappa. \tag{3.43}$$

After solving the integrals in (3.43), the CDF of R_{in} can be obtained and is given in the proposition below.

Proposition 5 *Let R_1 and X_1 are the real and imaginary part of Z_{01}, respectively. For a circular EA the CDF of its input resistance, R_{in}, is given as*

$$F_{R_{in}}(r_{in}) = \frac{1}{2} + \frac{r_{in} - R_0}{2\sqrt{M\left(X_1^2 + R_1^2\right) + \left(r_{in} - R_0\right)^2}}. \tag{3.44}$$

The PDF of input resistance is given as

$$f_{R_{in}}(r_{in}) = \frac{1}{2\sqrt{M\left(X_1^2 + R_1^2\right) + R_0^2}} - \frac{\left(r_{in} - R_0\right)^2}{2\left(M\left(X_1^2 + R_1^2\right) + \left(r_{in} - R_0\right)^2\right)^{3/2}}. \tag{3.45}$$

The probability that a circular EA can transmit an exact MRT precoded signal is

$$\begin{aligned} \mathcal{P} &= 1 - F_{R_{in}}(0) \\ &= \frac{1}{2} + \frac{R_0}{2\sqrt{M\left(X_1^2 + R_1^2\right) + R_0^2}}. \end{aligned} \tag{3.46}$$

Proof: See Appendix E.

From this proposition, it can be noted that the probability that a circular EA can support an exact MRT precoded signal, increases as the self-resistance of the active element increases. Furthermore, this probability decreases as the number of elements increases or the mutual coupling impedance between the active element and parasitic elements increases. These factors show that the probability increases as the mutual coupling is reduced. However, the basic work principle of an EA is the mutual coupling that exists due to the small distance between the elements, therefore, a relatively large mutual coupling is desired for EA operation. Thus, in this case, the probability $\mathcal{P}$ will decrease and our proposed EA-P will become crucial to achieve signal transmission using the EA.

Simulation Results

In Figure. 3.6, the CDF of R_{in}, plotted using (3.44), is compared with the CDF obtained via Monte Carlo simulation for different EAs. The CDFs are compared under different element numbers and antenna spacing for circular linear EAs in this figure. It can be noted that reducing the number of the elements or increasing antenna spacing reduces the probability on $R_{in} < 0$.

The SER performances, in the case of MRT, are compared for circular EAs with different

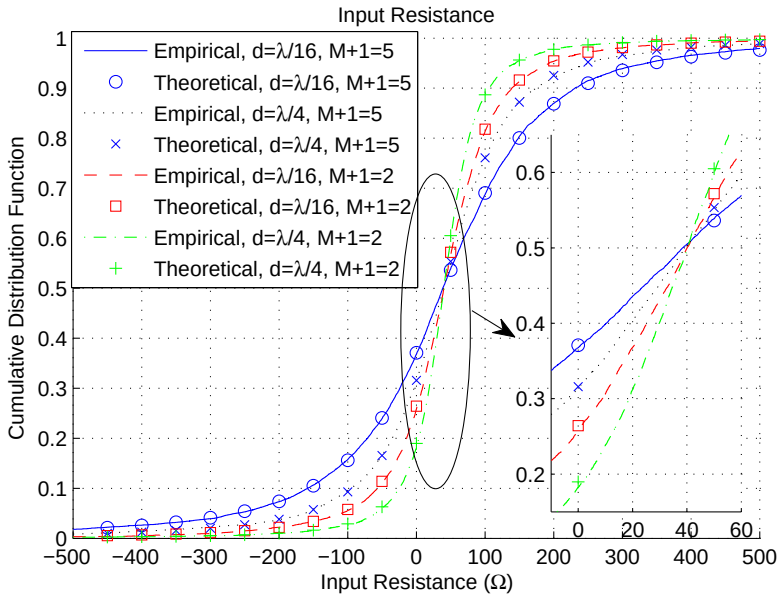

Figure 3.6: The CDF of input resistance with respect to different antenna spacings

number of elements and different spacings in Figure. 3.7. It can be observed from Figure. 3.7 that the SER performances vary with the number of antenna elements and the antenna spacing. Increasing the number of the elements or reducing antenna spacing reduces the SER. It can be observed for the EA-S that the SER performance is very poor and an error floor is obtained. In addition, the error floor can be avoided using EA-P and especially at low SNRs, the SER performance of the EA-P transmitter is similar to that of the standard multiple antenna transmitter. Thus, the SER performance can be improved significantly using EA-P. However, at high SNRs there is a slight loss in performance as the number of elements is increased. This happens because the proportion of unsupported signals increases with increasing antenna elements.

In Figure. 3.8, the SER performances of the EA-P is shown with varying ξ[4]. It can be observed that the SER increases with the increasing ξ. This happens due to a stronger requirement on the input resistance and results in an approximate signal that is more different from the ideal signal.

As ESPAR exploits the mutual coupling to transmit signals. the accurate mutual coupling is required for proposed algorithm. Most of these parameters that affect mutual coupling can

[4]The value of ξ affects the input power from the active element, and therefore, it will also affect the efficiency of an EA. However, this work focuses on the stability and feasibility of an EA.

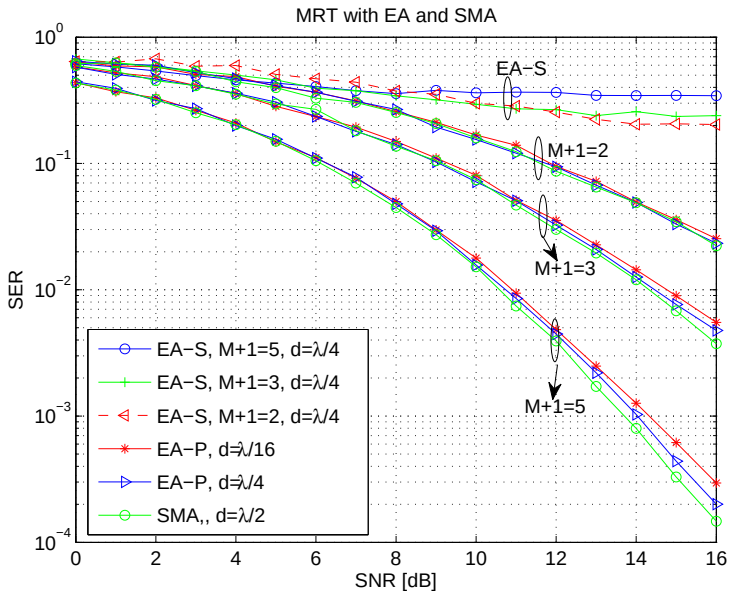

Figure 3.7: SER performance comparison of the EA transmitter and standard multiple antenna transmitter in the case of maximum ratio transmission under 16-QAM under the stability constraint.

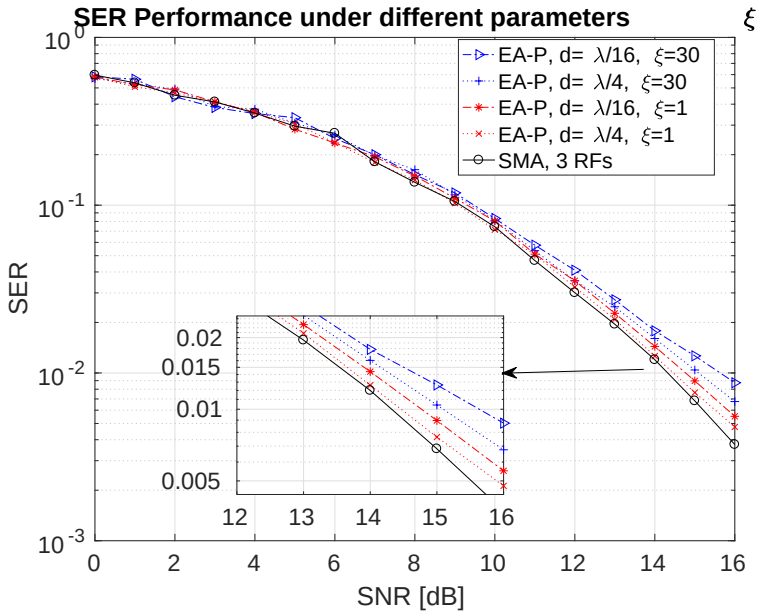

Figure 3.8: SER performance comparison of the 3 elements EA transmitter with varying ξ under 16-QAM under the stability constraint.

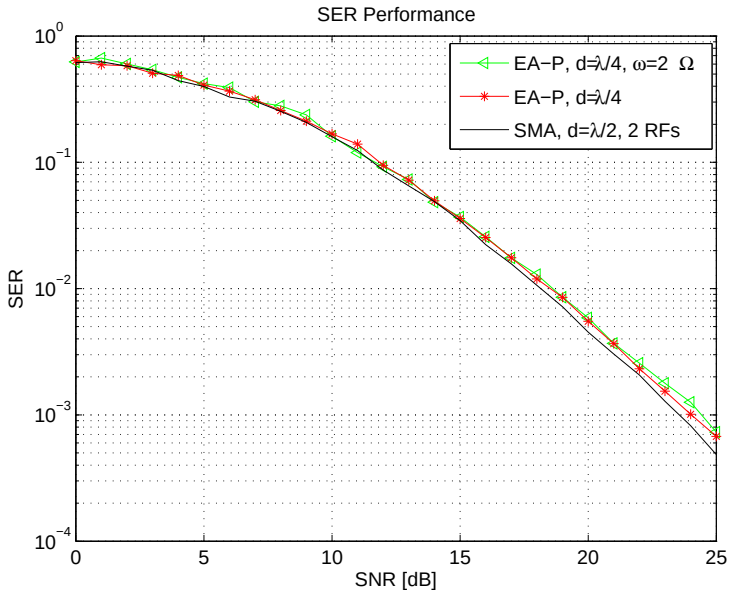

Figure 3.9: SER performance for proposed algorithm for 2-element ESPAR with uncertainty MCM under the stability constraint.

be measured or estimated except near field scatterers. As the near-field conductor can induce mutual coupling to the adjacent elements, conductive objects within a quarter wavelength proximity of antenna elements can have the near-field effects. It means that the impact of mutual coupling is more notable when ESPAR is used in mobile handsets. Since the occurrences of near field scatterers are unknown and uncontrollable to array applications, modeling of the mutual coupling is a significant and challenging for ESPAR transmitter. Hence, we model the configuration deviations between the calculated values of the loads and the practical values as Gaussian distributed with mean zero and variance ω. The SER performances for ESPAR considering the change of mutual coupling are presented by simulation. In Fig. 3.9, the modulation scheme considered is 16QAM. Taking into account the impact of mutual coupling in practice, the performance of ESPAR based system degrades in the high SNR region. It can be noted that in the low SNR region, the difference of SER performance between system with exact loads and practical values is very small. In the high SNR region, the difference becomes more obvious with increase of the number of antenna element.

3.5 Summary

For some signals, varying the parasitic loads results in a negative input resistance. A negative input resistance implies that the antenna structure is unstable for transmitting these signals. In order to achieve stable transmission using an EA, an approach is to design a new ESPAR by increasing its self-resistance as proposed in [16]. However, one issue with this approach is that, once an EA is designed, there are still some signals for which the ESPAR will be unstable, as such signals result in a negative input resistance. In order to transmit such signals, an alternative new EA needs to be designed. In this chapter, instead of those actual signals, one can transmit approximate signals that satisfy the input resistance constraint without much loss in performance. We have obtained simple closed-form expressions for calculating the approximate signals that can be easily implemented at the transmitter. The conclusions in this chapter are:

- To transmit signals that might lead to oscillatory/unstable behaviour of an EA transmitter, a novel approach has been proposed in this chapter. I.e., instead of trying to transmit the actual/ideal signals, which generate a negative input resistance at the EA, signals closely approximating the actual/ideal signals that do not lead to a negative input resistance are transmitted. In this way, the EA does not need to be redesigned.

- An optimisation problem has been proposed to minimise the MSE between the ideal and approximate signals while considering the implementation constraint of the EA. The underlying problem is originally not convex. We have recast it as a convex form via equivalent reformulation and Lagrange duality. As practical transmitters require real-time operation, the optimisation problem has been solved analytically, and novel closed-form expressions have been derived to easily calculate the approximate current signals for the EA system.

- The performance of EA-P has been compared with the performance of EA-S and of SMA in various communication scenarios. Specifically, when the transmitter does not possess the CSI, the spatial multiplexing scenario and space-time block precoding have been considered. When the transmitter possesses the CSI, the performances of EA-P, EA-S, and standard multiple antenna with MRT have been compared. The performance

metric compared is the SER. Our results have shown that the EA-P performs significantly better compared to the EA-S and gives almost the same performance as the standard multiple antenna transmitter. Moreover, considering the cost and complexity of the EA, the EA-P scheme performs well and is practical.

In general, we have addressed the issue of an EA transmitter by obtaining approximate signals for transmission that are close to the ideal signals in the MSE sense and satisfy the requirement that the input resistance be positive. Closed-form expressions to calculate the approximate signal vector from ideal signal vector have also been obtained, resulting in simplified processing at the transmitter. In the simulations, the standard transmitter system with one RF chain per antenna element is also provided as a benchmark. Our results, conducted for various communication scenarios, have shown that the EA-P transmitter gives significant improvement over the performance of the EA-S transmitter, and performs nearly the same as the standard multiple antenna systems.

Chapter 4
Transceiver Design With ESPAR antenna under Peak Power Constraints in MIMO Systems

4.1 Introduction

As discussed in Chapter 3, the authors in [16] provided the design conditions that an ESPAR antenna (EA) was required to satisfy in order to support an arbitrary precoding scheme which is that the input resistance should be positive. Satisfying this condition is essential because a negative input resistance implies that the EA is reflecting power back and exhibiting oscillatory/unstable behaviour [18]. In order to achieve stable transmission using an EA, two approaches are proposed. One is to increase the self-resistance of an EA as in [16], the other is to transmit signals closely approximating the actual signals that keep the EA stable as described in Chapter 3. In both approaches, no constraint on the transmission power of an EA was considered. This is not a case in actual systems, as the practical power amplifier normally has limited peak power [8]. Moreover, in the case of the standard multiple antenna with N elements, there are N power amplifiers, N mixers, and N DACs. Each antenna element can be fed power by its own power amplifier [8]. However, the single-RF antenna with N elements has only one power amplifier. When single-RF antennas are used to provide multiple antenna functionality, the power of all N antenna elements are fed by the single power amplifier. Unlike the standard multiple antenna system where each radio frequency (RF) chain has its own power amplifier and the transmitting power can be adjusted individually, in an EA, all the antennas are fed centrally by a single power amplifier and this power amplifier has to be sufficient to support all the elements of an ESPAR antenna. Thus, when an ESPAR antenna is applied to transmit same signals as standard multiple antenna with multiple RF chains, it is more probable that the power amplifier will reach maximum power while transmitting using an ESPAR antenna.

This highlights the importance of considering the peak power constraint of the power amplifier. It is noted that the peak power constraint of the power amplifier can be expressed as the twice of the power delivered to the antenna with conjugate matching as discussed at Equation 2.15 in Chapter 2. The power delivered to the antenna includes both the power radiated and the power dissipated by the antenna [17].

In this chapter, we extend the work of Chapter 3. It considers a more realistic scenario with the peak power constraint at the feeding element of an EA. For signals that result in the unstable operation of an EA, or that do not satisfy the requirement of maximum power, signals closely approximating the ideal signals are transmitted. These approximate signals guarantee the stability of the EA and also satisfy the peak power requirement. Specifically, to obtain the approximate signal, an optimisation problem is formulated to minimise the MSE between the ideal and approximate signals while considering the stability and peak power requirement of the EA. The underlying problem is originally not convex. There are a quadratic objective function and two non-convex quadratic constraints, and the strong duality conditions used in [19, 66] cannot be applied to this problem. Instead, coordinate transform and geometric methods are applied to find the optimal approximate signals. It is shown that these approximate signals can be easily obtained using well-known root finding and interior point algorithms.

For EA designs in [19, 55], the symbol error rate (SER) performance of our proposed algorithm is compared with the SER performance of a standard multiple antenna transmitter in various communication scenarios. Specifically, we consider both single-user and multi-user scenarios. For a single-user scenario, as an example, we analyse the SER performance of the EA for Alamouti coded transmission and maximum ratio transmission. For the multiuser case, the proposed scheme is analysed for channel inversion (CI) and regularised channel inversion (RCI) precoders. Our results show that a system employing EA transmitter and using our proposed algorithm gives performance similar to a system with a standard multiple antenna transmitter for some antenna design. Moreover, in [16], stable EA transmission is achieved by increasing the self-resistance of the active element. Our results show that if the EA has large self-resistance, as in [16], performance is significantly degraded. Due to large self-resistance, a large amount of power is dissipated by the self-resistance, and only limit-

ed power is actually transmitted. This results in significantly degraded performance, and to reduce the SER, the peak power needs to be increased substantially, which renders the EA with a large self-resistance highly power inefficient regardless of its improved stability. This shows that increasing its self-resistance is not a power efficient approach to improving the stability of an EA.

The rest of this chapter is organised as follows. The EA transmitter power model is explained in Section 4.2. The corresponding problem is formulated and discussed in Section 4.3, followed by application and some numerical results in Section 4.4. Finally, the main results and conclusions are summarised in Section 4.5.

4.2 Power Consideration Using an EA

The system model for EA has been described in Section 2.7. The power for EA based on circuit theory is considered in this section.

4.2.1 Power to an EA

Using the equivalent circuit model of an EA as shown in Figure. 4.1, the power delivered to an EA can be mathematically expressed as

$$P_E = \mid i_0 \mid^2 \Re\left\{Z_{in}\right\} = \left|\frac{v_s}{z_s + Z_{in}}\right|^2 \Re\left\{Z_{in}\right\}. \tag{4.1}$$

where Z_{in} denotes the input impedance of an EA, z_s denotes the total impedance from the source and matching circuit, and $\Re\left\{Z_{in}\right\}$ and $\Im\left\{Z_{in}\right\}$ denote its resistive and reactive components, respectively. As discussed in Section 2.4.2, the input power to the antenna should be positive to guarantee that there is power delivered to the antenna and to guarantee stable transmission, which implies the input resistance $\Re\{Z_{in}\}$ should be positive. If $\Re\{Z_{in}\}$ is not positive, it means that the EA is reflecting power back and exhibiting oscillatory/unstable behaviour [18].

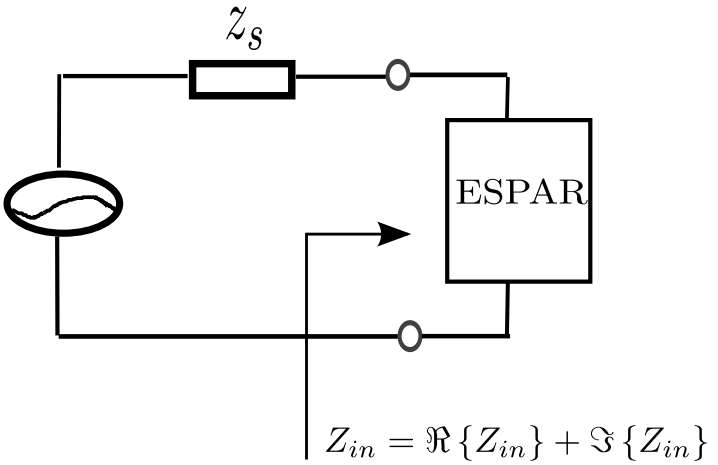

Figure 4.1: The equivalent circuit of the ESPAR antenna

Let w_{2m+1} and w_{2m+2} denote the real part and the imaginary part of i_m, the $m-$th entry of the vector $\mathbf{i}_m$. Representing the current values in terms of w_{2m+1} and w_{2m+2} and substituting it in (4.1), the input power to the active element can be simplified as

$$P_E = \left(w_1^2 + w_2^2\right) \Re\left\{ Z_{00} + \frac{\sum_{m=1}^{M-1} Z_{0m} i_m}{i_0} \right\}. \tag{4.2}$$

Following the method proposed in Appendix A for Chapter 3, the input power to the antenna element can be reformulated in the real domain as shown in the following proposition.

Proposition 6 *The power supplied to an EA from the active element is given as*

$$P_E = \mathbf{w}^T \mathbf{A} \mathbf{w}, \tag{4.3}$$

where $\mathbf{w} = [w_1, w_2, w_3, w_4, \ldots, w_{2M-1}, w_{2M}]^T$ *and its elements* w_{2m+1} *and* w_{2m+2} *denote*

the real part and the imaginary part of i_m, respectively. A is given as

$$\mathbf{A} = \begin{bmatrix} R_0 & 0 & \frac{R_1}{2} & -\frac{X_1}{2} & \dots & \frac{R_{M-1}}{2} & -\frac{X_{M-1}}{2} \\ 0 & R_0 & \frac{X_1}{2} & \frac{R_1}{2} & \dots & \frac{X_{M-1}}{2} & \frac{R_{M-1}}{2} \\ \frac{R_1}{2} & \frac{X_1}{2} & 0 & 0 & \dots & 0 & 0 \\ -\frac{X_1}{2} & \frac{R_1}{2} & 0 & 0 & \dots & 0 & 0 \\ \vdots & \vdots & \vdots & \vdots & \ddots & \vdots & \vdots \\ \frac{R_{M-1}}{2} & \frac{X_{M-1}}{2} & 0 & 0 & \dots & 0 & 0 \\ -\frac{X_{M-1}}{2} & \frac{R_{M-1}}{2} & 0 & 0 & \dots & 0 & 0 \end{bmatrix}, \tag{4.4}$$

where R_m and X_m denote the real part and the imaginary part of the mutual coupling from the active element to the m-th parasitic element, Z_{0m}.

As previously described, in order to radiate the signal, the currents at the antenna element need to be varied based on the transmission signals. In the case of the standard multiple antenna systems, the currents are varied by varying the input voltage at each antenna element. However, in the case of an EA, the loads at the parasitic elements and the voltage feeding at the active element needs to be varied. As $\mathbf{i}$ is denoted by its real part and imaginary part, using [16] and after some mathematical manipulations, the voltage feeding and load values can be calculated from $\mathbf{w}$ as

$$v_s = 2\sum_{j=0}^{M-1} Z_{0j}\left(w_{2j} + jw_{2j+1}\right), \tag{4.5a}$$

$$z_m = -\frac{\sum_{j=0}^{M-1} Z_{mj}\left(w_{2j} + jw_{2j+1}\right)}{\left(w_{2m} + jw_{2m+1}\right)},\ m = 1, 2, \dots, M-1. \tag{4.5b}$$

It is noted that the loads and the voltage feeding can be calculated using (4.5) once $\mathbf{w}$ is obtained.

4.2.2 Impedance Matching

As discussed in Chapter 2, in order to realise maximum power transfer, a dynamic impedance matching circuit is proposed to compensate the impedance mismatch between the source and

input impedance of the EA. The total power supplied by source in the active element is

$$P_S = \mid i_0 \mid^2 \Re\{z_s + Z_{in}\} = 2P_E. \tag{4.6}$$

4.3 Algorithm for Signal Transmission under Limited Power

4.3.1 Problem Formation

For signal transmission, the currents at the antenna elements need to be varied based on input symbols. This variation in current is achieved by varying the loads at the parasitic elements and the voltage feeding at the active element. In some cases, for a certain transmission signal, it is possible that the voltage and loads take values which lead to a negative input resistance, which causes an EA to exhibit unstable behaviour. For transmission of such signals, it was proposed to transmit signals closely approximating the ideal signal and which keep the EA stable [19]. However, in [19], no limit on the power of an EA was assumed. In real world systems, another important consideration is the limited power from the power amplifier. Thus, in this sequel, we ensure the stability of an EA with limited power.

The problem to obtain the values of the voltage and the loads can be formulated as an optimisation problem to minimise the MSE between the currents corresponding to the ideal and approximate transmission signals, and is given as

$$\min_{v_0, \mathbf{Z}_L} \quad \left\| \hat{\mathbf{i}} - (\mathbf{Z} + \mathrm{diag}(z_s, z_1, z_2, \ldots, z_{M-1}))^{-1}[v_0, 0, \ldots, 0] \right\|_2, \tag{4.7a}$$

$$\text{st.} \quad P_S = 2\left|\frac{v_0}{z_s + Z_{in}}\right|^2 \Re\{Z_{in}\} \geq P_S^{min}, \tag{4.7b}$$

$$P_S = 2\left|\frac{v_0}{z_s + Z_{in}}\right|^2 \Re\{Z_{in}\} \leq P_S^{max}, \tag{4.7c}$$

where $\hat{\mathbf{i}}$ denotes the desired current vector corresponding to ideal signal required to be transmitted by the EA. The objective of this optimisation problem is to find the voltage feeding v_0 and the loads $z_1, z_2, \ldots, z_{M-1}$ to minimise MSE between the ideal and approximate signal,

the constraint (4.7b) is similar to the constraint in [19] and guarantees that the input resistance is positive and that the EA does not exhibit unstable behaviour. The constraint (4.7c) is included to guarantee that the transmit power does not exceed the maximum power level supported by the transmitter.

4.3.2 Power Consumption for an EA and Problem Reformulation

Let $P_{min} = \frac{P_S^{min}}{2}$ and $P_{max} = \frac{P_S^{max}}{2}$, the optimisation problem can be reformulated and represented in terms of real and imaginary part of current in the antenna elements as

$$\min_{\mathbf{w}} \quad \|\mathbf{w} - \hat{\mathbf{w}}\|^2, \tag{4.8a}$$

$$\text{st.} \quad \mathbf{w}^T\mathbf{A}\mathbf{w} > P_{min}, \tag{4.8b}$$

$$\mathbf{w}^T\mathbf{A}\mathbf{w} \leq P_{max}. \tag{4.8c}$$

where $\hat{\mathbf{w}} = [\hat{w}_1, \hat{w}_2, \hat{w}_3, \hat{w}_4, \ldots, \hat{w}_{2M-1}, \hat{w}_{2M}]^T$, $\hat{w}_{2m+1}$ and $\hat{w}_{2m+2}$ denote the real part and the imaginary part of $\hat{i}_m$, respectively.

It can be noted that there are a quadratic objective function and two quadratic constraints in this problem. Moreover, the number of optimisation variables is $2M$. In addition, $\mathbf{A}$ is an indefinite matrix, as shown in the proposition below. Thus, the optimisation problem (4.8) is non-convex.

Proposition 7 *The $2M \times 2M$ matrix $\mathbf{A}$ which is defined as* (4.4) *is an indefinite matrix and the eigenvalues of $\mathbf{A}$ are*

$$\begin{cases} \lambda_1 = \lambda_2 = R_0 - \sqrt{R_0^2 + \sum_{m=1}^{M-1}(R_m^2 + X_m^2)} < 0 \\ \lambda_{2M-1} = \lambda_{2M} = R_0 + \sqrt{R_0^2 + \sum_{m=1}^{M-1}(R_m^2 + X_m^2)} > 0 \\ \lambda_n = 0 \quad \textit{for } n = 3, 4, \ldots, 2M-2 \end{cases}, \tag{4.9}$$

where $\lambda_1, \lambda_2, \ldots, \lambda_{2M-1}, \lambda_{2M}$ denotes the eigenvalues of the matrix $\mathbf{A}$ in ascending order.

Proof: The proof is provided in Appendix I. ■

Due to the non-convex nature of the constraint set, the strong duality employed in [19] and [66], cannot be applied to this problem. Instead, we use coordinate transform and geometric method to solve the optimisation problem.

In order to simplify this problem, we decompose $\mathbf{A}$ into its constituent eigenvalue and eigenvectors. As $\mathbf{A}$ is a real symmetric matrix and it can be diagonalized as

$$\mathbf{A} = \mathbf{Q}_A \mathbf{\Lambda}_A \mathbf{Q}_A^T,$$

where $\mathbf{\Lambda}_A = [\lambda_1, \lambda_2, \ldots, \lambda_{2M-1}, \lambda_{2M}]$ is a real diagonal matrix with its elements are eigenvalues of $\mathbf{A}$, the columns of the real orthogonal matrix $\mathbf{Q}_A$ are corresponding eigenvectors. In order to simplify this problem, simplified equivalent problem is stated in the following proposition. By using the decomposition of $\mathbf{A}$, we derive the simplified equivalent problem as stated in the following proposition.

Proposition 8 *By setting* $\mathbf{e} = \mathbf{Q}_A^T \mathbf{w}$ *and* $\mathbf{g} = \mathbf{Q}_A^T \hat{\mathbf{w}}$*, the minimal value of* (4.8a) *in the optimization problem* (4.8) *is obtained when* $e_m = g_m,$ for $m = 3, 4, \ldots, 2M-2$*, where* e_m *and* g_m *are the* m*-th element of* e_m *and* g_m*, respectively. Then the optimisation problem in* (4.8) *can be reformulated as*

$$\min_{\tilde{\mathbf{e}}} \quad \left\| \tilde{\mathbf{e}} - \tilde{\mathbf{g}} \right\|^2, \tag{4.10a}$$

$$\textit{st.} \quad \tilde{\mathbf{e}}^T \operatorname{diag}\left(\lambda_1, \lambda_2, \lambda_{2M-1}, \lambda_{2M}\right) \tilde{\mathbf{e}} > P_{min}, \tag{4.10b}$$

$$\tilde{\mathbf{e}}^T \operatorname{diag}\left(\lambda_1, \lambda_2, \lambda_{2M-1}, \lambda_{2M}\right) \tilde{\mathbf{e}} \leq P_{max}, \tag{4.10c}$$

where $\tilde{\mathbf{e}} = [e_1, e_2, e_{2M-1}, e_{2M}]^T$ *and* $\tilde{\mathbf{g}} = [g_1, g_2, g_{2M-1}, g_{2M}]^T$.

Proof: The proof is provided in Appendix J. ■

It can be noted that the optimisation problem in (4.10) is more simplified and has four optimisation variables instead of $2M$.

4.3.3 Solution of the Optimisation Problem

The optimisation problem in (4.10) can be further simplified using coordinate transformation. By representing the elements of $\tilde{\mathbf{e}}$ and $\tilde{\mathbf{g}}$ into the polar coordinate system, the problem can be further reformulated as shown in the following proposition.

Proposition 9 *By replacing Cartesian coordinate with the polar system in* (4.10)*, the objective function* $\|\tilde{\mathbf{e}} - \tilde{\mathbf{g}}\|^2$ *achieves its minimal value when* $\theta_a = \theta_c$ *and* $\theta_b = \theta_d$*.*

Therefore, the problem in (4.10) *can be further simplified as*

$$\min_{r_a, r_b} \quad r_a^2 + r_b^2 - 2r_a r_b - 2r_c r_d + r_c^2 + r_d^2, \tag{4.11a}$$

$$\textit{st.} \quad \lambda_1 r_a^2 + \lambda_{2M-1} r_b^2 \geq P_{min}, \tag{4.11b}$$

$$\lambda_1 r_a^2 + \lambda_{2M-1} r_b^2 \leq P_{max}. \tag{4.11c}$$

where the elements of $\tilde{\mathbf{e}}$ *and* $\tilde{\mathbf{g}}$ *are represented into the polar coordinate system as*

$$e_1 = r_a \cos\theta_a, \quad e_2 = r_a \sin\theta_a,$$

$$e_{2M-1} = r_b \cos\theta_b, \quad e_{2M} = r_b \sin\theta_b,$$

$$g_1 = r_c \cos\theta_c, \quad g_2 = r_c \sin\theta_c,$$

$$g_{2M-1} = r_d \cos\theta_d, \quad g_{2M} = r_d \sin\theta_d,$$

and

$$r_a = \sqrt{e_1^2 + e_2^2}, \quad \theta_a = \arctan\left(\frac{e_2}{e_1}\right),$$

$$r_b = \sqrt{s_{2M-1}^2 + e_{2M}^2}, \quad \theta_b = \arctan\left(\frac{e_{2M}}{e_{2M-1}}\right),$$

$$r_c = \sqrt{g_1^2 + g_2^2}, \quad \theta_c = \arctan\left(\frac{g_2}{g_1}\right),$$

$$r_d = \sqrt{g_{2M-1}^2 + g_{2M}^2}, \quad \theta_d = \arctan\left(\frac{g_{2M}}{g_{2M-1}}\right).$$

Proof: The proof is provided in Appendix K. ■

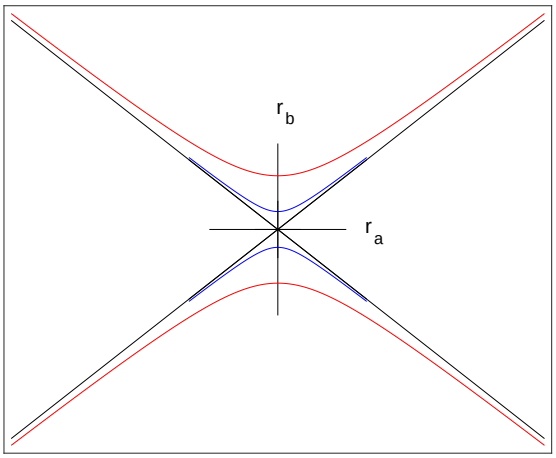

Figure 4.2: Two hyperbolas $\lambda_1 r_a^2 + \lambda_{2M-1} r_b^2 = P_{min}$ (blue) and $\lambda_1 r_a^2 + \lambda_{2M-1} r_b^2 = P_{max}$ (red) with same asymptotes and different focus points

It can be noted from Proposition 9 that the optimal value of θ_a and θ_b are obtained. Therefore, the number of optimisation variables has been reduce to two and it is required to obtain values of r_a and r_b which minimises (4.11a) under the constraints (4.11b) and (4.11c). The constraint set can be written as

$$\mathbb{S}_1 = \left\{ \mathbf{r}_e = [r_a, r_b]^T \mid \lambda_1 r_a^2 + \lambda_{2M-1} r_b^2 \geq P_{min}, \lambda_1 r_a^2 + \lambda_{2M-1} r_b^2 \leq P_{max} \right\}. \tag{4.12}$$

Note that $\lambda_1 r_a^2 + \lambda_{2M-1} r_b^2 = P_{min}$ and $\lambda_1 r_a^2 + \lambda_{2M-1} r_b^2 = P_{max}$ are two hyperbolas with same asymptotes and different focus points as shown Figure .4.2. The constraint set is the area between the hyperbola $\lambda_1 r_a^2 + \lambda_{2M-1} r_b^2 = P_{min}$ and hyperbola $\lambda_1 r_a^2 + \lambda_{2M-1} r_b^2 = P_{max}$, which is not a convex set.

The optimisation problem in (4.11) can be restarted to find the optimal $[r_a, r_b]^T$ to minimise the Euclidean distance between two points $[r_a, r_b]^T$ and $[r_c, r_d]^T$ when $[r_a, r_b]^T \in \mathbb{S}_1$. From the geometrical perspective, the problem is to find the distance from a point $\mathbf{r}_g = [r_c, r_d]^T \in$

$\mathbb{R}^2$ to the set $\mathbb{S}_1$. Thus, it can be expressed as

$$\textbf{dist}\left(\mathbf{r}_g, \mathbb{S}_1\right) = \inf_{\mathbf{r}_e \in \mathbb{S}_1} \left(\|\mathbf{r}_g - \mathbf{r}_e\|\right), \tag{4.13}$$

in which, $\textbf{dist}\left(\mathbf{r}_g, \mathbb{S}_1\right)$ is the distance between $\mathbf{r}_g$ and $\mathbb{S}_1$.

This problem can be solved by dividing into three sub-optimisation problems according to the position of the point $\mathbf{r}_g$.

4.3.3.1 Case 1: $\mathbf{r}_g \in \mathbb{S}_1$

If $\mathbf{r}_g \in \mathbb{S}_1$, then $\textbf{dist}\left(\mathbf{r}_g, \mathbb{S}_1\right) = 0$. In this case, $\mathbf{r}_e = \mathbf{r}_g$.

4.3.3.2 Case 2: $\mathbf{r}_g \in \left\{r_g = [r_c, r_d]^T \mid \lambda_1 r_c^2 + \lambda_{2M-1} r_d^2 > P_{max}\right\}$

In this case, $\mathbf{r}_e$ is the project of $\mathbf{r}_g$ on the hyperbola, which can be written as

$$\mathbb{S}_{c2} = \left\{\mathbf{r}_e = [r_a, r_b]^T \mid \lambda_1 r_a^2 + \lambda_{2M-1} r_b^2 = P_{max}\right\}, \tag{4.14}$$

and the optimisation problem can be reformulated as

$$\textbf{dist}\left(\mathbf{r}_g, \mathbb{S}_1\right) = \inf_{r_e \in \mathbb{S}_{c2}} \left(\|\mathbf{r}_g - \mathbf{r}_e\|\right). \tag{4.15}$$

Proposition 10 *When* $\mathbf{r}_g \in \left\{r_g = [r_c, r_d]^T \mid \lambda_1 r_c^2 + \lambda_{2M-1} r_d^2 > P_{max}\right\}$, *the projection of the point* $\mathbf{r}_g$ *onto the subspace* $\mathbb{S}_{c2}$ *is the point* $\mathbf{r}_e$ *with the coordinate* $\left[\frac{r_c}{1+\lambda_1 t}, \frac{r_d}{1+\lambda_{2M-1} t}\right]^T$, *where* t *is the unique root of the function*

$$G\left(t\right) = \lambda_1 \left(\frac{r_c}{1+\lambda_1 t}\right)^2 + \lambda_{2M-1} \left(\frac{r_d}{1+\lambda_{2M-1} t}\right)^2 - P_{max} = 0$$

on the domain

$$\left\{t| -\frac{1}{\lambda_1} \leq t \leq -\frac{1}{\lambda_{2M-1}}\right\}.$$

Proof: The proof is provided in Appendix L. ■

In order to obtain the point $\mathbf{r}_e$ of the problem, a root is required. Any root finding algorithm can be used. In our algorithm, we use the method which combines the bisection and Newton's method which was proposed in [93]. Firstly, the bisection method is utilised to reduce the search area. Then Newton's method is applied to find the root and the steps are outlined in Algorithm 2.

4.3.3.3 Case 3: $\mathbf{r}_g \in \left\{\mathbf{r}_g = [r_c, r_d]^T \mid \lambda_1 r_c^2 + \lambda_{2M-1} r_d^2 \leq P_{min}\right\}$

Similarly, in this case, $\mathbf{r}_e$ is the projection of $\mathbf{r}_g$ onto the hyperbola, which can be expressed as

$$\mathbb{S}_{c3} = \left\{[r_a, r_b]^T \mid \lambda_1 r_a^2 + \lambda_{2M-1} r_b^2 = P_{min}\right\}. \tag{4.16}$$

The problem can be reformulated as

$$\textbf{dist}\left(\mathbf{r}_g, \mathbb{S}_1\right) = \inf_{\mathbf{r}_e \in \mathbb{S}_{c3}} \left(\|\mathbf{r}_g - \mathbf{r}_e\|\right). \tag{4.17}$$

Note that the problem in (4.17) is similar to (4.15) when replacing P_{max} in (4.15) by P_{min} in (4.17). Hence, we can use the same approach in Algorithm 2 to obtain the optimal point.

Once the optimisation problem is solved, the optimal approximate signals can be obtained for the EA. The main steps for calculation of the optimal approximate signals are outlined in Algorithm 3.

4.3.4 Complexity Analysis of Proposed Algorithm

From Algorithm 3, the solution of the optimization problem is solved from Step 4 to Step 12. Below we calculate the complexity of our proposed algorithm. In the proposed algorithm, during the signal transmission, the steps from step 1 to step 3 can be calculated once, and can be used for the subsequent signal transmissions. Only step 4 to step 12 require to be calculated for every transmitted signal.

Step 4: Step 4 involves a matrix multiplication operation, thus it requires $2n^2 - n = 8M^2 - 2M$ floating point (flop) operations [67] [69].

Algorithm 2 Finding the projection of $\mathbf{r}_g$ onto the hyperbola $\mathbb{S}_1$

Input: $\mathbf{r}_g$, $\lambda_1^{(A)}$, $\lambda_{2M-1}^{(A)}$, P;

Output: $\mathbf{r}_e$;

Step 1: Choose the inflection points as the initial data point in canonical coordinates, and calculate inflection point t_0 and the corresponding $G(t_0)$.

Step 2: If $G(t_0) < 0$, then pick the interval $\mathbb{D} = \left(-\frac{1}{\lambda_{2M-1}}, t_0\right]$.

for $j = 1 : N_{div}$

$t_0^{old} = t_0^{new}$; $\quad t_0^{new} = \left(-\frac{1}{\lambda_1}\right)^2 - \frac{\left(-t_0^{old} + \left(-\frac{1}{\lambda_1}\right)\right)}{2^j}$;

if $G(t_0^{new}) < 0$ break; end;

end;

for $iter = 1 : N$

$t_0^{old} = t_0^{new}$;

if $G\left(t_0^{old}\right) > 0$ break; end;

if $\left|\frac{G\left(t_0^{old}\right)}{G'\left(t_0^{old}\right)}\right| < \xi$ break; end

$t_0^{new} = t_0^{old} - \frac{G\left(t_0^{old}\right)}{G'\left(t_0^{old}\right)}$;

end

Step 4: If $G(t_0) > 0$ then pick the initial interval $\mathbb{D} = \left[t_0, -\frac{1}{\lambda_1}\right)$.

for $j = 1 : N_{div}$

$t_0^{old} = t_0^{new}$; $\quad t_0^{new} = -\left(-\frac{1}{\lambda_{2M-1}}\right)^2 - \frac{\left(t_0^{old} - \left(-\frac{1}{\lambda_{2M-1}}\right)\right)}{2^j}$;

if $G(t_0^{new}) > 0$ break; end;

end;

for $iter = 1 : N$

$t_0^{old} = t_0^{new}$;

if $G\left(t_0^{old}\right) < 0$ break; end;

if $\left|\frac{G\left(t_0^{old}\right)}{G'\left(t_0^{old}\right)}\right| < \xi$ break; end

$t_0^{new} = t_0^{old} - \frac{G\left(t_0^{old}\right)}{G'\left(t_0^{old}\right)}$;

end

Step 5:Substitute t_0^{new} to $\left(\frac{r_c}{1+\lambda_1 t}, \frac{r_d}{1+\lambda_{2M-1} t}\right)$ to obtain $\mathbf{r}_e$.

Algorithm 3 Finding optimal transmission signals and corresponding values of voltage feeding and load for an EA

Input: Required ideal currents vector $\hat{\mathbf{i}}$

Output: EA-P loads and voltage feeding for $\hat{\mathbf{i}}$,

Step 1: if $\hat{\mathbf{i}} \in \mathbb{I}_{P\xi}$ {Goto Step 6. } else {Goto Step 2.}

Step 2: Obtain $\hat{\mathbf{w}}$ by separating real and imaginary parts of $\hat{\mathbf{i}}$. Calculate $\mathbf{A}$.

Step 3: Calculate λ_1, λ_{2M-1}, and $\mathbf{Q}$ from the eigenvalue decomposition of $\mathbf{A}$.

Step 4: Calculate $\mathbf{g}$ by $\mathbf{g} = \mathbf{Q}_A^T \hat{\mathbf{w}}$.

Step 5: Calculate r_c, r_d, θ_c and θ_d by $r_c = \sqrt{g_1^2 + g_2^2}$, $\theta_c = \arctan\left(\frac{g_2}{g_1}\right)$, $r_d = \sqrt{g_{2M-1}^2 + g_{2M}^2}$, and $\theta_d = \arctan\left(\frac{g_{2M}}{g_{2M-1}}\right)$.

Step 6: Calculate e_m, for $m = 3, 4, \ldots, 2M_t - 2$, θ_a and θ_b by $e_m = g_m$, for $m = 3, 4, \ldots, 2M_t - 2$, $\theta_a = \theta_c$ and $\theta_b = \theta_d$, respectively.

Step 7: Calculate $\lambda_1 r_c^2 + \lambda_{2M-1} r_d^2$

if $\lambda_1 r_c^2 + \lambda_{2M-1} r_d^2 < P_{min}$

Goto Step 8;

else if $\lambda_1 r_c^2 + \lambda_{2M-1} r_d^2 > P_{max}$

Goto Step 9;

else $\mathbf{r}_e = \mathbf{r}_g$; Goto Step 9;

end;

Step 8: Calculate r_a, r_b by Algorithm 2 when the input $P = P_{min}$.

Step 9: Calculate r_a, r_b by Algorithm 2 when the input $P = P_{max}$.

Step 10: Using Proposition 9, $\theta_a = \theta_c$ and $\theta_b = \theta_d$.

Step 11: Calculate the elements of $\mathbf{s}$ by $e_1 = r_a \cos\theta_a$, $e_2 = r_a \sin\theta_a$, $e_{2M-1} = r_b \cos\theta_b$, $e_{2M} = r_b \sin\theta_b$, $e_m = g_m$, for $m = 3, 4, \ldots, 2M$.

Step 12: Calculate $\mathbf{w}$ from $\mathbf{w} = \mathbf{Q}\mathbf{e}$.

Step 13: Calculate the corresponding loads $z_1, z_2, \ldots, z_{M-1}$ and feeding v_0 as (4.5).

Step 5 to Step 7: Step 5 to step 7 involves 6 operations of scalar multiplication, 2 operations of scalar division and 2 operations of inverse tangent based on scalars.

Step 8 or 9: Step 9 requires calculating the root. The number of optimization variables is one. The complexity of the root finding algorithm is $\mathcal{O}\left(log\frac{1}{\xi}\right)$ [93] [94].

Step 10 to Step 11: Step 10 involves operations of scalar assignment, 4 operations of scalar multiplication, 2 scalar sine operations and 2 scalar cosine operations.

Step 12: Step 12 involves matrix operations and it requires $2n^2 - n = 8M^2 - 2M$ flops.

Adding the complexity of each step, the worst case complexity of the proposed algorithm is $\mathcal{O}\left(16M^2 - 4M + \log\frac{1}{\xi}\right)$.

4.4 Applications and Numerical Results

In this section, using numerical simulations, we analyse the performances of an EA using our proposed Algorithm 3 in various communication scenarios.

4.4.1 Single-user Scenario

Consider a point-to-point link consisting of a transmitter having an array of M antenna elements and a receiver having N_r antennas. The corresponding signal model is

$$\mathbf{y} = \mathbf{H}\mathbf{i} + \mathbf{n}, \tag{4.18}$$

where $\mathbf{y}$ is the received signal at the receiver, $\mathbf{H} \in \mathbb{C}^{N_r \times M}$ is the channel matrix as $N_t = M$, $\mathbf{i}$ is the vector of currents flowing through the transmit antennas, and $\mathbf{n} \in \mathbb{C}^{N_r \times 1}$ denotes the noise vector. In order to radiate the signal, the currents at the antenna elements need to be varied based on the transmission signals [55, 64, 65]. Without loss of generality, as we focus on the transmitter scheme with an EA, in our simulations, we assume that the receiver has a single antenna. The channel is assumed to be Rayleigh faded.

Diversity gain is one of the main advantages of multiple antennas which results in significant performance improvement. There are different approaches to achieve transmit diversity gain depending on the CSI availability at the transmitter [20]. To be best of the authors' knowledge, diversity concepts for the EA have been initially proposed based on beamspace concepts in [12,52,68]. However, there are several weaknesses in beamspace MIMO model. The receiver cannot guarantee the orthogonality of basic beam patterns and the radiating modes cannot be computed accurately for an arbitrary EA. Moreover, arbitrary channel-dependent precoding cannot be realised for an arbitrary antenna array [54]. Therefore, an alternate model based on the currents at the ports of the transmit antenna was introduced in [55]. The authors in [16] provided design conditions that an EA has to satisfy in order to support an Alamouti Code. In order to guarantee the stability of the EA, one approach in [16] is to increase the self-resistance of an EA and redesign an antenna with a new MC matrix. However, one issue with the approach in [16] is that, once an EA is designed, there are still some signals for which the EA will be unstable, as such signals result in a negative input resistance. In order to transmit such signals, a new EA needs to be designed. Thus, we propose a novel approach to transmit signals which closely approximate the actual signals that maintain EA stability. In this subsection, we analyse two different scenarios based on the CSI availability after considering peak power constraint.

4.4.1.1 Transmitter without CSI

In this case, the diversity gain can be achieved by using Alamouti scheme, which extracts transmit diversity without CSI at the transmitter. For a 2-element EA, given a transmission symbol vector $[s_0, s_1]^T$, the ideal port current vector is $\hat{\mathbf{i}} = \sqrt{P_T}\begin{bmatrix} s_0 & -\overline{s_1} \\ s_1 & \overline{s_0} \end{bmatrix}$ and $[s_0, s_1]^T$ is assumed to be independent and identically distributed (i.i.d.) with unit power. The corresponding power consumption for these two symbol periods is

$$\begin{aligned} P_E^{(1)} &= i_0^2 R_{in} = P_T \left|s_0\right|^2 \left(R_0 + \Re\left(\frac{Z_{01} s_1}{s_0}\right)\right), \\ P_E^{(2)} &= i_0^2 R_{in} = P_T \left|s_1\right|^2 \left(R_0 + \Re\left(\frac{Z_{01} \overline{s_0}}{-\overline{s_1}}\right)\right). \end{aligned} \tag{4.19}$$

The supported signal vector set $[s_0, s_1]^T$, which can be exactly transmitted using the Alamouti code by an EA, is

$$\mathbb{S}_{P\xi} = \left\{ [s_0, s_1]^T \middle| P_{min} < P_E^{(1)} \leq P_{max}, P_{min} < P_E^{(2)} \leq P_{max} \right\}. \tag{4.20}$$

It can be noted from (4.19) and (4.20) that whether a signal can be supported depends on the MCM and also the transmission signals which are dependant on the modulation scheme employed. For example, considering N-PSK modulation scheme, the signal at the $(m+1)$-th element is denoted as $s_m = \exp(j\phi_m)$, where $\phi_m = \frac{2\pi n_m}{N}, n_m \in \{0, 1, ..., (N-1)\}$ is the phase of the signal at the $(m+1)$-th antenna element and N is the order of the PSK signal constellation [51]. In this case, the input power for the combination of N-PSK signals can be expressed as

$$\begin{aligned} P_E = i_0^2 R_{in} &= P_T |s_0|^2 \Re \left(Z_{00} + \sum_{m=1}^{M-1} Z_{0m} \exp\left(j\left(\phi_m - \phi_0\right)\right) \right) \\ &= P_T \left(R_0 + \sum_{m=1}^{M-1} \left(R_m \cos \frac{2\pi\left(n_m - n_0\right)}{N} - X_m \sin \frac{2\pi\left(n_m - n_0\right)}{N} \right) \right), \end{aligned} \tag{4.21}$$

The corresponding input power for two signal periods is

$$\begin{aligned} P_E^{(1)} = i_0^2 R_{in} &= P_T \left(R_0 + R_1 \cos \frac{2\pi\left(n_m - n_0\right)}{N} - X_1 \sin \frac{2\pi\left(n_m - n_0\right)}{N} \right), \\ P_E^{(2)} = i_0^2 R_{in} &= P_T \left(R_0 - R_1 \cos \frac{2\pi\left(n_m - n_0\right)}{N} + X_1 \sin \frac{2\pi\left(n_m - n_0\right)}{N} \right). \end{aligned} \tag{4.22}$$

Therefore, in order to transmit different N-PSK signals for each antenna element, the MCM of the EA is required to satisfy

$$\mathbf{Z} \in \left\{ \mathbf{Z} \middle| \frac{P_{min}}{P_T} < R_0 \pm \left(R_1 \cos\left(\phi_1 - \phi_0\right) - X_1 \sin\left(\phi_1 - \phi_0\right)\right) < \frac{P_{max}}{P_T} \right\}. \tag{4.23}$$

It can be noted that the input power varies with R_0, R_1 and X_1 (defined by the MCM), the required transmitted power and the phases of transmitted signals. When the transmitter

uses BPSK, then the MCM is required to satisfy that $P_{min} < P_T\left(R_0 \pm R_1\right) < P_{max}$. Note that the power of an EA increases linearly with R_0. Based on recent studies [16, 19], two approaches to achieve stable transmission using an ESPAR antenna (EA) are to increase the self-resistance of an EA [16] or to transmit signals closely approximating the actual signals that keep the EA stable as proposed in Chapter 3. Both approaches did not take into account the impact of limited power on an EA transmission, which is a practical constraint on power amplifier design. After taking into account the instantaneous total power requirement in this chapter, as shown in 5.21, when P_T is a fixed value and the mutual coupling impedance are fixed, increasing R_0 would increase the input power to the EA $P_E^{(1)}$ and $P_E^{(2)}$, which could be greater than P_{max}. It is desirable to have a reasonable value of self resistance, which is not too large and neither too small. The larger the value of R_0, the more likely that the input impedance will remain positive and the EA will remain stable for most transmission signals. However, it will consume a large amount of power as can be noted from (4.1). Small values of R_0 will more likely cause the input impedance to become negative for more transmission signals. This implies that, the larger the value of R_0, the more likely EA will remain stable for the majority of signals. The lower the value of R_0, the more likely the EA will exhibit unstable behaviour for a large set of signals. A more detailed discussion on this is given in [19]. Thus, for a system with limited power, P_{max}, it is undesirable to have a high R_0 when considering the peak power constraint of the power amplifier. However, as shown in [19], a higher value of R_0 increases the stability of an EA. This also highlights the importance of considering the peak power constraint of the power amplifier in this chapter.

Simulation Results

The SER performance of the system where the transmitter employs Alamouti code is shown in Figure 4.3. The performance is plotted against SNR and it is defined as the ratio of the radiated power to the noise power i.e. SNR$= P_T/N_0$. P_T is the transmitted signal power from the EA. Noise is assumed to be additive white Gaussian noise (AWGN) with zero mean and unit variance, therefore, it is equivalent to the transmission SNR. The modulation scheme is 16-QAM and the SER performance of an EA using our proposed algorithm is compared to the SER performance of a standard multiple antenna transmitter. The EA using our proposed algorithm is denoted by EA-P and the standard multiple antenna transmitter is denoted

by SMA. For the simulation, we select three practical 2-element EAs, $\mathbf{Z}^{(1)}$, $\mathbf{Z}^{(2)}$, and $\mathbf{Z}^{(3)}$, whose MCMs have been given in Chapter 3.4.2. The values of self-resistance for $\mathbf{Z}^{(1)}$, $\mathbf{Z}^{(2)}$ and $\mathbf{Z}^{(3)}$ are 45.12, 52.81 and 465.4 , respectively. The EA with $\mathbf{Z}^{(3)}$ has the largest self-resistance designed to overcome the stability problem for an EA transmitter [16]. Without loss of generality $P_{min} = 0$ and $P_{max} = 100, 150$. p_{max} is the amount of power delivered to the antenna and it includes the power radiated and dissipated by the antenna [17]. For the EAs with $\mathbf{Z}^{(1)}$ and $\mathbf{Z}^{(2)}$, the SER for the EA transmission is slightly higher compared to the SMA system. This can be expected because, unlike the SMA, the EA is transmitting approximate signals instead of the ideal signals. It is noted that the performances of $\mathbf{Z}^{(1)}$, $\mathbf{Z}^{(2)}$ and , $\mathbf{Z}^{(3)}$ are similar to the results in Figure 3.5 in Chapter 3 up to $P_T = 12$ dB. However, after $P_T = 12$dB, the performance here degraded and this is due to the limited input power constraint from the single power amplifier of an ESPAR antenna when it is used to provide multiple antenna functionality. The EA with $\mathbf{Z}^{(3)}$ was designed to overcome the stability problem for an EA transmitter in [16]. However, considering the maximal power requirement of EA, it consumes large power as the self-resistance at the active element is large. Due to this large self-resistance, in order to meet the power constraint the symbol transmission power is reduced which results in significantly degraded performance. This shows that achieving stability by increasing the self-resistance is highly power inefficient approach.

4.4.1.2 Transmitter with CSI

When the transmitter has CSI, transmit diversity can be achieved by employing maximal ratio transmission (MRT) [74]. Assuming that symbol s is to be transmitted, the symbols are precoded and mapped to the antenna currents. Let $\mathbf{h} = [h_0, h_1, \ldots, h_{M-1}]^H \in \mathbb{C}^{M\times 1}$ and h_m denotes the channel from the $(m+1)$-th element of EA transmitter to the signal antenna receiver. h_m is a Rayleigh random variable with unit variance. The ideal port current at the transmitter is $\hat{\mathbf{i}} = \sqrt{P_T}\frac{\mathbf{h}}{\|\mathbf{h}\|}s$. For N-PSK modulation, the corresponding power consumption

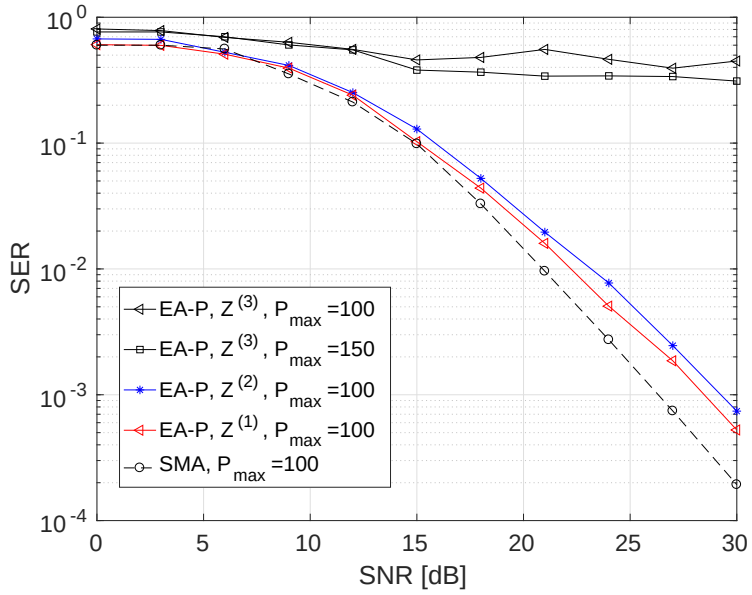

Figure 4.3: SER performance comparison of the ESPAR transmitter and the standard multiple antenna transmitter employing Almouti scheme with 16-QAM modulation under stability and power constraints.

at the active element can be obtained as

$$\begin{aligned} P_E &= P_T \left(\frac{h_1 s}{\|\mathbf{h}\|}\right)^2 \Re\left(Z_{00} + \frac{\sum_{m=1}^{M-1} Z_{0m} h_j}{h_0}\right) \\ &= P_T \|s\|^2 \left(\frac{h_0}{\|\mathbf{h}\|}\right)^2 \left(R_0 + \Re\left(\frac{\sum_{m=1}^{M-1} Z_{0m} h_j}{h_0}\right)\right). \end{aligned} \tag{4.24}$$

It can be noted that the input power varies with channel and the MCM, and that it is independent of the data symbols. This implies that, for the EA, in the case of a block fading channel, in which the channel is constant over a block of symbols, the antenna only needs to be preprocessed once in the beginning of the block for Step 1 to Step 7 in the algorithm 3.

Simulation Results

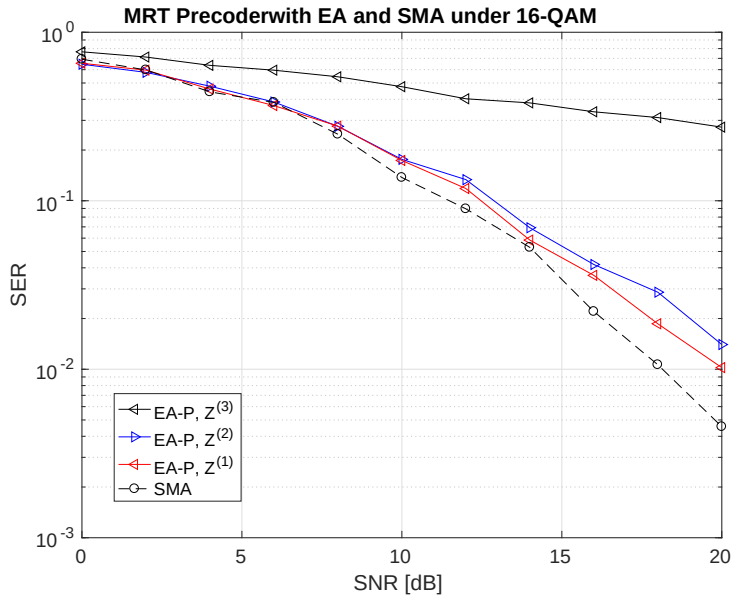

Figure 4.4: SER performance comparison of the EA transmitter and the standard multiple antenna transmitter employing MRT scheme with 16-QAM modulation under stability and power constraints.

Considering MRT scheme, the SER performances are compared for EAs with different number of elements and spacings in Fig. 4.4 and Fig. 4.5. In Fig. 4.4, it can be observed that the SER performance of EAs with MCM $\mathbf{Z}_1$ and $\mathbf{Z}_2$ is similar to that of the standard multiple antenna transmitter especially at low SNRs. Similar to Fig. 4.3 as P_T increases, the power consumed by the antenna approaches P_{max} and an error floor occurs. However, again, with the maximal power constraint, the EA with $\mathbf{Z}^{(3)}$ is unable to achieve SER close to the SER of a standard multiple antenna system.

As shown in Fig. 4.5, The mutual coupling matrices for different number of antenna elements are obtained using the induced electromotive force method (IEFM) for different antenna spacing [73]. The SER performance for two different antenna spacing $d = \frac{\lambda}{4}$ for linear EAs are shown in the Fig. 4.5. It can be observed from this figure that the SER performance varies with the number of antenna elements and the antenna spacing. Increasing the number of the elements or reducing antenna spacing reduces the SER.

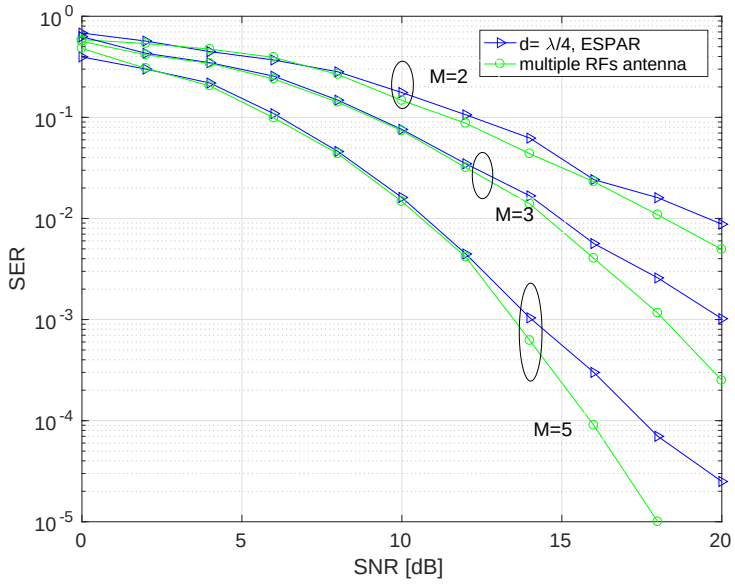

Figure 4.5: SER performance comparison of the EA transmitter and the standard multiple antenna transmitter with different number of antenna elements employing MRT scheme under stability and power constraints.

4.4.2 Multi-user Scenario

Next, we investigate the application of the proposed antenna to MU-MIMO systems. We consider the downlink multi-user scenario where the base station communicates with several single-antenna users. Let us assume the transmitting vector $\mathbf{s} = \{s_1, s_2, \ldots, s_K\}$, in which, u_k denotes the transmit symbol to the k-th user. the ideal current vector is the function of transmit symbol. The desired transmitted current vector $\mathbf{i}$ can be expressed as

$$\mathbf{i} = \mathbf{F}\mathbf{s}. \tag{4.25}$$

At the base station, the symbol vector for user is precoded. We consider CI and RCI as precoding schemes for downlink transmissions. Denoting the precoding matrix by $\mathbf{F} \in \mathbb{S}^{M\times K}$, we have that

$$\mathbf{F} = \begin{cases} \mathbf{H}^H \left(\mathbf{H}\mathbf{H}^H\right)^{-1} & CI, \\ \mathbf{H}^H \left(\mathbf{H}\mathbf{H}^H + \sigma^2 \mathbf{I}_{M-1}\right)^{-1} & RCI. \end{cases} \tag{4.26}$$

Then the transmit current vector can be expressed as $\hat{\mathbf{i}} = \sqrt{P_T}\mathbf{Fs}$, and the corresponding power consumption for an EA is

$$P_E^{(1)} = i_1^2 R_{in} = P_T \left|(\mathbf{Fs})^{(0)}\right|^2 \Re\left(Z_{00} + \frac{\sum_{m=1}^{M-1} Z_{0m}(\mathbf{Fs})}{(\mathbf{Fs})^{(0)}}\right), \tag{4.27}$$

where $(\mathbf{Fs})^{(0)}$ denotes the first elemnent of the vector $(\mathbf{Fs})$.

Simulation Results

In the simulation, EA is employed at the base station and serve two single-antenna users. The MCM is calculated by induced electromotive force method (IEFM) [95] for thin half-wavelength electrical dipoles EA. The antenna spacing is assumed to $d = \lambda/4$, where λ denotes the wavelength at 2.6 GHz. The modulation scheme in the simulations is QPSK. The SER performances are compared for EAs with different number of antenna elements in Figure 4.6 for CI and RCI algorithms. Again, the SER performance of the EA transmitter is similar to that of the standard multiple antenna transmitter at low P_T. At high P_T, the performance saturates due to limited maximum power. The SER performance at the high P_T is limited by the constraint of the maximal power. Due to this constraint, the SER performance cannot keep increasing when the desired transmitted power reaches a certain limit value. Moreover, RCI gives better performance compared to CI as it takes into account the noise power.

4.5 Summary

Considering limited power availability, we have proposed a new algorithm to achieve stable signal transmission using an EA in this chapter.

The conclusions in this chapter are:

- To transmit signals that might lead to power consumption beyond the limits of the transmitter and might lead to oscillatory/unstable behaviour of an EA transmitter, we have proposed a new method to formulate and solve this problem. Signals closely

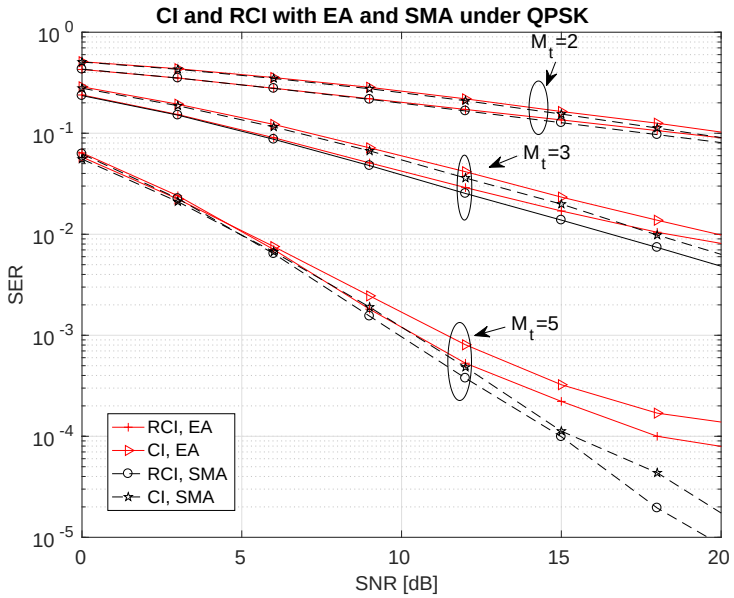

Figure 4.6: SER performance comparison of the EA transmitter and standard multiple antenna transmitter in the case of RCI and CI scheme with QPSK under stability and power constraints.

approximating the ideal signals are transmitted. These approximate signals guarantee the stability of the EA and satisfy the peak power requirements. Specifically, to obtain the approximate signal, an optimisation problem has been formulated to minimise the MSE between the ideal and the approximated signal while considering the stability and peak power requirements of the EA.

- Considering the implementation stability of the EA and the maximum power requirements, an optimisation problem has been proposed to minimise the MSE between the ideal and the approximated signals. The underlying problem is originally not convex. There are a quadratic objective function and two non-convex quadratic constraints, and the strong duality conditions used in chapter 3 cannot be applied to this problem. Instead, coordinate transformations and geometric methods have been applied to find the optimal approximate signals.

- The SER performance of our proposed algorithm has been compared to that of a standard multiple antenna transmitter in both single-user and multi-user scenarios. As an example, we have analysed the SER performances of the EA for Alamouti coded transmission and the maximum ratio transmission in the single-user scenario. Moreover,

the proposed scheme has been analysed for CI and RCI precoders for the multi-user case. Our results have shown that a system employing an EA transmitter and using our proposed algorithm gives performance similar to a system with a standard multiple antenna transmitter for some antenna design.

In general, it has been seen that the system employing the proposed transmission scheme gives similar performance to that of a standard multiple antenna system, especially at low SNRs. In addition, it has been shown that improving the stability by increasing the self-resistance [55] proportionally increases the power consumption, and thus for practical systems with limited power, it is highly power inefficient and infeasible. These results have been verified through extensive simulation of an EA system in various communication scenarios.

The transceiver design with ESPAR antennain MIMO systems has been considered in Chapter 3 and chapter 4. In Chapter 5, we also consider another single-RF antenna with load modulated array architecture as proposed in HARP project [8, 58] and this antenna has been applied into CRANs.

Chapter 5
Energy Efficiency of Cloud Radio Access Network with Single RF Chain Antennas

5.1 Introduction

As discussed in Chapter 2, cloud ran access networks (CRANs) have recently triggered enormous research interest as one possible way to enable highly efficient resource utilisation in 5G and beyond mobile networks [76, 77]. In CRANs, multiple remote radio heads (RRHs) are connected to a baseband unit (BBU) via optical fibre [78]. One advantage of this system is its flexibility and adaptability to enable optimised energy consumption [79, 80]. Moreover, due to greatly increased data rates, economic reasons, and environmental concerns about sustainable growth, energy consumption is one of the most urgent and critical challenges in the design of future mobile networks. Therefore, energy efficiency (EE) has been widely utilised as a metric to find an optimal approach for the trade-off between the achievable data transmission rate and energy consumption in wireless communications. Recently, many efforts have been devoted to optimising EE performance [9, 10, 81–83]. In [81], a transmission scheme with proportional fairness between spectral efficiency (SE) and energy consumption has been proposed for the downlink multi-user CRANs. The SE-EE trade-off and a power control scheme to maximise EE have been studied for a single element antenna user and single antenna RRHs in [9, 83] respectively. Large scale distributed CRANs with a single antenna element at the transmitter and the receiver have been investigated in [10]. Meanwhile, a precoding scheme for CRANs with multiple radio frequency (RF) chains has been studied to maximise capacity in [82]. However, most of the studies focus on a system where RRHs and users are equipped with a single antenna element or standard multiple antenna with multiple RF chains.

In this chapter, we consider CRANs employing a single-RF antenna at RRHs for single- and multi-user systems. RRHs are placed at different locations in a cell and connected to a BBU

through optical fibres. In this chapter, the transmission strategy (precoding and power allocation) is designed to maximize the energy efficiency when the instantaneous channel gains are known perfectly at both the transmitter and the receiver. For a single-user system, closed-form expressions for precoding and power allocation are derived that are applicable not only for single-RF MIMO systems, but also for standard multiple antenna systems with multiple RF chains. We then consider the multi-user generalisation of this optimisation problem. Furthermore, we compare the EE performance of single-RF and standard multiple antenna systems for single- and multi-user systems. It is shown that the system with a single-RF antenna provides superior EE performance. After that, the proposed algorithms are applied into EA.

The contributions in this chapter are

- An EE maximisation problem is formulated to obtain optimal precoding and power allocation schemes during signal transmission; it is solved by a suboptimal decomposition strategy.
- In the single-user system, the optimisation problem is simplified. We obtain the closed-form expressions for precoding and power allocation among different RRHs to maximise the EE in the system.
- In the multi-user system, the optimisation problem is formulated by introducing zero-forcing (ZF) constraints for multi-user interference cancellation. We obtain the closed-form expressions for precoding and power allocation among different users to maximise the EE.
- We compare the EE performance of single-RF antenna and standard multiple antenna systems for both single- and multiple-user scenarios. It is shown that the EE systems outperform the standard multiple antenna systems in all cases.
- We discuss the applications and constraints of CRANS with ESPAR antennas and load modulated array at RRHs with the proposed algorithms. Moreover, for both single- and multi-user systems, the optimal configuration of a circular EA is derived to achieve the maximal EE during signal transmission.

The remainder of this chapter is organised as follows. The system model is presented in Section 5.2. In Section 5.3, an EE maximisation optimisation problem is formulated. The optimal precoding and power allocation are then described for the single-user scenario in Section 5.4. The multi-user generalisation of this optimisation problem is investigated in Section 5.5. The applications and constraints of CRANS with ESPAR antennas and load modulated array at RRHs with the proposed algorithms are discussed in section 5.6. Numerical results are presented in section 5.7, followed by conclusions in Section 5.8.

5.2 System Model

As described in Chapter 2 and as shown in Fig. 5.1 , we consider downlink transmission from N RRHs to K users. RRHs are connected with a BBU via optical fibre. The RRHs have single-RF antennas, which can provide multi-antenna-like functionality. All users are equipped with a single antenna element. All RRH ports and the users are assumed to possess perfect CSI. After transmission from RRHs, the signal received by the k-th user is given by

$$y_k = \underbrace{\sum_{t=1}^{N} \mathbf{h}_{k,t}^H \mathbf{w}_{k,t} s_k^{DL}}_{\text{desired signal}} + \underbrace{\sum_{t=1}^{N} \left(\sum_{j=1, j\neq k}^{K} \mathbf{h}_{k,t}^H \mathbf{w}_{j,t} s_j^{DL} \right)}_{\text{interference}} + \underbrace{n_k}_{\text{noise}}, \tag{5.1}$$

The corresponding EE, η_{ee}, which is definited as the ratio of data transmission rate (in bit/second) and the total power consumption (in Watt = Joule/second) [85] in chapter 2, is given by

$$\eta_{ee} = \frac{R}{P_{tot}} = \frac{\Omega \sum_{k=1}^{K} \log_2 \left(1 + \frac{\left| \mathbf{h}_k^H \mathbf{w}_k \right|^2}{\sum_{j=1, j\neq k}^{K} \left| \mathbf{h}_k^H \mathbf{w}_j \right|^2 + \sigma_n^2} \right)}{P_{bbu} + P_{fibre} + P_{rrh} + K P_{user}^{DL}}. \tag{5.2}$$

It is noted that the rate clearly R in the numerator goes down with distance. However, the power consumption on the fiber, $P_{fibre} = N P_{op} R$ in the denominator, goes down with distance due to dependence on the rate R. Then it is difficult to know how η_{ee} changes with the distance.

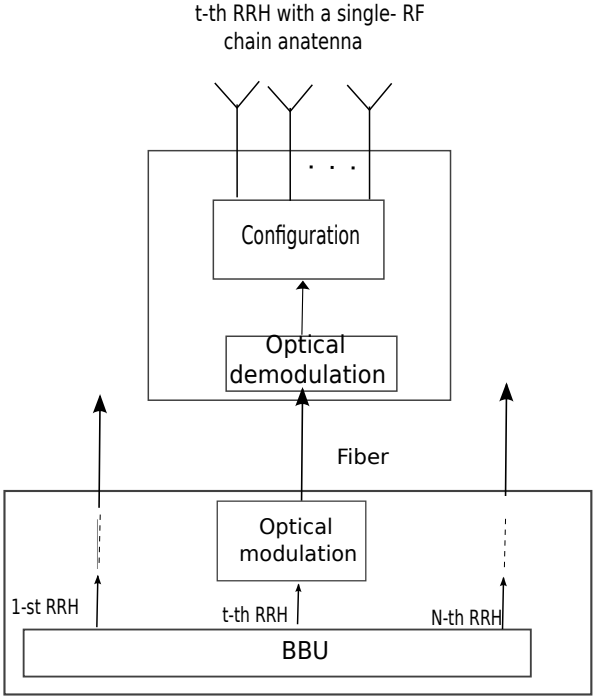

Figure 5.1: A BBU and N RRHs with single-RF chain antennas

5.3 Problem Formulation

To derive low-complexity precoders to eliminate multi-user interference, we introduce ZF constraints [86] into the optimisation problem and the ZF constraints can be expressed as

$$\mathbf{h}_k^H \mathbf{w}_j = 0, \text{for } j, k = 1, 2, \ldots, K \text{ and } j \neq k.$$

Therefore, in order to realise signal transmission, the problem to obtain precoding and power allocation at each RRH can be formulated as an optimisation problem to maximise the EE, and it can be written as

$$\max_{\mathbf{w}_1, \mathbf{w}_2, \ldots, \mathbf{w}_k, \mathbf{p}^U} \quad \eta_{ee} = \frac{\Omega \sum_{k=1}^{K} \log_2 \left(1 + \frac{\left|\mathbf{h}_k^H \mathbf{w}_k\right|^2}{\sigma_n^2}\right)}{P_{bbu} + P_{fibre} + P_{rrh} + K P_{user}^{DL}} \tag{5.3a}$$

$$\text{s.t.} \quad \sum_{k=1}^{K} \mathbf{w}_{k,t}^H \mathbf{w}_{k,t} = P_t^{RRH}, \tag{5.3b}$$

$$\sum_{t=1}^{N} \mathbf{w}_{k,t}^H \mathbf{w}_{k,t} = P_k^U, \tag{5.3c}$$

$$\mathbf{h}_k^H \mathbf{w}_j = 0, \text{for } j \neq k, \tag{5.3d}$$

$$\forall\, t \in \{1, 2, \ldots, N\}, k \in \{1, 2, \ldots, K\},$$

$$j \in \{1, 2, \ldots, K\},$$

where (5.3a) is the objective function involving the EE for the whole system. (5.3b) and (5.3c) are the average transmission power constraints for each RRH and each user, respectively. The problem is not convex. In order to obtain closed-form expressions, suboptimal decomposition is applied to solve this problem. This optimisation problem is simplified for the single-user scenario in Section 5.4. The mathematical analysis and approaches are then extended to the multi-user scenario to solve this optimisation problem in Section 5.5.

5.4 Energy Efficiency for Single-user Systems

In this section, we assume that $K = 1$. In a single-user system, the optimisation problem in (5.3) is simplified as

$$\max_{\mathbf{w}_{1,t}, P_t^{RRH}} \quad \eta_{ee} = \frac{\Omega \log_2\left(1 + \frac{|\mathbf{h}_1^H \mathbf{w}_1|^2}{\sigma_n^2}\right)}{P_{bbu} + P_{fibre} + P_{rrh} + P_{user}^{DL}} = \frac{\Omega \log_2\left(1 + \frac{|\sum_{t=1}^{N} \mathbf{h}_{1,t}^H \mathbf{w}_{1,t}|^2}{\sigma_n^2}\right)}{P_{bbu} + P_{fibre} + P_{rrh} + P_{user}^{DL}} \tag{5.4a}$$

$$\text{s.t.} \quad \mathbf{w}_{1,t}^H \mathbf{w}_{1,t} = P_t^{RRH}, \tag{5.4b}$$

We obtain the closed-form expression of $\mathbf{w}_{1,t}$ to maximise EE, which depends on the beamformer and the allocated power scheme at t-th RRH.

5.4.1 Optimal Precoding Vectors

The power allocated to the t-th RRH is assumed to be P_t and the optimal value will be discussed later. The optimal precoder is formulated as an optimisation problem to maximise

EE under the power constraint (5.4b) and is given by

$$\left(\mathbf{w}_{1,1}^{*}, \mathbf{w}_{1,2}^{*}, \ldots, \mathbf{w}_{1,N}^{*}\right) = \underset{\mathbf{w}_{1,1},\mathbf{w}_{1,2},\ldots,\mathbf{w}_{1,N}}{\arg\max} \ \eta_{ee}, \tag{5.5a}$$

$$\text{s.t.} \quad \mathbf{w}_{1,t}^{H}\mathbf{w}_{1,t} = P_{t}^{RRH}, \forall t \in \{1, 2, \ldots, N\}.$$

Proposition 11 *The closed-form expressions of the precoders at the t-th RRH in CRANs to the optimisation problem* (5.5) *are*

$$\mathbf{w}_{1,t}^{*} = \sqrt{P_{t}^{RRH}} \frac{\mathbf{h}_{1,t}}{\|\mathbf{h}_{1,t}\|}, \forall t \in \{1, 2, \ldots, N\},$$

with power constraint for the t-th RRH, P_{t}^{RRH}.

Proof: The proof is provided in Appendix F. ■

It is noted that the precoder for the RRHs obtained depends on the channel conditions and is similar to the ones used for MRT [74].

5.4.2 Power Allocation for Distributed RRHs

In order to find the optimal allocated power to RRHs, we list the following lemma which has been proved in [11, Lemma3] as

Lemma 1 *The optimisation problem*

$$\max_{a+bx\geq 0,\ a,b,c,d\geq 0} \frac{\log_2(a+bx)}{c+dx}, \tag{5.6}$$

has a unique solution for x and it is given as

$$x = \frac{\exp(w(\frac{bc}{de} - \frac{a}{e}) + 1) - a}{b}, \tag{5.7}$$

where $w(x)$ is the Lambert W function.

From now on, we derive the optimal power allocation scheme by using this lemma. Substituting Proposition 11 into (2.54), the rate simplifies as

$$R = r_1 = \Omega \log_2 \left(1 + \frac{\left(\sum_{t=1}^{N} \sqrt{P_t} \|\mathbf{h}_{1,t}\| \right)^2}{\sigma_n^2} \right). \tag{5.8}$$

Substituting (5.8) into (2.55), the EE is given by

$$\begin{aligned} \eta_{ee} &= \frac{\Omega \log_2 \left(1 + \frac{\left(\sum_{t=1}^{N} \sqrt{P_t^{RRH}} \|\mathbf{h}_{1,t}\| \right)^2}{\sigma_n^2} \right)}{P_{bbu} + N P_{op} \Omega \log_2 \left(1 + \frac{\left(\sum_{t=1}^{N} \sqrt{P_t^{RRH}} \|\mathbf{h}_{1,t}\| \right)^2}{\sigma_n^2} \right) + \sum_{t=1}^{N} \left(P_t^{RRH} \frac{\zeta}{\eta} + \left(N_{RF}^{(t)} P_t^c \right) \right) + P_{user}^{DL}} \\ &= \frac{\Omega}{1/\delta + N P_{op} \Omega} \end{aligned} \tag{5.9}$$

where

$$\delta = \frac{\log_2 \left(1 + \left(\sum_{t=1}^{N} \sqrt{P_t^{RRH}} \frac{\|\mathbf{h}_{1,t}\|}{\sigma_n} \right)^2 \right)}{P_{bbu} + \sum_{t=1}^{N} \left(N_{RF}^{(t)} P_t^c \right) + P_{user}^{DL} + \frac{\zeta}{\eta} \sum_{t=1}^{N} P_t^{RRH}}. \tag{5.10}$$

Let

$$\rho_t = \frac{\|\mathbf{h}_{1,t}\|}{\sigma_n}$$

and

$$P_{tpi} = P_{bbu} + \sum_{t=1}^{N} \left(N_{RF}^{(t)} P_t^c \right) + P_{user}^{DL},$$

then δ can be simplified as

$$\delta = \frac{\log_2 \left(1 + \left(\sum_{t=1}^{N} \sqrt{P_t^{RRH}} \rho_t \right)^2 \right)}{P_{tpi} + \frac{\zeta}{\eta} \sum_{t=1}^{N} P_t^{RRH}}. \tag{5.11}$$

As δ and η_{ee} are positive, η_{ee} increases monotonically with δ from (5.9). The objective function in (5.4a) can be replaced by maximising δ. Thus, we have an optimisation problem with

respect to $\mathbf{p}^{RRH} = \left[P_1^{RRH}, P_2^{RRH}, \ldots, P_N^{RRH}\right]^T$ as

$$\mathbf{p}^{RRH*} = \arg\max_{\mathbf{p}^{RRH}} (\eta_{ee}) = \arg\max_{\mathbf{p}^{RRH}} (\delta). \tag{5.12}$$

Proposition 12 *In order to maximise EE for CRANs in which all RRHs serve one user, the power allocated to different RRHs satisfies*

$$\frac{P_1^{RRH}}{\rho_1^2} = \frac{P_2^{RRH}}{\rho_2^2} = \cdots = \frac{P_N^{RRH}}{\rho_N^2}, \tag{5.13}$$

where P_t^{RRH} is the power allocated to the t-th RRH, and $\rho_t = \frac{\|\mathbf{h}_{1,t}\|}{\sigma_n}$.

Proof: By applying the first-order necessary condition for optimality, it is required to satisfy the condition $\forall t, \frac{\partial \delta}{\partial P_t^{RRH}} = 0$ when the allocated power vector $\mathbf{p}^{RRH*}$ is an optimal point.

The partial derivative equation of δ with respect to P_t^{RRH} is

$$\begin{aligned}\frac{\partial \delta}{\partial P_t^{RRH}} = & \frac{\rho_t}{\sqrt{P_t^{RRH}}} \frac{\log_2 e}{2\left(1 + \left(\sum_{t=1}^{N} \sqrt{P_t^{RRH}}\rho_t\right)^2\right)\left(P_{tpi} + \frac{\zeta}{\eta}\sum_{t=1}^{N} P_t^{RRH}\right)} \\ & - \frac{\frac{\zeta}{\eta}\log_2\left(1 + \left(\sum_{t=1}^{N} \sqrt{P_t^{RRH}}\rho_t\right)^2\right)}{\left(P_{tpi} + \frac{\zeta}{\eta}\sum_{t=1}^{N} P_t^{RRH}\right)^2}.\end{aligned} \tag{5.14}$$

As $\forall t, \frac{\partial \delta}{\partial P_t^{RRH}} = 0$, Proposition 12 is proved. ■

Let $P_b = \frac{P_t^{RRH}}{\rho_t^2}$, we have $P_t^{RRH} = \rho_t^2 P_b$. By substituting it into (5.11), we have

$$\delta = \frac{\log_2\left(1 + P_b\left(\sum_{t=1}^{N} \rho_t^2\right)^2\right)}{P_{tpi} + P_b\frac{\zeta}{\eta}\sum_{t=1}^{N} \rho_t^2}. \tag{5.15}$$

The problem (5.12) can be further reformulated as

$$\begin{aligned} P_t^{RRH*} &= \rho_t^2 P_b^*, \quad \text{for } t = 1, 2, \ldots, N, \\ P_b^* &= \arg\max_{P_b} (\delta) . \end{aligned} \tag{5.16}$$

The solution of this optimisation problem is provided in the following proposition.

Proposition 13 *In order to maximise EE for CRANs in which all RRHs serve one user, the closed-form expression for the power allocated to the t-th RRH is given by*

$$P_t^{RRH*} = \rho_t^2 \frac{\exp(w(\frac{\left(\sum_{t=1}^N \rho_t^2\right) P_{tpi}}{e\frac{\zeta}{\eta}} - \frac{1}{e}) + 1) - 1}{\left(\sum_{t=1}^N \rho_t^2\right)^2}, \tag{5.17}$$

where

$$P_{tpi} = P_{bbu} + \sum_{t=1}^{N} \left(N_{RF}^{(t)} P_t^c \right) + P_{user}^{DL}.$$

Proof: From Lemma 1, by setting $a = 1$, $b = \left(\sum_{t=1}^N \rho_t^2\right)^2$, $c = P_{tpi}$, and $d = \frac{\zeta}{\eta} \sum_{t=1}^N \rho_t^2$, the optimal P_b^* is given by

$$P_b^* = \frac{\exp\left(w\left(\frac{\left(\sum_{t=1}^N \rho_t^2\right) P_{tpi}}{e\frac{\zeta}{\eta}} - \frac{1}{e}\right) + 1\right) - 1}{\left(\sum_{t=1}^N \rho_t^2\right)^2}. \tag{5.18}$$

After substituting (5.18) into (5.16), we obtain (5.17). ■

It is to be noted that the allocated power among different RRHs depends on the channel condition. The amount of power is proportional to the channel condition. We allocate higher power to the RRH which has better channel condition, and less power to the RRH when its channel is poor. We can obtain the optimal $\mathbf{w}_{1,t}$ by substituting Proposition 13 into Proposition 11.

5.5 Energy Efficiency for Multi-user Systems

The analysis on single-user systems in the previous section reveals a number of interesting results regarding the CRANs with single-RF antennas. However, practical CRANs support multiple users with interference among each other, and it is therefore intriguing to explore how single-RF antennas are employed at the RRHs to support multiple users. In this section, we investigate the application of the multi-user CRANs where all RRHs are equipped with single-RF antennas. The closed-form expressions of precoding under ZF constraints are derived to maximise the EE, and power allocation among different users and different RRHs is proposed in this subsection.

5.5.1 Optimal Precoding

When the power allocated to the k-th user is assumed to be P_k^U, from (5.3), the optimal precoders for all users can be formulated as an optimisation problem to maximise EE under the user power and ZF constraints, and it is given by

$$(\mathbf{w}_1^*, \mathbf{w}_2^*, \ldots, \mathbf{w}_k^*) = \underset{\mathbf{w}_1, \mathbf{w}_2, \ldots, \mathbf{w}_k}{\arg\max} \quad \eta_{ee}, \tag{5.19a}$$

$$\text{s.t.} \quad \mathbf{w}_k^H \mathbf{w}_k = P_k^U, \tag{5.19b}$$

$$\mathbf{h}_j^H \mathbf{w}_k = 0, \tag{5.19c}$$

$$k \neq j. \tag{5.19d}$$

The subspace decomposition method [86] is introduced to find precoders under ZF constraints. Let $\mathbf{H}^{DL}$ denote the total downlink channel from all RRHs to all users and it can be expressed as $\mathbf{H}^{DL} = [\mathbf{h}_1, \mathbf{h}_2, \ldots, \mathbf{h}_K]^H \in \mathbb{C}^{K \times M_{tot}}$. The pseudo-inverse of $\mathbf{H}^{DL}$ can be expressed as $\mathbf{H}^{\dagger} = \left(\mathbf{H}^{DL}\left(\mathbf{H}^{DL}\right)^H\right)^{-1}\mathbf{H}^{DL}$. Let $\mathbf{a}_k \in \mathbb{C}^{M_{tot} \times 1}$ denotes the k-th coloum of $\mathbf{H}^{\dagger}$ and $\mathbf{U}$ denotes a matrix whose columns are orthonormal basis for the null space of $\mathbf{H}^{DL}$. Then we have $\mathbf{h}_j^H \mathbf{a}_k = 0$ for $j \neq k$ and $\mathbf{h}_j^H \mathbf{U} = 0$. The precoders for the k-th user under the

ZF constraints can be expressed as

$$\mathbf{w}_k = \xi_k \mathbf{a}_k + \mathbf{U}\mathbf{q}_k, \tag{5.20}$$

where ξ_k and $\mathbf{q}_k$ are corresponding weighting coefficients. By substituting it into (5.3c), the total transmit power to the k-th user can be rewritten as

$$\begin{aligned} P_k^U &= \mathbf{w}_k^H \mathbf{w}_k = \left(\xi_k \mathbf{a}_k + \mathbf{U}\mathbf{q}_k\right)^H \left(\xi_k \mathbf{a}_k + \mathbf{U}\mathbf{q}_k\right) \\ &= \xi_k^2 \mathbf{a}_k^H \mathbf{a}_k + \|\mathbf{U}\mathbf{q}_k\|^2. \end{aligned} \tag{5.21}$$

After substituting (5.20) and (5.21) into (5.19), the optimisation problem is reformulated as

$$(\xi_1^*, \mathbf{q}_1^*, \xi_2^*, \mathbf{q}_2^*, \ldots \xi_K^*, \mathbf{q}_K^*) = \underset{\xi_1, \mathbf{q}_1, \xi_2, \mathbf{q}_2, \ldots \xi_K, \mathbf{q}_K}{\arg\max} \eta_{ee}, \tag{5.22a}$$

$$\text{s.t.} \quad \xi_k^2 \mathbf{a}_k^H \mathbf{a}_k + \|\mathbf{U}\mathbf{q}_k\|^2 = P_k^U. \tag{5.22b}$$

Proposition 14 *The closed-form expression of the precoder for the k-th user to maximise the EE in CRANs is given as*

$$\mathbf{w}_k^* = \sqrt{\frac{P_k^U}{\mathbf{a}_k^H \mathbf{a}_k}} \mathbf{a}_k, \tag{5.23}$$

with power constraint for the k-th user, P_k^U and ZF constraints.

The precoders for the k-th user at the t-th RRH is

$$\mathbf{w}_{k,t}^* = \sqrt{\frac{P_k^U}{\mathbf{a}_k^H \mathbf{a}_k}} a_k^{\left(\sum_{j=1}^{t-1} M_j + 1 : \sum_{j=1}^{t} M_j\right)} \tag{5.24}$$

where $a_k^{\left(\sum_{j=1}^{t-1} M_j + 1 : \sum_{j=1}^{t} M_j\right)}$ denotes a vector whose elements is from $\left(\sum_{j=1}^{t-1} M_j + 1\right)$-th to the $\left(\sum_{j=1}^{t} M_j\right)$-th element of the vector $\mathbf{a}_k$.

Proof: The proof is provided in Appendix G. ■

It should be noted that the precoder depends on the channel conditions and it is implemented at the base station.

5.5.2 Optimal Power Allocation for Multiple Users

By substituting Proposition 14 into (2.54), the rate simplifies as

$$R = \Omega \sum_{k=1}^{K} \log_2 \left(1 + \frac{P_k^U}{\left(\mathbf{a}_k^H \mathbf{a}_k\right) \sigma_n^2} \right). \tag{5.25}$$

We follow the same algebraic manipulations from (5.9) in the Section 5.4.2 for the single-user scenario, the EE can be written as

$$\begin{aligned} \eta_{ee} &= \frac{R}{P_{bbu} + NP_{op}R + \sum_{t=1}^{N} \left(\frac{\zeta}{\eta} \sum_{k=1}^{K} P_{k,t} + N_{RF}^{(t)} P_t^c \right) + KP_{user}^{DL}} \\ &= \frac{\Omega}{1/\delta + NP_{op}\Omega}, \end{aligned} \tag{5.26}$$

where

$$\delta = \frac{\sum_{k=1}^{K} \log_2 \left(1 + \frac{P_k^U}{\left(\mathbf{a}_k^H \mathbf{a}_k\right)\sigma_k^2} \right)}{P_{tpi} + \frac{\zeta}{\eta} \sum_{k=1}^{K} P_k^U}, \tag{5.27}$$

and

$$P_{tpi} = P_{bbu} + \sum_{t=1}^{N} \left(N_{RF}^{(t)} P_t^c \right) + KP_{user}^{DL}. \tag{5.28}$$

The optimisation problem to maximise EE with respect to $\mathbf{p}^U = \left[P_1^U, P_2^U, \ldots, P_k^U\right]^T$ can be reformulated as

$$\mathbf{p}^{U*} = \left[P_1^{U*}, P_2^{U*}, \ldots, P_K^{U*}\right]^T = \arg\max_{\mathbf{p}^U} \left(\eta_{ee}\right) = \arg\max_{\mathbf{p}^U} \left(\delta\right). \tag{5.29}$$

Proposition 15 *To maximise the EE for CRANs in which all RRHs serve K users, the power*

allocated to different users, P_k^U, satisfies

$$\begin{aligned} &\left(\mathbf{a}_{j_m}^H \mathbf{a}_{j_m}\right) \sigma_n^2 + P_1^U = \left(\mathbf{a}_{j_n}^H \mathbf{a}_{j_n}\right) \sigma_n^2 + P_2^U, \quad \forall j_m, j_n \in \mathbb{J}_P \\ &P_{j_m}^U = 0, \quad \forall j_m \notin \mathbb{J}_P \end{aligned} \tag{5.30}$$

where the element j_m in the set $\mathbb{J}_P$ satisfies the conditions that $\frac{\partial \delta}{\partial P_{j_m}^U} = 0$ and that $P_{j_m}^U$ is positive, and $\mathbf{a}_k \in \mathbb{C}^{M_{tot} \times 1}$ is the k-th coloum of $\mathbf{H}^\dagger$ and $\mathbf{H}^\dagger = \left(\mathbf{H}^{DL}\left(\mathbf{H}^{DL}\right)^H\right)^{-1}\mathbf{H}^{DL}$.

Proof: By applying the necessary conditions for optimality, when the allocated power vector $\mathbf{p}^U$ is an optimal point, as [Page 214] [20], the Kuhn-Tucker conditions for the optimality of a power allocation is

$$\begin{aligned} &\frac{\partial \delta}{\partial P_k^U} = 0 \quad \text{if } P_k^U > 0 \\ &\frac{\partial \delta}{\partial P_k^U} \leq 0 \quad \text{if } P_k^U = 0. \end{aligned} \tag{5.31}$$

The partial derivative equation of δ with respect to P_k^U is

$$\begin{aligned} \frac{\partial \delta}{\partial P_k^U} &= \frac{1}{\left(\mathbf{a}_k^H \mathbf{a}_k\right) \sigma_n^2} \frac{1}{1 + \frac{P_k^U}{\left(\mathbf{a}_k^H \mathbf{a}_k\right)\sigma_n^2}} \frac{\log_2 e}{P_{tpi} + \frac{\zeta}{\eta}\sum_{k=1}^K \delta_k} - \frac{\zeta}{\eta} \frac{\sum_{k=1}^K \log_2\left(1 + \frac{P_k^U}{\left(\mathbf{a}_k^H \mathbf{a}_k\right)\sigma_n^2}\right)}{\left(P_{tpi} + \frac{\zeta}{\eta}\sum_{k=1}^K P_k^U\right)^2} \\ &= \left(\frac{1}{\left(\mathbf{a}_k^H \mathbf{a}_k\right) \sigma_n^2 + P_k^U}\right) \frac{\log_2 e}{P_{tpi} + \frac{\zeta}{\eta}\sum_{k=1}^K P_k^U} - \frac{\zeta}{\eta} \frac{\sum_{k=1}^K \log_2\left(1 + \frac{P_k^U}{\left(\mathbf{a}_k^H \mathbf{a}_k\right)\sigma_n^2}\right)}{\left(P_{tpi} + \frac{\zeta}{\eta}\sum_{k=1}^K P_k^U\right)^2}. \end{aligned} \tag{5.32}$$

By setting the set $\mathbb{J}_P$ which contains all the users whose power is positive, based on (5.31) and (5.32), we have (5.30). ■

Let L_J denote the number of elements in the set $\mathbb{J}_P$ and its element are $j_1, j_2, \ldots, j_L$ in an

ascending order. From the proposition 15, for j_m ($j_m \in \mathbb{J}_P$) , we have

$$P_{b1} = \left(\mathbf{a}_{j_m}^H \mathbf{a}_{j_m}\right) \sigma_n^2 + P_{j_m}^U - \frac{\left(\sum_{k=1}^{L_J} \left(\mathbf{a}_{j_k}^H \mathbf{a}_{j_k}\right) \sigma_n^2\right)}{L_J} \tag{5.33}$$

is equal for all users with positive transmitting power levels. By setting

$$x = \sum_{k=1}^{L_J} \log_2 \left(\mathbf{a}_{j_k}^H \mathbf{a}_{j_k} \sigma_n^2\right), \tag{5.34}$$

we have

$$P_{j_m}^U = P_{b1} + \frac{\left(\sum_{j=1}^{L_J} \left(\mathbf{a}_{j_k}^H \mathbf{a}_{j_k}\right) \sigma_n^2\right)}{L_J} - \left(\mathbf{a}_{j_m}^H \mathbf{a}_{j_m}\right) \sigma_n^2. \tag{5.35}$$

After some algebraic manipulations, δ can be further simplified as

$$\begin{aligned} \delta &= \frac{L_J \log_2 \left(P_{b1} + \frac{\sum_{k=1}^{L_J} \left(\mathbf{a}_{j_k}^H \mathbf{a}_{j_k}\right) \sigma_n^2}{L_J}\right) - \sum_{j_k=1}^{L_J} \log_2 \left(\mathbf{a}_{j_k}^H \mathbf{a}_{j_k} \sigma_n^2\right)}{P_{tpi} + \frac{\zeta}{\eta} \sum_{j_k=1}^{L_J} \left(P_{b1} + \frac{\left(\sum_{j_k=1}^{L_J} \left(\mathbf{a}_{j_k}^H \mathbf{a}_{j_k}\right) \sigma_n^2\right)}{L_J} - \left(\mathbf{a}_{j_k}^H \mathbf{a}_{j_k}\right) \sigma_n^2\right)} \\ &= \frac{L_J \log_2 2^{-x/L_J} \left(P_{b1} + \frac{\sum_{k=1}^{L_J} \left(\mathbf{a}_{j_k}^H \mathbf{a}_{j_k}\right) \sigma_n^2}{L_J}\right)}{P_{tpi} + \frac{\zeta}{\eta} L_J P_{b1}}. \end{aligned} \tag{5.36}$$

By substituting it into (5.29), the resulting closed-form expression of P_k^U is given in following proposition.

Proposition 16 *In order to maximise EE for CRANs in which all RRHs serve K users, the closed-form expression for the power allocated to k-th user, P_k^U, is given by*

$$\begin{aligned} P_{j_m}^{U*} &= \frac{\exp\left(w\left(\frac{2^{-x/L_J} P_{tpi}}{\frac{\zeta}{\eta} L_J e} - \frac{2^{-x/L_J} \sum_{k=1}^{L_J} \left(\mathbf{a}_{j_k}^H \mathbf{a}_{j_k}\right) \sigma_n^2}{L_J e}\right) + 1\right)}{2^{-x/L_J}} - \left(\mathbf{a}_{j_m}^H \mathbf{a}_{j_m}\right) \sigma_n^2, \forall j_m \in \mathbb{J}_P \\ P_{j_m}^{U*} &= 0, \qquad \forall j_m \notin \mathbb{J}_P \end{aligned} \tag{5.37}$$

Proof: From Lemma 1, by setting $a = \frac{2^{-x/L_J}\sum_{k=1}^{L_J}\left(\mathbf{a}_{j_k}^H\mathbf{a}_{j_k}\right)\sigma_n^2}{L_J}$, $b = 2^{-x/L_J}$, $c = P_{tpi}$, and $d = \frac{\zeta}{\eta}L_J$, the optimal P_{b1}^* is

$$P_{b1}^* = \frac{\exp\left(w\left(\frac{2^{-x/L_J}P_{tpi}}{\frac{\zeta}{\eta}L_J e} - \frac{2^{-x/L_J}\sum_{k=1}^{L_J}\left(\mathbf{a}_{j_k}^H\mathbf{a}_{j_k}\right)\sigma_n^2}{L_J e}\right)+1\right)}{2^{-x/L_J}} - \frac{\sum_{k=1}^{L_J}\left(\mathbf{a}_{j_k}^H\mathbf{a}_{j_k}\right)\sigma_n^2}{L_J}. \quad (5.38)$$

Substitute this result into P_k^U in (5.35), this proposition is proved. ■

Now we need to calculate the set J_P. From (5.32), it is noted that $\frac{\partial\delta}{\partial P_k^U}$ increases monotonically with P_k^U and the sign of $\frac{\partial\delta}{\partial P_k^U}$ depends on the value $\left(\mathbf{a}_k^H\mathbf{a}_k\right)\sigma_n^2 + P_k^U$. Thus, we can find the set $\mathbb{J}_P$ from the value of $\frac{\partial\delta}{\partial P_k^U}$. Based on (5.30) and (5.38), the steps to obtain the configuration for the EA-P for every transmitted signal are summarised in Algorithm 4.

Algorithm 4 The Positive User Set for Power Allocation

Initialization:

Initial sets: $\mathbb{J} = \{1, 2, \ldots, K\}$ and $\mathbb{J}_P = \mathbb{J}$;

Initial the number of the elements in the set $\mathbb{J}_P$: $L_J = K$.

Outputs: the set $\mathbb{J}_P$;

Steps:

Step 1: Based on perfect CSI, calculate $\left(\mathbf{a}_1^H\mathbf{a}_1\right), \left(\mathbf{a}_2^H\mathbf{a}_2\right), \ldots, \left(\mathbf{a}_K^H\mathbf{a}_K\right)$.

Step 2: Reorder these values in an ascending order as $\left(\mathbf{a}_{j_1}^H\mathbf{a}_{j_2}\right), \left(\mathbf{a}_{j_2}^H\mathbf{a}_{j_2}\right), \ldots, \left(\mathbf{a}_{j_k}^H\mathbf{a}_{j_k}\right)$, which satisfy $\left(\mathbf{a}_{j_1}^H\mathbf{a}_{j_1}\right) \leq \left(\mathbf{a}_{j_2}^H\mathbf{a}_{j_2}\right) \leq \ldots \leq \left(\mathbf{a}_{j_K}^H\mathbf{a}_{j_K}\right)$.

Step 3: Set $n = K$.

Step 4: Calculate P_{b1} and $P_{j_{L_J}}^U$ from (5.38) and (5.35) based on $\mathbb{J}_P$.

Step 5: If $P_{b1} < 0$, goto step 7;

Step 6: If $P_{j_{L_J}}^U >= 0$, goto step 9;

Step 7: Update $\mathbb{J}_P$ by removing the element j_n.

Step 8: $n = n - 1$ and $L_J = L_J - 1$, goto step 4;

Step 9: Finished;

5.6 Discussions

Our proposed algorithm is based on generic type of the single-RF antenna. In this section, we discuss its application to the practical ESPAR and load modulated array.

5.6.1 Application of the Algorithm to ESPAR antenna

This chapter considers energy-efficient CRANs in which single-RF antennas are employed at the RRHs. There are still some potential research points that need to be considered when using the algorithm directly for ESPAR antennas, such as the practical power model for ESPAR transmitters. In other words, the power model still require further research, and the realistic power consumption model for ESPAR antenna design depends on the specific implementation of the antenna. It is necessary and important to consider realistic power consumption models in the future.

5.6.2 Application of the Algorithm to Load Modulated Antenna

As discussed in chapter 2, load modulated array architecture was proposed in [58]. All antenna elements are connected to a common carrier source by two-port loading networks, and these networks are passive and lossless. These loads are tuned to control the input currents to all radiating elements, thereby implementing a desired signal constellation [8]. The power consumption model for this antenna has been analysed and utilised in [59], and it is similar to the power model used in our algorithm, which shows that our proposed approach can be used for the practical load modulated array to obtain the optimal current vector. Based on the obtained current vector, the antenna parameters can be calculated and designed fro practical application with the guidances in [60].

5.7 Simulation Results

In this section, we present the simulation results, showing the EE performance of CRANs with single-RF and multi-RF antennas. In order to gain more insights into the performance

Parameter	**Value**
Transmission bandwidth: Ω	10MHz
PA efficiency at the RRHs: η	0.39
Fraction of downlink transmission: ζ	0.6
Fixed power consumption (control signals, backhaul, etc.): P_{tpi}	34 W
Power required to run the RF circuit components at at the t-th RRH: P_t^c	1W
Total noise power: σ_n^2	$-174dBm/Hz$
Power required for optical traffic: p_{op}	0.5 W/Gbit
The distance from users to RRH: d	$[3m, 40m]$
Path loss model (2GHz): $l_t(\alpha)$	$g - 128.1 + 37.6\log_{10}(d/d_0)$
Path loss coefficient:	3.76

Table 5.1: Simulation Parameters for Chapter 5 [10, 87, 105]

of our scheme, the EE performance of a standard multiple antenna transmitter system is also shown as the benchmark. We numerically compare the proposed algorithm with the single-RF and multi-RF antenna under the 3GPP LTE specifications for small cell deployments [87].

The downlink transmission from the RRHs to the users are considered in the simulation. RRHs are connected with a BBU via optical fibre. All users are equipped with a single antenna element. It is assumed that all RRHs and the users possess perfect CSI. Note in the transmission strategy (precoding and power allocation) is designed to maximize the energy efficiency when the instantaneous channel gains are known perfectly at both the transmitter and the receiver. In other words, the transmission strategy is based on the instantaneous channel state, and not on the statistical fading model. The fading model is only required when generating the constant instantaneous channel gains in the simulations. As the possibility of line of sight increases when the distance between the transmitter and receivers decreases, the Rician fading model is used in the simulations. Thus, the channel between RRH and users are assumed to experience the path loss model for line-of-sight (LOS) communications and

it is

$$P_{\text{LOS}} = 103.8 + 20.9 \log_{10} \frac{d}{d_0}$$

from [87, 105]. In this model, $d_0 = 1$km and P_{LOS} is expressed in dB. The small-scale fading channel is modelled as Rician fading with a Rician factor 4dB. The thermal noise density is -174dBm/Hz and the bandwidth is set to 10MHz. The parameters for the system model for each link are adopted from [87, 105].

The simulation is performed under a typical RRH scenario, in which the fixed circuit power consumption is dominant compared to the transmitted power consumption due to the low power transmission of RRHs as [10]. As the BBU performs the centralize and complex processing and the RRHs cover small areas. Thus, unless stated otherwise, BBU power consumption follows BS's power consumption model for BBU and RRH follow a small cell BS, which are obtained from recent studies [10]. For the sake of simplification, in the simulations, we denote the system with single-RF antennas as SRFA and with standard multiple antenna as SMA.

5.7.1 Single-user Case

From the analytical result in Proposition 13, the EE performance depends highly on the power consumption models, i.e., the power consumption of the RF circuit and the fixed circuit. As the main difference of the power consumption between the single-RF antenna and standard multiple antenna systems are the power consumption values for the RF circuit. For a standard multiple antenna, the number of RF chains is equal to the number of antenna elements M_t. However, the number of RF chain equals to 1 in the case of a single-RF antenna. Figure. 5.2 and Figure. 5.3 illustrate the achievable maximal EE under different power consumption of RF circuit and fixed circuit,respectively.

As shown in Figure. 5.2 and Figure. 5.3, the achievable EE performance of the single-RF antenna system is similar to the standard multiple antenna with single antenna element employed at the RRHs. This matches our analytical results in Proposition 12 and Proposition 13. From these results, it can be noted that the difference of the optimal allocated power for different RRHs depends on the norm of the channel from each RRH to the user $\|\mathbf{h}_{1,t}\|, t \in$

$\{1, 2, \ldots, N\}$. Thus, with the similar norm of the channel, the achievable EE performance of the single-RF antenna system is similar to the standard multiple antenna with single element antennas (one RF chain circuit) employed at the RRHs.

As illustrated in Figure. 5.2, as the RF power consumption increase, the gap in EE results between the single-RF chain antenna and standard multiple antenna systems increases. This is due to the fact that the total power consumption gap increases when the RF power consumption increases. Moreover, when the number of antenna elements M_t increases, the EE decreases for standard multiple antenna systems. However, increasing M_t has no impact on EE for single-RF antenna systems, this is due to the fact that increasing M_t does not increase the power consumption of the RF circuitry in the single-RF chain antenna system and the optimal allocated power to the different RRHs only depends on the norm of channel from each RRH to the user $\|\mathbf{h}_{1,t}\|, t \in \{1, 2, \ldots, N\}$ based on Proposition 12 and Proposition 13.

In Figure. 5.3, it is can be noted that the EE gap between different numbers of antenna elements for single-RF and multiple antenna systems varies with the fixed power consumption level. When the fixed power consumption increases to a certain number, the achievable EE performance of the single-RF chain antenna system tends to be similar to the standard multiple antenna configuration. This matches our assumptions that the main difference among standard multiple antenna and single-RF antenna with different antenna elements are the RF power consumption. With the increase of fixed power consumption, the impact from the power consumption of the fixed circuit becomes more importance compared with the RF circuit power consumption.

Figures. 5.4 and 5.5 illustrate the achievable EE performance for different distances d from the RRHs to the user. As discussed in [10, 84], it is assumed that the t-th RRH is located at coordinates $\left(d_t \cos \frac{2\pi(t-1)}{N}, d_t \sin \frac{2\pi(t-1)}{N}\right)$. The optimal precoding scheme for different RRHs follows Proposition 11 and Proposition 13. As shown in Figure. 5.4, the achievable EE performance of the single-RF chain antenna system is similar to the standard multiple antenna with one antenna employed at the RRHs. This is similar with Figure. 5.2 and Figure. 5.3 and it matches our analytical results in Proposition 12 and Proposition 13. Moreover, when the number of antenna elements M_t increases, the EE decreases for standard multiple antenna systems, and thus the achievable EE performance of the single-RF chain antenna

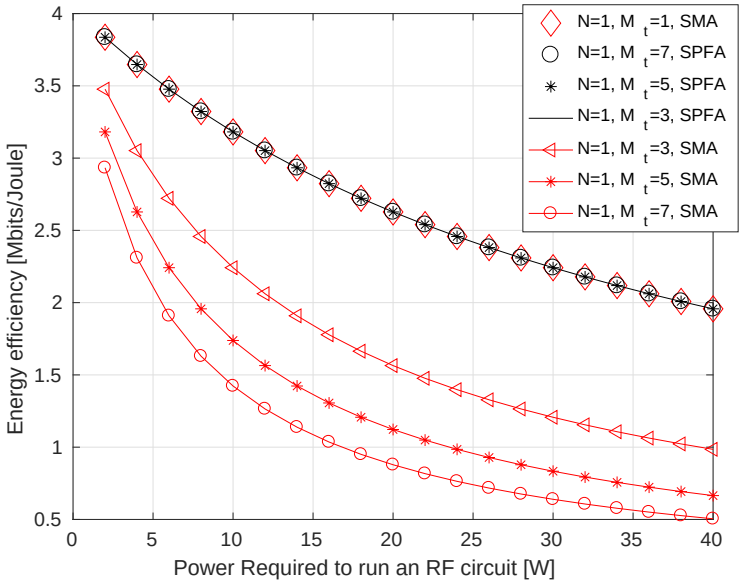

Figure 5.2: Energy Efficiency with standard multiple antennas and single-RF antennas under different power consumption from RF circuit

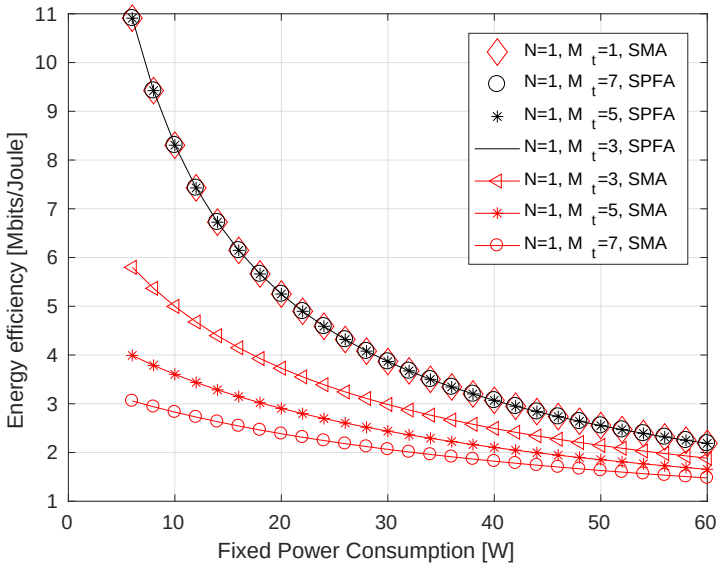

Figure 5.3: Energy Efficiency with standard multiple antennas and single-RF antennas under different power consumption from fixed circuit

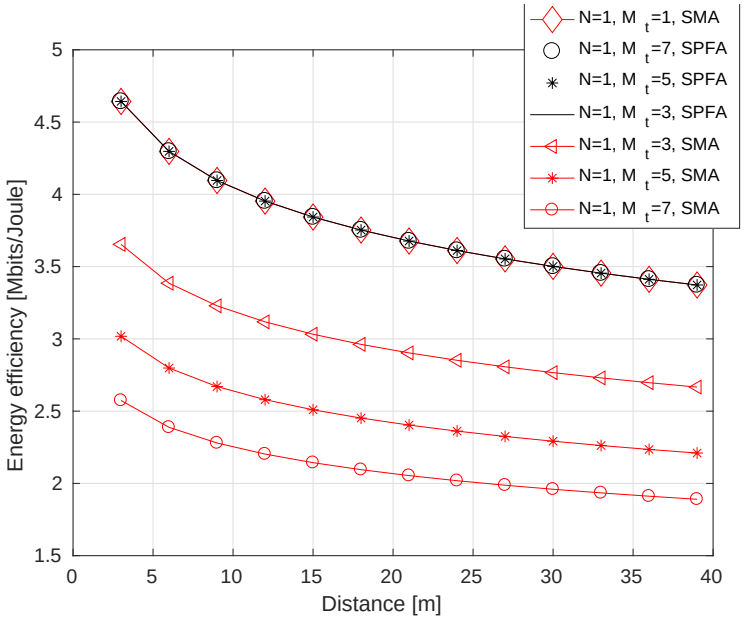

Figure 5.4: Energy Efficiency with standard multiple antennas and single-RF antennas under different number of antenna elements

system is better than that of the standard multiple antenna system with more than one RF chain antenna employed at the RRFs.

In Figure. 5.5, it shows the combined impact of the number of RRHs and the distance on EE. Assuming $N \in \{1, 3\}$ and $M_t = 3$, it can be observed that more RRHs with single-RF chain antennas could cooperate to serve the user in order to obtain better EE performance.

Table. 5.2 illustrate the achievable maximal EE under different numbers of serving RRHs. From this table, three RRHs are around the user, and the distance from the RRHs to the user are 35m, 40m and 40m, respectively. It can be noted that the EE increases when the number of serving RRHs increases. However, when the distances are 5m, 35m and 40m, respectively, we can have three options of RRHs to sever the user, which are only one RRH with the distance 5m, two RRHs with the distance 5m and 35m, and all three RRHs respectively. As shown in Table. 5.2, the EE which is obtained when only the nearest RRH serves the user is similar to that when two RRHs or three RRHs serve the user simultaneously. When the user is close to a specific RRH, having only this RRH serve the user provides similar EE performance compared with that when more RRHs serve the user. According to the comparison of these

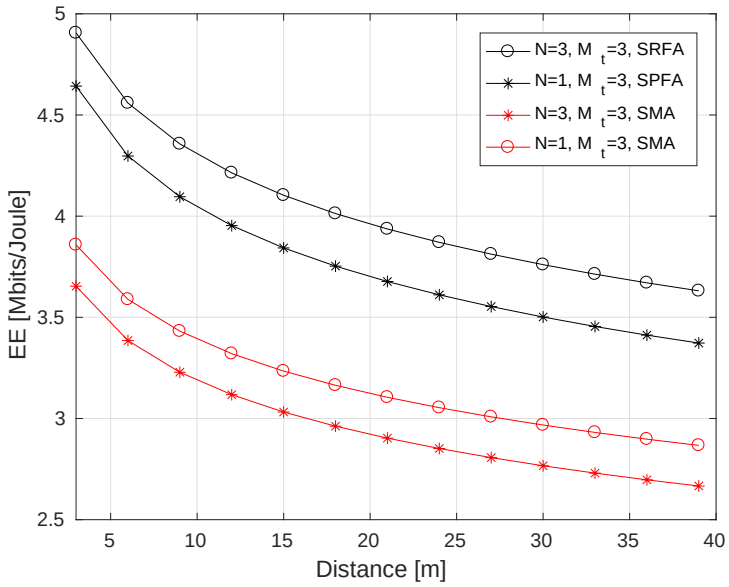

Figure 5.5: Energy Efficiency with the standard multiple antenna and single-RF antenna under different number of serving RRHs

two scenarios, when the user is near to the edge of the cell, the EE performance can be improved by increasing the number of serving RRHs and the number of antenna elements for single-RF antenna based systems. When the user is close to a specific RRH, having only this RRH serve the user provides the similar EE performance as that when several RRHs serve the user simultaneously. This highlights the significance of CRANs with single-RF chain antennas as it can provide better EE performance.

The EE (Mbits/Joule)	$\mathbf{d} = [35m, 40m, 40m]$			$\mathbf{d} = [5m, 35m, 40m]$		
	$N = 1$	$N = 2$	$N = 3$	$N = 1$	$N = 2$	$N = 3$
SMA	3.42	3.55	3.64	3.46	3.46	3.46
SRFA	2.72	2.81	2.86	4.39	4.39	4.39

Table 5.2: The Energy Efficiency with the standard multiple antenna and single-RF antenna considering the different number of serving RRHs, when there are three RRHs around the user

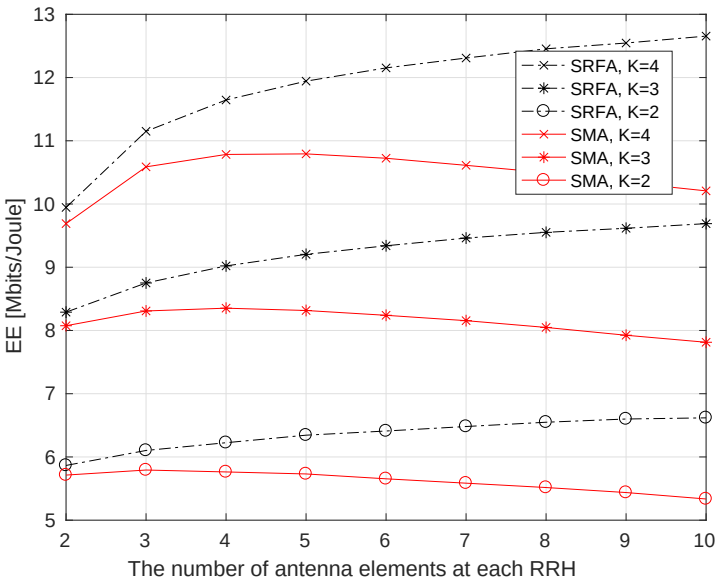

Figure 5.6: Energy efficiency with the standard multiple antenna and single-RF antenna under different antenna elements at each RRH and different numbers of users when $N = 3$.

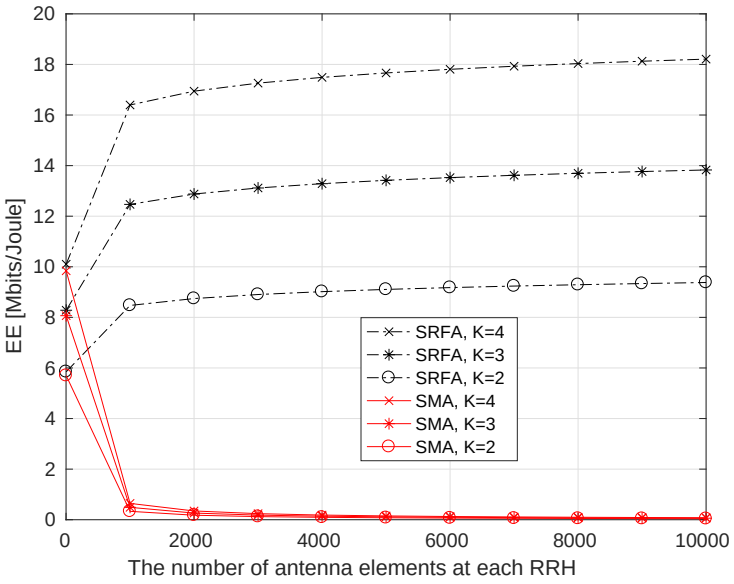

Figure 5.7: Energy efficiency with the standard multiple antenna (SMA) and single-RF antenna (SRFA) under large number of antenna elements at each RRH and different numbers of users (all users are equipped with a single antenna element) when $N = 3$.

5.7.2 Multi-user Case

The achievable EEs for the single-RF antenna and standard multiple antenna systems with respect to the number of antenna elements at each RRH are compared under different number of users in Figures. 5.6 and 5.7. The optimal precoders to different RRHs follow Proposition 14 and Proposition 16. The number of RRHs is set to $N = 3$. We evaluate EEs with three different number of users with $K = \{2, 3, 4\}$. As shown in Figure. 5.6, the EE increases as the number of the users increases. Moreover, for the single-RF antenna based system, the EE performance increases with the number of transmitting antennas and it tends towards to a constant asymptote when the number of antenna elements goes infinity. However, in the case of standard multiple antenna systems, the achievable EE becomes stable and then decreases with the increase in the number of transmitting antenna elements. It is noted the negative impact on EE of M_t is not as significant as that in the single-user scenario. This is because the total rate of all users increases more compared with the increasing power consumption from the increasing M_t.

When the number of antenna elements at the RRHs at the transmitter goes to infinity, the energy efficiency for the multi-use case is shown in Figure. 5.7. From the curve, the energy efficiency tends to an asymptotic value when the number of antenna elements at each RRH increases for the single-RF antenna based system. In the case of standard multiple antenna systems, with the dramatic increase in the number of antenna elements at the RRHs, the energy efficiency decreases. As the number of users K is setting to $K = \{2, 3, 4\}$ in this simulation and all users are equipped with a single antenna element, when the number of antenna elements at each RRH goes to infinity, the energy efficiency performance tends to be zeros. This is due to the fact that the RF power consumption increases dramatically when the number of antenna elements at the transmitter goes to infinity and the number of users (each user is employed with single element antenna) at the receiver K is $K = \{2, 3, 4\}$. From the mathematical point of view, as given in (5.26) and (5.27), the EE is

$$\eta_{ee} = \frac{\sum_{k=1}^{K} \log_2 \left(1 + \frac{P_k^U}{(\mathbf{a}_k^H \mathbf{a}_k)\sigma_k^2}\right)}{P_{bbu} + NP_{op}R + \sum_{t=1}^{N} \left(\frac{\zeta}{\eta} \sum_{k=1}^{K} P_{k,t} + N_{RF}^{(t)} P_t^c\right) + KP_{user}^{DL}}, \tag{5.39}$$

in which, the number of users K is setting to $K = \{2, 3, 4\}$ in the simulations for Figure (5.7). It is noted that the denominator increases linearly with the number of RF chain at each RRH. As observed in Lemma 1 and Proposition 16, the numerator varies with the number of RF chains at each RRH roughly by Lambert W and Logarithmic functions when the number of users K is setting to $K = \{2, 3, 4\}$ in this simulation. In the case of the single-RF antena, N_{RF} keeps one when the number of antenna elements goes infinity. However, N_{RF} equals to the number of transmitting antenna elements in the case of a standard multiple antennas based system as each antenna element has one RF chain. Thus, in the case of a standard multiple antennas based system, the numerator increases much slower compared with the increase of the denominator when the number of antenna elements at each RRH at the transmitter goes to infinity.

5.8 Summary

In this chapter, we have studied the EE of CRANs that deploy single-RF antennas at RRHs by formulating an EE optimisation problem. The closed-form expressions for precoding and power allocation have been obtained to maximise EE for both the single-user and multi-user systems that can be used for both single-RF antenna and standard multiple antenna based systems. Moreover, we have derived the closed-form expressions for configuring the single-RF antenna to transmit the desired signals in single- and multi-user scenarios. The EE performance of CRANs has been compared for single-RF antennas and standard multiple antenna systems. The CRANs with single-RF antennas provide superior EE performance compared to the standard multiple antenna systems.

The conclusions of this chapter are:

- For CRANs employed at RRHs, an EE maximisation problem has been formulated and solved by a suboptimal decomposition strategy.
- In the single-user system, the closed-form expressions for precoding and power allocation among different RRHs have been derived to maximise the EE. Our results are applicable to not only single-RF antennas, but also other types of antennas.

- To cancel multi-user interference, ZF constraints have been introduced into the optimisation problem for the multi-user system. By a suboptimal decomposition strategy, closed-form expressions for precoding and power allocation among different users have been obtained to maximise the EE. These results are also applicable to single-RF antennas and other types of antennas.
- The EE performances of standard multiple antenna and single-RF antenna systems have been compared for both single- and multiple-user scenarios. It has been shown that the EE of single-RF antenna-based systems outperform the standard multiple antenna systems.

Generally speaking, the performance of CRANs can be greatly improved by employing compact single-RF antennas at RRHs. According to our results, when the user is near to the edge of the cell, the EE performance can be improved by increasing the number of serving RRHs and the number of antenna elements for single-RF antenna-based systems. When the user is close to a specific RRH, having only this RRH serve the user provides the similar EE performance as that when several RRHs serve the user simultaneously.

Chapter 6
Conclusions and Future Work

This thesis has focused on the real challenges in modern wireless networks; it has discussed novel and promising transmission techniques, CRANs with single RF chain antennas, to help overcome them.

In this chapter, we draw together the main results of our research and highlight the key findings of this thesis. Suggestions for possible future research directions are also discussed.

6.1 Conclusions

Multiple-input multiple-output (MIMO) transmission has been proposed in wireless communication standards including Long Term Evolution (LTE) and LTE advanced (LTE-A) [116]. The benefits improves with increasing the number of antennas [20] [26]. A consequence of increasing the number of antennas is that the number of required radio frequency (RF) chains increases linearly with the number of antenna elements, resulting in an increase in the cost and complexity of the device. Moreover, the antenna elements are required to be placed at least half a wavelength apart from each other to minimize the mutual coupling, causing the size of the device to increase [8]. In this thesis, we have addressed the issue by studying single-RF antennas and ESPAR solutions in order to reduce the cost and the physical size of multiple antenna devices by providing multi-antenna functionality utilizing a single RF chain [15]. It has shown that nearly the same performance as that of the standard multiple antenna system is achieved by using ESPAR antennas with proposed algorithms in the thesis. Additionally, an energy efficiency (EE) maximisation problem is formulated and solved to obtain optimal precoding and power allocation schemes in the CRANs applying single-RF antennas to CRANs. According to the results, when the user is near to the edge of the cell, the EE performance can be improved by increasing the number of serving RRHs and

the number of antenna elements for EA based systems. When the user is close to a specific RRH, having only this RRH serve the user provides similar EE performance with that more RRHs serve the user. Compared with SMA based systems, single-RF antennas can provide better EE performance. This gain mainly comes from the lower RF power consumption of single-RF antennas compared with standard multiple antennas with multiple-RF chains. This highlights the significance of CRANs with single-RF antennas and our work.

The conclusions of the whole thesis can be summarized as follows:

To overcome hardware limitation in wireless cellular networks, this thesis explores approaches that enable an ESPAR antenna to provide multi-antenna functionality and the application of single RF chain antennas into CRANs. Firstly, while considering the oscillatory behaviour of an ESPAR antenna to transmit signals, this thesis proposes a novel algorithm to guarantee stable ESPAR antenna transmission. Secondly, as all elements of a single-RF antenna are fed centrally by a single power amplifier. This makes it more probable that an ESPAR antenna power amplifier might reach maximum power when it is used to transmit same information as a multi-RF antenna. Thus, this thesis proposes a practical and new transmission scheme that enables an ESPAR antenna to provide stable multi-antenna functionality with peak power constraint from the power amplifier. Furthermore, it considers energy-efficient CRANs in which single-RF antennas are employed at the RRHs. By exploring the difference of RF circuit power consumption between single-RF antennas and standard multiple antennas with multiple-RF chains, this thesis introduces precoding and power allocation techniques that can deliver better EE when compared to standard multiple antenna systems.

Based on my experience during my PhD, we find that it is very important to explore new mathematical approaches and novel algorithms for new applications of single-RF antennas. With appropriate mathematical methods, it is possible that some solutions are simpler compared with standard multiple antenna systems in some circumstances, such as MRT with an ESPAR antenna transmitter in Chapter 3. Another example is the mathematical model and method proposed in Chapter 4. In Chapter 4, the optimal solution can be obtained via conventional semi-definite relaxation (SDR). We would like to mention here that we tried to solve the problem using SDR previously, but the algorithm did not perform satisfactorily due to the complexity and simulation time. Because of this, we resorted to the existing proposed ap-

proach. The worst case complexity of the proposed algorithm is $\mathcal{O}\left(16M^2 - 4M + 8\log\frac{1}{\xi}\right)$, where M is the total number of transmitting antenna elements as mentioned before. The complexity of SDR of $\mathcal{O}\left((2M)^{4.5}\log\frac{1}{\xi}\right)$ by counting the arithmetic operations of a specific interior-point method in [117]. Thus, the complexity of SDR based approach is much higher compared to our proposed method.

Moreover, apart from size and cost saving, there are some differences between a single-RF antenna and a standard multiple antenna with multi-RF chain, such as loaded modulation scheme, single RF circuit, the mutual coupling among different antenna elements, and so on. We can focus on these different areas to explore more benefits and more applications to a single-RF antenna. An example of this is the work in Chapter 5. In Chapter 5, based on the difference of RF chain power consumption, we are exploring the link between RF chain power consumption and energy efficiency in CRAN systems.

6.2 Limitations and Future Work

This thesis achieves many remarkable results; however, some constraints limit the application of these results in practice. The next section contains some promising future research directions that could help make forthcoming work more general and practically appealing.

6.2.1 Design and Implementation of an ESPAR Antenna

This thesis has considered the use of an EA to provide multiple antenna functionality; the results can be used as a guide for future realisation and measurement. A similar process has been applied in the prior literature involving EA. The idea of creating a multiplexing gain by ESPAR has been first presented in [12], and later a proof-of-concept implementation and corresponding measurements have been shown in [53]. Therefore, our proposed algorithms can be implemented and measured in the same way. In practice, the parasitic elements for an EA can be implemented in multiple ways. Several promising options are discussed in [58] [71]. For imaginary part, one approach is using varactor diodes. Another implementation of imaginary part is digitally using a network of pin diodes. For real part, the authors [71] then

presented some design schemes for active loads at the parasitic elements. Circuit implementation experiments are important and necessary for future work.

6.2.2 Further Consideration on the Implementation of an EA

As earlier mentioned in Chapter 3, the proposed algorithm can realise stable EA transmission. In Chapter 4, we have derived a novel algorithm to satisfy the peak power limit. As there are limitations on the range (real and imaginary parts) of load impedances, based on the results in Chapter 3, some simulations have been carried out to observe the distribution of the load values. to show the range of the real and imaginary parts of impedance values, respectively. The results show that the range of load values is $[-200\Omega, 200\Omega]$ for STBC, and $[-500\Omega, 500\Omega]$ for MRT. It is shown in [51] that load values in this range are acceptable for antenna design. the real and imaginary part range of realized impedance for EA-P and EA-S is $[-200\Omega, 200\Omega]$, and $[-600\Omega, 600\Omega]$ under STBC transmission, respectively. Thus, the range for EA-P outperform EA-S scheme. It is shown in [51] that load values in this range are acceptable for antenna design. However, since the range of load values is a realistic constraint, it is also desirable to consider this limitation in the range of load impedances. This practical limitation can be formulated by adding constraints on the real and imaginary parts of impedance values in the optimisation problem. The new constraints result in a modified optimisation problem. In this case, strong duality in chapter 3, and coordinate transformation and geometric methods in chapter 5, do not hold together. A new approach will be required to solve this problem.

6.2.3 Further Exploitation on Wideband Applications of an EA

This thesis has considered the application of an EA for narrowband applications. Many applications of further wireless communication systems will be wideband and able to support one or multiple types of multi-carrier modulation and multiple access. The main challenge for applying an EA into the multi-carrier transmission is the implementation of different loads for sub-carriers for wideband applications. Thus, a novel approach to implementing is required in practice for the realisation of EAs in wideband applications. The exploration of

the EA application into wideband systems is an important step toward the integration of EA technology into 5G and further wireless communication systems.

6.2.4 Power Model and Radiation Efficiency for an EA

ESPAR had been initially proposed with passive loads at the parasitic elements and could realise remarkable hardware savings. However, it is not possible to find appropriate loads that emulate arbitrary MIMO transmission with only passive loads [55]. To alleviate this issue, the authors in [55] have proposed complex loads at the parasitic elements to enable ESPAR to support more transmitted signals, and the authors [71] then presented some design schemes for active loads at the parasitic elements. Based on complex loads, this thesis has proposed the optimization problems in Chapters 3 and 4. However, other important concerns for ESPAR antenna design are the power consumption model and antenna efficiency, which partly depend on the specific implementation of the antenna. The exploration of the power consumption model and the antenna efficiency of the EA is necessary and important for the practical application of an EA in the future.

6.2.5 Energy Efficiency for CRANs with ESPAR antennas

This thesis has considered energy-efficient CRANs in which single-RF antennas are employed at the RRHs. Energy Efficiency for CRANs with ESPAR antennas can be further considered as a practical application of ESPAR antennas. There are some potential research points that need to be considered when using the algorithm for ESPAR antennas, such as the practical power model for ESPAR transmitters. The realistic power consumption model for ESPAR antennas depends on the specific implementation of the antenna. It is necessary and important to consider realistic power consumption models in the future.

6.2.6 Mutual Coupling Estimation

ESPAR transmitters require a priori knowledge of accurate mutual coupling. In general, mutual coupling between antenna elements depends on different parameters, including inter-

element spacing, the antenna element pattern, array geometry, relative positioning of the antenna elements in the array, operational frequency, and near-field scatterers [40, 41]. Except for the near field scatterers, most of these parameters can be measured or estimated. Therefore, the mutual coupling might in practice vary with different scenarios. Modelling of the mutual coupling in practice is a significant challenge for the ESPAR transmitter. In order to model this impact, the SER performances for ESPAR considering the change of mutual coupling are presented by simulation in the section 3.4.3.2 of Chapter 3. It can be noted that the difference of SER performance between system with exact loads and practical values is very small. However, for a standard MIMO system with a compact antenna, the impact of mutual coupling was considered indirectly through channel estimation in [109] [110]. The channel with parasitic antennas was estimated by varying the loads at the parasitic elements in [111]. These two ideas can be combined to estimate mutual coupling coefficients for an ESPAR transmitter. Different signals are transmitted by varying loads and feeds at the ESPAR transmitter. The receiver estimates the channel and mutual coupling coefficients when the values of the loads and feeds are known at the receiver.

6.2.7 Pilot Design and Channel Estimation for single-RF transmitter

Channel estimation for single-RF antenna transmitter based communication has not been discussed much in literature. One of the issues which arises in single-RF antenna transmitter based systems is that the active antenna elements must work all the time. For the standard multiple antenna transmission, one antenna element may be activated in a time slot and its channel may be estimated. For a single-RF antenna transmitter, this is not possible. A challenge, in this case, is to design training signals to estimate the channel. Take an ESPAR antenna transmitter as an example, channel matrix can be recovered on the knowledge of training signals and received signals by estimation process.

As we discussed, the main difference between standard MIMO antenna and ESPAR is training sequence. The optimum training sequence can be obtained by solving an MSE optimization problem between practical and estimated channel. Take least square (LS) estimator as an example, the channel matrix can be estimated by LS approach. In order to obtain the optimal training, an optimization could be formulated to minimize the error between real and

estimated channel under the power and ESPAR stability constraints. By solving this optimization problem, we can find a training sequence which satisfies the requirements, and then the channel estimation can be achieved for an ESPAR transmitter.

6.2.8 Load Modulated Array

As described in Chapter 2, a load modulated array architecture has been proposed in [58]. Compared with an ESPAR transmitter, the load modulated array can support a large range of transmitted signals. This scheme can be applied to the massive MIMO systems with large numbers of antennas, as explained in [8]. In addition, load modulated arrays can realise arbitrary modulation with passive loads, which greatly improves antenna efficiency. Therefore, it is a promising type of antenna that can be used in an area of massive array architectures with single RF chains. The application of load modulated arrays is another necessary and important topic for the future.

Appendix A
Proof of Proposition 1

From (3.2), the input resistance is

$$
\begin{aligned}
&\Re\left\{ Z_{00} + \frac{\sum_{m=1}^{M} Z_{0m} i_m}{i_0} \right\} \\
&= \Re\left\{ R_0 + jX_0 + \frac{\sum_{m=1}^{M-1} (R_m + jX_m)(w_{2m+1} + jw_{2m+2})}{w_1 + jw_2} \right\} \\
&= R_0 + \\
&\Re\left\{ \frac{\sum_{m=1}^{M-1} \{((R_m w_{2m+1} - X_m w_{2m+2}) + j\,(R_m w_{2m+2} + X_m w_{2m+1}))\,(w_1 - jw_2)\}}{w_1^2 + w_2^2} \right\} \\
&= R_0 + \frac{\sum_{m=1}^{M} ((R_m w_{2m+1} - X_m w_{2m+2})\, w_1 + (R_m w_{2m+2} + X_1 w_{2m+1})\, w_2)}{w_1^2 + w_2^2} \\
&= \frac{R_0 w_1^2 + R_0 w_2^2 + \sum_{k=1}^{M} (R_m w_{2m+1} w_1 - X_m w_{2m+2} w_1 + R_m w_{2m+2} w_2 + X_1 w_{2m+1} w_2)}{w_1^2 + w_2^2}.
\end{aligned}
\tag{A.1}
$$

Eq. (3.5) follows as a simple consequence of rewriting the quadratic form in (A.1) in the form of an appropriate matrix expansion.

Appendix B
Proof of Proposition 2

As $\mathbf{B}$ is a real symmetric matrix and it can be diagonalized as $\mathbf{B} = \mathbf{Q}_B \Lambda \mathbf{Q}_B^T$, where $\mathbf{\Lambda}$ is a real diagonal matrix and its elements are eigenvalues of $\mathbf{B}$, the columns of the real orthogonal matrix $\mathbf{Q}_B$ are corresponding eigenvectors of $\mathbf{B}$. For the sake of simplification, the eigenvalues $\mathbf{\Lambda}$ are set in ascending order. Let ζ denote the eigenvalues of $\mathbf{B}$, the matrix $\mathbf{B} - \zeta\mathbf{I}$ can be written as

$$\mathbf{B} - \zeta\mathbf{I} = \begin{bmatrix} \mathbf{B}_{11} & \mathbf{B}_{12} \\ \mathbf{B}_{21} & \mathbf{B}_{22} \end{bmatrix}, \tag{B.1}$$

where

$$\begin{aligned}
\mathbf{B}_{11} &= \begin{bmatrix} R_0 - \xi - \zeta & 0 \\ 0 & R_0 - \xi - \zeta \end{bmatrix}, \\
\mathbf{B}_{12} &= \begin{bmatrix} \frac{R_1}{2} & -\frac{X_1}{2} & \cdots & \frac{R_M}{2} & -\frac{X_M}{2} \\ \frac{X_1}{2} & \frac{R_1}{2} & \cdots & \frac{X_M}{2} & \frac{R_M}{2} \end{bmatrix}, \\
\mathbf{B}_{21} &= \begin{bmatrix} \frac{R_1}{2} & -\frac{X_1}{2} & \cdots & \frac{R_M}{2} & -\frac{X_M}{2} \\ \frac{X_1}{2} & \frac{R_1}{2} & \cdots & \frac{X_M}{2} & \frac{R_M}{2} \end{bmatrix}^T, \\
\mathbf{B}_{22} &= \operatorname{diag}\left(-\zeta, -\zeta, \ldots, -\zeta\right).
\end{aligned}$$

As $\mathbf{B_{22}}$ is invertible, the determinant of the matrix $\mathbf{B} - \zeta\mathbf{I}$ can be rewritten as

$$\begin{aligned}
&\det\left(\mathbf{B} - \zeta\mathbf{I}\right) \\
&= \det\left(\mathbf{B}_{22}\right) \det\left(\mathbf{B}_{11} - \mathbf{B}_{12}\mathbf{B}_{22}^{-1}\mathbf{B}_{21}\right) \\
&= \left(-\zeta\right)^{2M-2} \left(\zeta^2 - 2\left(R_0 - \xi\right)\zeta - \sum_{m=1}^{M}\left(R_m^2 + X_m^2\right)\right)^2.
\end{aligned} \tag{B.3}$$

Setting $\det(\mathbf{B} - \zeta\mathbf{I}) = 0$, the eigenvalues of $\mathbf{B}$ are (3.11). We can find that ζ_1 and ζ_2 are negative whereas ζ_3 and ζ_4 are positive eigenvalues, thus $\mathbf{\Lambda}$ is $\mathrm{diag}(\zeta_1, \zeta_2, 0, \ldots, 0, \zeta_3, \zeta_4)$. The matrix $\mathbf{B}$ is not a positive or a negative semidefinite matrix. The constraint (3.10b) is nonconvex and the optimisation problem (3.10) is a noncovex problem.

Appendix C
Proof of Proposition 3

From proposition 2, $\mathbf{B}$ is a real symmetric matrix and it can be eigenvalue decomposed as

$$\mathbf{B} = \mathbf{Q}_B \mathbf{\Lambda} \mathbf{Q}_B^T, \tag{C.1}$$

where $\mathbf{\Lambda} = \mathrm{diag}(\zeta_1, \zeta_2, 0, \ldots, 0, \zeta_3, \zeta_4)$ is a diagonal matrix whose diagonal elements are the eigenvalues of $\mathbf{B}$ in ascending order. $\mathbf{Q}_B$ is an orthogonal matrix whose columns are the corresponding eigenvectors. Then we have

$$\mathbf{I} - \delta_B \mathbf{B} = \mathbf{Q}_B \left(\mathbf{I} - \delta_B \mathbf{\Lambda}\right) \mathbf{Q}_B^T. \tag{C.2}$$

The eigenvalues of $(\mathbf{I} - \delta_B \mathbf{B})$ are $1 - \delta_B\zeta_1, 1 - \delta_B\zeta_2, 1, \ldots, 1, 1 - \delta_B\zeta_3, 1 - \delta_B\zeta_4$ and the columns of $\mathbf{Q}_B$ are corresponding eigenvectors of $(\mathbf{I} - \delta_B \mathbf{B})$. Therefore, the feasible set of the optimisation problem (3.16) is

$$\mathbb{C} = \left\{\delta_B | 0 \leq \delta_B \leq 1/\zeta_3\right\}, \tag{C.3}$$

and it can be rewritten as the optimisation conditions as (3.17c).

For the objective function (3.16a), $\hat{\mathbf{w}}^T\hat{\mathbf{w}}$ can be simply removed form the objective function as it is constant. Similarly, the objective function is reformulated as

$$\hat{\mathbf{w}}^T \left(\mathbf{I} - \delta_B \mathbf{B}\right)^{-1} \hat{\mathbf{w}} = \left(\mathbf{Q}_B^T \hat{\mathbf{w}}\right)^T \left(\mathbf{I} - \delta_B \mathbf{\Lambda}\right)^{-1} \left(\mathbf{Q}_B^T \hat{\mathbf{w}}\right)^T. \tag{C.4}$$

Setting $\mathbf{g} = [g_1, g_2, \ldots, g_{2M+1}, g_{2M+2}]^T = \mathbf{Q}^T\hat{\mathbf{w}} \in \mathbb{R}^{2(M+1)}$, (C.4) can be written as

$$\begin{aligned} &\hat{\mathbf{w}}^T \left(\mathbf{I} - \delta_B \mathbf{B}\right)^{-1} \hat{\mathbf{w}} \\ &= \frac{g_1^2 + g_2^2}{1 - \delta\zeta_1} + \frac{g_{2M+1}^2 + g_{2M+2}^2}{1 - \delta\zeta_3} + \sum_{k=3}^{2M} g_k. \end{aligned} \tag{C.5}$$

From (C.5), $\sum_{k=3}^{2M} g_k$ depends on the ideal currents $\hat{\mathbf{w}}$ and matrix $\mathbf{B}$, and it is independent of the optimal value δ_B. It can be removed from the objective function. Setting $r_1 = g_1^2 + g_2^2$, $r_2 = g_{2M+1}^2 + g_{2M+2}^2$, the objective function (3.16a) can be further reformulated as

$$\frac{r_1}{1 - \delta_B\zeta_1} + \frac{r_2}{1 - \delta_B\zeta_3}. \tag{C.6}$$

The optimisation problem can be reformulated as (3.17) from (C.3) and (C.6).

Appendix D
Proof of Proposition 4

As when $\delta_B = \frac{1}{\zeta_3}$ or $\delta_B = \frac{1}{\zeta_1}$, the objective function of (3.17a) cannot obtain minimal value, there are two possible cases from (3.20).

D.0.9 Case 1: $\sigma_2 = 0$, $\delta_B = 0$, and $\sigma_1 \geq 0$

In this case, we can rewrite (3.19) as

$$\nabla_{\delta_B} L_{\delta_B}(\delta_B, \sigma_1, \sigma_2) = \zeta_1 r_1 + \zeta_3 r_2 - \sigma_1 = 0. \tag{D.1}$$

Thus, we have

$$\sigma_1 = \zeta_1 r_1 + \zeta_3 r_2, \tag{D.2}$$

which means $\zeta_1 r_1 + \zeta_3 r_2 \geq 0$.

D.0.10 Case 2: $\sigma_2 = 0$, $\sigma_1 = 0$, and $\delta_B \geq 0$

The stationarity condition of the KKT conditions (3.20) can be written as

$$\nabla_{\delta_B} L_{\delta_B}(\delta_B, \sigma_1, \sigma_2) = -\frac{\zeta_1 r_1}{(1 - \delta_B \zeta_1)^2} - \frac{\zeta_3 r_2}{(1 - \delta_B \zeta_3)^2} = 0. \tag{D.3}$$

As $\zeta_1 < 0$, $\zeta_3 > 0$, $r_1, r_2 > 0$, (3.20) can be further simplified as

$$\frac{\sqrt{-\zeta_1 r_1}}{1 - \delta_B \zeta_1} = \frac{\sqrt{\zeta_3 r_2}}{1 - \delta_B \zeta_3}. \tag{D.4}$$

Then the value of δ_B is

$$\delta_B = \frac{\sqrt{-\zeta_1 r_1} - \sqrt{\zeta_3 r_2}}{\zeta_3\sqrt{-\zeta_1 r_1} - \zeta_1\sqrt{\zeta_3 r_2}}. \tag{D.5}$$

In this case, we have

$$\frac{\zeta_1 r_1 + \zeta_3 r_2}{\left(1-\delta_B\zeta_1\right)^2} < \frac{\zeta_1 r_1}{\left(1-\delta_B\zeta_1\right)^2} + \frac{\zeta_3 r_2}{\left(1-\delta_B\zeta_3\right)^2} = 0. \tag{D.6}$$

Then, we have

$$\zeta_1 r_1 + \zeta_3 r_2 < 0. \tag{D.7}$$

D.0.11 Discussion

In this subsection, we apply logic to prove that the case 1 and the case 2 are logically equivalent to the statement that the ideal signal can be transmitted by EA and the statement that the ideal signal cannot be supported by EA, respectively. Let C_1 and C_2 denote the statement case 1 and case 2, respectively. D_P for the statement $\hat{\mathbf{i}} \in \mathbb{I}_{P\xi}$ and D_N for the statement $\hat{\mathbf{i}} \in \mathbb{I}_{N\xi}$. D_1 for $\hat{\mathbf{w}}_T^T\mathbf{B}\hat{\mathbf{w}} \geq 0$ and D_2 for $\hat{\mathbf{w}}_T^T\mathbf{B}\hat{\mathbf{w}} < 0$. D_3 for $\zeta_1 r_1 + \zeta_3 r_2 \geq 0$ and D_4 for $\zeta_1 r_1 + \zeta_3 r_2 < 0$.

From (3.10b), we have $D_P \Leftrightarrow D_1$ and $D_N \Leftrightarrow D_2$, where $\Leftrightarrow$ means if and only if.

Now, we can see the practical meaning of these two cases. Substituting ideal currents into constraint (3.10b), we have

$$\hat{\mathbf{w}}_T^T\mathbf{B}\hat{\mathbf{w}} = \left(\mathbf{Q}^\mathbf{T}\hat{\mathbf{w}}\right)^T \mathbf{\Lambda}\mathbf{Q}^\mathbf{T}\hat{\mathbf{w}} = \mathbf{g}^T\Lambda\mathbf{g} = \zeta_1 r_1 + \zeta_3 r_2. \tag{D.8}$$

Thus, we have $D_1 \Leftrightarrow D_3$ and $D_2 \Leftrightarrow D_4$.

In the case 1, as $\sigma_1 \geq 0$, $\zeta_1 r_1 + \zeta_3 r_2 \geq 0$. Thus, $C_1 \Rightarrow D_3$ and then $C_1 \Rightarrow D_P$. If D_P is true, then we have $\zeta_1 r_1 + \zeta_3 r_2 \geq 0$ as $D_P \Leftrightarrow D_1 \Leftrightarrow D_3$. Since there are only two cases of solutions, we have C_1 is true, which means $D_P \Rightarrow C_1$. Thus, we have $C_1 \Leftrightarrow D_P$, which implies that case 1 is equivalent that the ideal currents $\hat{\mathbf{i}}$ can be supported by EA . Similarly,

we have $C_2 \Leftrightarrow D_N$, the ideal currents cannot be implemented by ESPAR antenna. Then we have

$$\delta_B^* = \begin{cases} 0 & \text{for } \hat{\mathbf{i}} \in \mathbb{I}_{P\xi} \\ \frac{\sqrt{-\zeta_1 r_1}-\sqrt{\zeta_3 r_2}}{\zeta_3\sqrt{-\zeta_1 r_1}-\zeta_1\sqrt{\zeta_3 r_2}} & \text{for } \hat{\mathbf{i}} \in \mathbb{I}_{N\xi} \end{cases}. \tag{D.9}$$

Appendix E
Proof of Proposition 5

From (3.43), the proposition can be proved in these two cases.

E.0.12 Case 1, $R_1 > 0$

In this case, by setting $l_1 = \frac{X_1}{R_1}$, $l_2 = \frac{r_{in}-R_0}{R_1}$, the CDF of input resistance is

$$\begin{aligned} F_{R_{in}}(r_{in}) &= \iint_{r_\kappa \leq \frac{X_1}{R_1} x_\kappa + \frac{r_{in}-R_0}{R_1}} f(r_\kappa, x_\kappa) \mathrm{d}r_\kappa \mathrm{d}x_\kappa \\ &= \frac{M}{\pi} \int_{-\infty}^{+\infty} \int_{-\infty}^{l_1 x_\kappa + l_2} \left(r_\kappa^2 + x_\kappa^2 + M\right)^{-2} \mathrm{d}r_\kappa \mathrm{d}x_\kappa. \end{aligned} \tag{E.1}$$

The indefinite integral with respect to r_κ can be calculated by using [114, eq. (2.110.2)] and [114, eq. (2.01.15)] and it is

$$\begin{aligned} \int \left(r_\kappa^2 + x_\kappa^2 + M\right)^{-2} \mathrm{d}r_\kappa = &\frac{r_\kappa}{2(M + x_\kappa^2)(M + x_\kappa^2 + r_\kappa^2)} \\ &+ \frac{\arctan\left(\frac{r_\kappa}{\sqrt{M+x_\kappa^2}}\right)}{2(M + x_\kappa^2)^{3/2}}. \end{aligned} \tag{E.2}$$

Applying Newton-Leibniz formula, the definite integral with respect to r_κ is

$$\begin{aligned} &\int_{-\infty}^{l_1 x_\kappa + l_2} \left(r_\kappa^2 + x_\kappa^2 + M\right)^{-2} \mathrm{d}r_\kappa \\ &= \frac{l_1 x_\kappa + l_2}{2(M + x_\kappa^2)\left(M + x_\kappa^2 + (l_1 x_\kappa + l_2)^2\right)} + \frac{\pi/2}{2(M + x_\kappa^2)^{3/2}} + \frac{\arctan\left(\frac{l_1 x_\kappa + l_2}{\sqrt{M+x_\kappa^2}}\right)}{2(M + x_\kappa^2)^{3/2}}. \end{aligned} \tag{E.3}$$

Substituting (E.3) into (E.1), the double integral can be separated into the sum of three integrals. The indefinite integral of the first part, $F_1(x_\kappa)$, can be calculated by using [114, eq. (2.01.15)] and [114, eq. (2.01.2)] and doing some algebraic manipulations, and it is

$$\begin{aligned} F_1(x_\kappa) &= \int \frac{l_1 x_\kappa + l_2}{2(M + x_\kappa^2)\left(M + x_\kappa^2 + (l_1 x_\kappa + l_2)^2\right)} \mathrm{d}x_\kappa \\ &= \frac{2 l_2 \arctan\left(\frac{x_\kappa}{\sqrt{M}}\right)}{4\left(l_1^2 M + l_2^2\right)\sqrt{M}} \\ &\quad - \frac{2 l_2 \arctan\left(\left(x_\kappa + x_\kappa l_1^2 + l_1 l_2\right)/\sqrt{M + l_1^2 M + l_2^2}\right)}{4\left(l_1^2 M + l_2^2\right)\sqrt{M + l_1^2 M + l_2^2}} \\ &\quad + \frac{l_1}{4\left(l_1^2 M + l_2^2\right)} \ln \frac{M + x_\kappa^2\left(1 + l_1^2\right) + 2 x_\kappa l_1 l_2 + l_2^2}{M + x_\kappa^2}. \end{aligned} \tag{E.4}$$

Similarly, the indefinite integral of the second part, $F_2(x_\kappa)$, can be calculated from [114, eq. (2.264.5)] and it is

$$F_2(x_\kappa) = \int \frac{\pi/2}{2(M + x_\kappa^2)^{3/2}} \mathrm{d}x_\kappa = \frac{\pi}{4} \frac{x_\kappa}{M\sqrt{M + x_\kappa^2}}. \tag{E.5}$$

The indefinite integral of third part, $F_3(x_\kappa)$, can be firstly simplified by applying the theorem of integration by parts, and then calculated by using [114, eq. (2.01.15)] and [114, eq.

(2.01.2)]. After some algebraic manipulations, we have

$$
\begin{aligned}
F_3\left(x_\kappa\right) &= \int \frac{\arctan\left(\frac{l_1 x_\kappa + l_2}{\sqrt{M+x_\kappa^2}}\right)}{2(M+x_\kappa^2)^{3/2}}\mathrm{d}x_\kappa \\
&= \frac{1}{2}\int \arctan\left(\frac{l_1 x_\kappa + l_2}{\sqrt{M+x_\kappa^2}}\right)\mathrm{d}\frac{x_\kappa}{M\sqrt{M+x_\kappa^2}} \\
&= \frac{x_\kappa}{2M\sqrt{M+x_\kappa^2}}\arctan\left(\frac{l_1 x_\kappa + l_2}{\sqrt{M+x_\kappa^2}}\right) - \int \frac{x_\kappa}{2M\sqrt{M+x_\kappa^2}}\mathrm{d}\left(\arctan\left(\frac{\mathrm{l_1 x_\kappa + l_2}}{\sqrt{\mathrm{M+x_\kappa^2}}}\right)\right) \\
&= -\frac{l_2\arctan\left(\frac{x_\kappa}{\sqrt{M}}\right)}{2\sqrt{M}\left(l_1^2M+l_2^2\right)} + \frac{x_\kappa\arctan\left(\left(x_\kappa l_1+l_2\right)/\sqrt{M+x_\kappa^2}\right)}{2M\sqrt{M+x_\kappa^2}} \\
&+ \frac{l_2\sqrt{M+l_1^2M+l_2^2}\arctan\left(\left(x_\kappa+x_\kappa l_1^2+l_1l_2\right)/\sqrt{M+l_1^2M+l_2^2}\right)}{2M\left(l_1^2M+l_2^2\right)} \\
&+ \frac{l_1\ln\frac{M+x_\kappa^2}{M+x_\kappa^2(1+l_1^2)+2x_\kappa l_1 l_2+l_2^2}}{4\left(l_1^2M+l_2^2\right)}.
\end{aligned}
\tag{E.6}
$$

According to Newton-Leibniz formula and after some algebraic manipulations, the probability when the real part of the input impedance is less than r_{in} under the condition $R_1 \geq 0$ is

$$
F_{R_{in}}(r_{in}) = \frac{1}{2} + \frac{l_2}{2\sqrt{M+l_1^2M+l_2^2}}. \tag{E.7}
$$

As $l_1 = \frac{X_1}{R_1}$ and $l_2 = \frac{r_{in}-R_0}{R_1}$, putting them into (E.7), we have (3.44). The PDF of R_{in} can be obtained from its CDF as (3.45). The probability of the real part of the input impedance is bigger than 0 under the condition $R_1 > 0$ is (3.46).

E.0.13 Case 2: $R_1 < 0$

From (3.42), in this case, the probability is

$$\begin{aligned} F_{R_{in}}(r_{in}) &= \iint_{r_\kappa > \frac{X_1}{R_1}x_\kappa + \frac{r_{in}-R_0}{R_1}} f(r_\kappa, x_\kappa)\mathrm{d}r_\kappa \mathrm{d}x_\kappa \\ &= \frac{M}{\pi}\int_{-\infty}^{+\infty}\int_{l_1 x_\kappa + l_2}^{+\infty} \left(r_\kappa^2 + x_\kappa^2 + M\right)^{-2} \mathrm{d}r_\kappa \mathrm{d}x_\kappa. \end{aligned} \tag{E.8}$$

Applying Newton-Leibniz formula based on (E.2), we have

$$\begin{aligned} &\int_{l_1 x_\kappa + l_2}^{+\infty} \left(r_\kappa^2 + x_\kappa^2 + M\right)^{-2} \mathrm{d}r_\kappa \\ &= \frac{\pi/2}{2(M + x_\kappa^2)^{3/2}} - \frac{\arctan\left(\frac{l_1 x_\kappa + l_2}{\sqrt{M + x_\kappa^2}}\right)}{2(M + x_\kappa^2)^{3/2}} \\ &- \frac{l_1 x_\kappa + l_2}{2(M + x_\kappa^2)\left(M + x_\kappa^2 + (l_1 x_\kappa + l_2)^2\right)}. \end{aligned} \tag{E.9}$$

Substituting (E.9) into (E.8) and after some algebraic manipulations, the CDF and PDF when $R_1 < 0$ is (3.44), (3.45), respectively. Similarly, the probability of the real part of the input impedance is bigger than 0 under the condition $R_1 < 0$ is (3.46).

Appendix F
Proof of Proposition 11

As the function $\log_2(1+x)$ is a monotonic increasing function with respect to x, with the allocated power P_t at the t-th RRH, the optimisation problem (5.5) can be written as

$$\begin{aligned} \max_{\mathbf{w}_{1,1},\mathbf{w}_{1,2},\ldots,\mathbf{w}_{1,N}} \quad & |\sum_{t=1}^{N} \mathbf{h}_{1,t}^H \mathbf{w}_{1,t}|^2, \\ \text{s.t.} \quad & \text{tr}\left\{\mathbf{w}_{1,t}\mathbf{w}_{1,t}^H\right\} = P_t, \quad \text{for } t = 1,2,\ldots,N. \end{aligned} \tag{F.1}$$

Let $\mathbf{h}$, $\mathbf{w}$ and $\mathbf{Q}$ denotes $\mathbf{h} = [\mathbf{h}_1^H, \mathbf{h}_2^H, \ldots, \mathbf{h}_N^H]^H$, $\mathbf{w} = [\mathbf{w}_{1,1}^H, \mathbf{w}_{1,2}^H, \ldots, \mathbf{w}_{1,N}^H]^H$ and $\mathbf{Q} = \mathbf{w}\mathbf{w}^H$, respectively. The τ-th row and j-th column element of matrix Q is denoted as $q_{\tau j}$. The constraint can be relaxed to 2×2 principle minors of Q and the principle minors are given as [82, 115]. Then we have

$$\mathbf{T}_{\tau j} = \begin{bmatrix} q_{\tau\tau} & \overline{q_{\tau j}} \\ q_{\tau j} & q_{jj} \end{bmatrix}, \tag{F.2}$$

where a minor $\mathbf{T}_{\tau j}$ is achieved by removing $M_t - 2$ rows (except column τ and j) and corresponding columns of $\mathbf{Q}$. The relaxation form of the second constraint of (5.5) can be relaxed as $\mathbf{T}_{\tau j} \geq 0$, and it is identical to $|q_{\tau j}|^2 = q_{\tau\tau} q_{jj}$ [82, 115]. The optimisation problem can be expressed as:

$$\begin{aligned} \max_{\mathbf{Q}} \quad & \mathbf{h}\mathbf{Q}\mathbf{h}^H \\ \text{s.t.} \quad & \sum_{t=M_{(i-1)}+1}^{M_i} q_{tt} = P_t, \quad \text{for} \quad i = 1,2,\ldots,N, \\ & |q_{\tau j}|^2 \leq q_{\tau\tau} q_{jj}, \quad \text{for} \quad \tau, j = 1,2,\ldots,M_t - 1. \end{aligned} \tag{F.3}$$

By using KKT conditions and the rank of $\mathbf{w}_{1,t}$ is equal to one, the optimal precoder vectors

for RRHs are obtained as Proposition 11.

Appendix G
Proof of Proposition 14

When the power allocated to the k-th user is assumed to be $P_k^{(U)}$ and the optimal value will be discussed later. The total system power consumption can be written as $P_{tot} = P_{bbu} + P_{fiber} + \left(\frac{\zeta}{\eta}\sum_{k=1}^{K} P_k^{(U)} + n_t P_{tc}\right) + KP_u$, which is independent to the values of $(\xi_1, \mathbf{q}_1, \xi_2, \mathbf{q}_2, \ldots \xi_K, \mathbf{q}_K)$. Thus, (5.22) can be reformulated as

$$\begin{aligned}
&(\xi_1^*, \mathbf{q}_1^*, \xi_2^*, \mathbf{q}_2^*, \ldots \xi_K^*, \mathbf{q}_K^*) \\
&= \underset{\xi_k^2 \mathbf{g}_k^H \mathbf{g}_k + \mathbf{L}_k^H \mathbf{U}^H \mathbf{U} \mathbf{L}_k = P_k^{(U)}}{\arg\max} \eta_{EE} \\
&= \underset{\xi_k^2 \mathbf{g}_k^H \mathbf{g}_k + \mathbf{L}_k^H \mathbf{U}^H \mathbf{U} \mathbf{L}_k = P_k^{(U)}}{\arg\max} R \\
&= \underset{\xi_k^2 \mathbf{g}_k^H \mathbf{g}_k + \mathbf{L}_k^H \mathbf{U}^H \mathbf{U} \mathbf{L}_k = P_k^{(U)}}{\arg\max} \sum_{k=1}^{K} r_k \\
&= \underset{\xi_k^2 \mathbf{g}_k^H \mathbf{g}_k + \mathbf{L}_k^H \mathbf{U}^H \mathbf{U} \mathbf{L}_k = P_k^{(U)}}{\arg\max} \sum_{k=1}^{K} \Omega \log_2 \left(1 + \frac{\left|\mathbf{h}_k^H \mathbf{w}_k\right|^2}{\sum_{j=1, j\neq k}^{K} \left|\mathbf{h}_k^H \mathbf{w}_j\right|^2 + \sigma_k^2}\right) \\
&= \underset{\xi_k^2 \mathbf{g}_k^H \mathbf{g}_k + \mathbf{L}_k^H \mathbf{U}^H \mathbf{U} \mathbf{L}_k = P_k^{(U)}}{\arg\max} \sum_{k=1}^{K} \Omega \log_2 \left(1 + \frac{\left|\mathbf{h}_k^H \left(\xi_k \mathbf{g}_k + \mathbf{U}\mathbf{q}_k\right)\right|^2}{\sigma_k^2}\right) \\
&= \underset{\xi_k^2 \mathbf{g}_k^H \mathbf{g}_k + \mathbf{L}_k^H \mathbf{U}^H \mathbf{U} \mathbf{L}_k = P_k^{(U)}}{\arg\max} \sum_{k=1}^{K} \Omega \log_2 \left(1 + \frac{\xi_k^2}{\sigma_k^2}\right)
\end{aligned} \tag{G.1}$$

This problem can be divided into K sub-optimziation problems as

$$\begin{aligned}
(\xi_k^*, \mathbf{q}_k^*) &= \underset{\xi_k^2 \mathbf{g}_k^H \mathbf{g}_k + \mathbf{q}_k^H \mathbf{U}^H \mathbf{U} \mathbf{q}_k = P_k^{(U)}}{\arg\max} \Omega \log_2 \left(1 + \frac{\xi_k^2}{\sigma_k^2}\right) \\
&= \underset{\xi_k^2 \mathbf{g}_k^H \mathbf{g}_k + \mathbf{q}_k^H \mathbf{U}^H \mathbf{U} \mathbf{q}_k = P_k^{(U)}}{\arg\max} \xi_k^2, \ k = 1, 2, \ldots, K.
\end{aligned} \tag{G.2}$$

As $\xi_k^2 > 0$, $\mathbf{g}_k^H \mathbf{g}_k = \|\mathbf{g}_k\|^2 > 0$ and $\mathbf{q}_k^H \mathbf{U}^H \mathbf{U} \mathbf{q}_k = \|\mathbf{U}\mathbf{q}_k\|^2 > 0$, then the optimal value of ξ_k, $\mathbf{q}_k$ to maximise the EE is

$$\xi_k^* = \sqrt{\frac{P_k^{(U)}}{\mathbf{g}_k^H \mathbf{g}_k}}, \mathbf{q}_k^* = \mathbf{0}. \tag{G.3}$$

By substituting (G.3) into (5.20), the global precoder for the k-th user is given as

$$\mathbf{w}_k^* = \sqrt{\frac{P_k^{(U)}}{\mathbf{g}_k^H \mathbf{g}_k}} \mathbf{g}_k \tag{G.4}$$

Then, the precoder to the k-th user at the t-th RRH is derived as (5.24).

Appendix H
Proof of non-convexity of (4.3)

Proof: Let w_{2m+1} and w_{2m+2} from the vector $\mathbf{i}$ denote the real part and the imaginary part of i_m. Representing the current values in (2.46) in terms of w_{2m+1} and w_{2m+2} and substituting it in (4.1), the input power to the active element can be simplified as

$$\begin{aligned} P_E &= \left(w_1^2 + w_2^2\right) \Re\left\{ Z_{00} + \frac{\sum_{m=1}^{M-1} Z_{0m} i_m}{i_0} \right\} \\ &= \left(w_1^2 + w_2^2\right) \Re\left\{ R_0 + jX_{Z0} + \frac{\sum_{m=1}^{M-1} \left[\left(R_m w_{2m+1} - X_m w_{2m+2}\right) + j\left(R_m w_{2m+2} + X_m w_{2m+1}\right)\right]}{w_1 + jw_2} \right\} \\ &= R_0 w_1^2 + R_0 w_2^2 + \sum_{k=1}^{M-1} \left(R_m w_{2m+1} w_1 - X_m w_{2m+2} w_1 + R_m w_{2k+2} w_2 + X_1 w_{2m+1} w_2\right), \end{aligned} \tag{H.1}$$

and it can be expressed in vector form as (4.3). ■

Appendix I
Proof of non-convexity of (4.8)

Proof: As $\mathbf{A}$ is a real symmetric matrix and it can be diagonalized as $\mathbf{A} = \mathbf{Q}_A \Lambda_A \mathbf{Q}_A^T$,

$$\mathbf{A} = \mathbf{Q}_A \Lambda_A \mathbf{Q}_A^T, \tag{I.1}$$

where $\mathbf{\Lambda_A}$ is a real diagonal matrix and its elements are eigenvalues of $\mathbf{A}$, the columns of the real orthogonal matrix $\mathbf{Q}_A$ are corresponding eigenvectors of $\mathbf{A}$. For the sake of simplification, the eigenvalues $\mathbf{\Lambda_A}$ are set in ascending order. Let λ denotes the eigenvalues of $\mathbf{A}$, the matrix $\mathbf{A} - \lambda\mathbf{I}$ can be written as

$$\begin{aligned}\mathbf{A} - \lambda\mathbf{I} &= \begin{bmatrix} R_0 - \xi - \lambda & 0 & \frac{R_1}{2} & -\frac{X_1}{2} & \dots & \frac{R_{M-1}}{2} & -\frac{X_{M-1}}{2} \\ 0 & R_0 - \xi - \lambda & \frac{X_1}{2} & \frac{R_1}{2} & \dots & \frac{X_{M-1}}{2} & \frac{R_{M-1}}{2} \\ \frac{R_1}{2} & \frac{X_1}{2} & -\lambda & 0 & \dots & 0 & 0 \\ -\frac{X_1}{2} & \frac{R_1}{2} & 0 & -\lambda & \dots & 0 & 0 \\ \vdots & \vdots & \vdots & \vdots & \ddots & \vdots & \vdots \\ \frac{R_{M-1}}{2} & \frac{X_{M-1}}{2} & 0 & 0 & \dots & -\lambda & 0 \\ -\frac{X_{M-1}}{2} & \frac{R_{M-1}}{2} & 0 & 0 & \dots & 0 & -\lambda \end{bmatrix} \\ &= \begin{bmatrix} \mathbf{A}_{11} & \mathbf{A}_{12} \\ \mathbf{A}_{21} & \mathbf{A}_{22} \end{bmatrix},\end{aligned} \tag{I.2}$$

where

$$\begin{aligned}\mathbf{A}_{11} &= \begin{bmatrix} R_0 - \lambda & 0 \\ 0 & R_0 - \lambda \end{bmatrix}, \\ \mathbf{A}_{12} &= \begin{bmatrix} \frac{R_1}{2} & -\frac{X_1}{2} & \frac{R_1}{2} & -\frac{X_1}{2} & \dots & \frac{R_{M-1}}{2} & -\frac{X_{M-1}}{2} \\ \frac{X_1}{2} & \frac{R_1}{2} & \frac{X_1}{2} & \frac{R_1}{2} & \dots & \frac{X_{M-1}}{2} & \frac{R_{M-1}}{2} \end{bmatrix}, \\ \mathbf{A}_{21} &= \mathbf{A}_{12}^T,\end{aligned}$$

$$\mathbf{A}_{22} = \mathrm{diag}\left(-\lambda, -\lambda, \ldots, -\lambda\right).$$

The determinant of $\mathbf{A} - \lambda\mathbf{I}$ As $\mathbf{A}_{22}$ is invertible, the determinant of the matrix $\mathbf{A} - \lambda\mathbf{I}$ can be derived as in Appendix (B). Following similar steps as in Appendix (B), the eigenvalues of $\mathbf{A}$ are (I.4).

$$\begin{cases} \lambda_1 = \lambda_2 = R_0 - \sqrt{R_0^2 + \sum_{m=1}^{M-1}\left(R_m^2 + X_m^2\right)} < 0 \\ \lambda_{2M-1} = \lambda_{2M} = R_0 + \sqrt{R_0^2 + \sum_{m=1}^{M-1}\left(R_m^2 + X_m^2\right)} > 0 \\ \lambda_n = 0 \quad \text{for } n = 3, 4, \ldots, 2(M-2) \end{cases} . \tag{I.4}$$

We can find that λ_1 and λ_2 are negative whereas λ_{2M-1} and λ_4 are positive eigenvalues, thus $\mathbf{\Lambda_A}$ is $\mathrm{diag}(\lambda_1, \lambda_2, 0, \ldots, 0, \lambda_{2M-1}, \lambda_{2M})$. The matrix $\mathbf{A}$ is not a positive or a negative semidefinite matrix. The constraints (4.7b) and (4.7c) are non-convex and therefore the optimisation problem (4.7) is a non-covex problem. ■

Appendix J
Proof of Proposition 8

Proof: As $\mathbf{A}$ is a real symmetric matrix and it can be diagonalized as $\mathbf{A} = \mathbf{Q}_A \mathbf{\Lambda}_A \mathbf{Q}_A^T$, where $\mathbf{\Lambda}_A$ is a real diagonal matrix whose elements are eigenvalues of $\mathbf{A}$, the columns of the real orthogonal matrix $\mathbf{Q}_A$ are corresponding eigenvectors. Let $\mathbf{e} = \mathbf{Q^T w}$, $\mathbf{g} = \mathbf{Q}_A^T \hat{\mathbf{w}}$. By substituting them into (4.8a), the objective function of this optimisation problem can be written as

$$\begin{aligned} \|\mathbf{w} - \hat{\mathbf{w}}\|^2 &= (\mathbf{Q}(\mathbf{e} - \mathbf{g}))^T (\mathbf{Q}(\mathbf{e} - \mathbf{g})) \\ &= (\mathbf{e} - \mathbf{g})^T (\mathbf{e} - \mathbf{g}) = \|\mathbf{e} - \mathbf{g}\|^2 . \end{aligned} \tag{J.1}$$

Similarly, the left side of the constraints (4.8b) and (4.8c) can be written as

$$\mathbf{w}^T \mathbf{A} \mathbf{w} = \mathbf{e}^T \mathbf{\Lambda_A} \mathbf{e}. \tag{J.2}$$

Thus, the optimisation problem can be reformulated as

$$\min_{\mathbf{e}} \quad \|\mathbf{e} - \mathbf{g}\|_2^2 , \tag{J.3a}$$

$$\text{st.} \quad \mathbf{e}^T \mathbf{\Lambda_A} \mathbf{e} \geq P_{min}, \tag{J.3b}$$

$$\mathbf{e}^T \mathbf{\Lambda_A} \mathbf{e} \leq P_{max}. \tag{J.3c}$$

By substituting the elements of $\mathbf{g}$ and $\mathbf{e}$ into (J.3), its objective function can be further reformulated as

$$\|\mathbf{e} - \mathbf{g}\|_2^2 = \sum_{m=1}^{2} (e_m - g_m)^2 + \sum_{m=3}^{2M-2} (e_m - g_m)^2 + \sum_{m=2M-1}^{2M} (e_m - g_m)^2 , \tag{J.4}$$

and the corresponding constraints are

$$\begin{aligned} \mathbf{e}^T \mathbf{\Lambda_A} \mathbf{e} &= \lambda_1 \left(e_1^2 + e_2^2\right) + \lambda_{2M-1} \left(e_{2M-1}^2 + e_{2M}^2\right) \geq P_{min}, \\ \mathbf{e}^T \mathbf{\Lambda_A} \mathbf{e} &= \lambda_1 \left(e_1^2 + e_2^2\right) + \lambda_{2M-1} \left(e_{2M-1}^2 + e_{2M}^2\right) \leq P_{max}. \end{aligned} \tag{J.5}$$

From (J.4) (J.5), it is noted that the element $e_m,\ m = 3, 4, \ldots, 2M$ is not in the constraints. In order to minimize (J.4), we have $e_m = g_m,\ \text{for}\ m = 3, 4, \ldots, 2M$. (J.3) can be further reformulated as

$$\min_{\tilde{\mathbf{e}}} \quad \left\|\tilde{\mathbf{e}} - \tilde{\mathbf{g}}\right\|^2, \tag{J.6a}$$

$$\text{st.} \quad \lambda_1 \left(e_1^2 + e_2^2\right) + \lambda_{2M-1} \left(e_{2M-1}^2 + e_{2M}^2\right) > P_{min}, \tag{J.6b}$$

$$\lambda_1 \left(e_1^2 + e_2^2\right) + \lambda_{2M-1} \left(e_{2M-1}^2 + e_{2M}^2\right) \leq P_{max}. \tag{J.6c}$$

By setting $\tilde{\mathbf{e}} = [e_1, e_2, e_{2M-1}, e_{2M}]^T$, $\tilde{\mathbf{g}} = [g_1, g_2, g_{2M-1}, g_{2M}]^T$ and $\mathbf{\Lambda 1} = diag\left(\lambda_1, \lambda_1, \lambda_{2M-1}, \lambda_{2M-1}\right)$, this can be written in matrix form as (4.10). ■

Appendix K
Proof of Proposition 9

Proof: By substituting the polar coordinate forms into (4.10), its constraints can be rewritten as

$$\begin{aligned}\lambda_1\left(e_1^2+e_2^2\right)+\lambda_{2M-1}\left(e_{2M-1}^2+e_{2M}^2\right)&=\lambda_1 r_a^2+\lambda_{2M-1}r_b^2\geq P_{min},\\ \lambda_1\left(e_1^2+e_2^2\right)+\lambda_{2M-1}\left(s_{2M-1}^2+e_{2M}^2\right)&=\lambda_1 r_a^2+\lambda_{2M-1}r_b^2\leq P_{max}.\end{aligned} \tag{K.1}$$

As $r_a \geq 0$, $r_b \geq 0$, $\lambda_1 < 0$, $\lambda_{2M-1} > 0$, the objective function (4.10a) can be changed as

$$\begin{aligned}\left\|\tilde{\mathbf{e}}-\tilde{\mathbf{g}}\right\|^2=&\sum_{m=1}^{2}\left(e_m-g_m\right)^2+\sum_{m=2M-1}^{2M}\left(e_m-g_m\right)^2\\ =&r_a^2+r_b^2-2r_a r_c\left(\cos\theta_a\cos\theta_c-\sin\theta_a\sin\theta_c\right)\\ &+r_c^2+r_d^2-2r_b r_c\left(\cos\theta_b\cos\theta_d-\sin\theta_b\sin\theta_d\right)\\ =&r_a^2+r_b^2-2r_a r_c\cos\left(\theta_a-\theta_c\right)-2r_b r_c\cos\left(\theta_b-\theta_d\right)+r_c^2+r_d^2.\end{aligned} \tag{K.2}$$

As there is no constraint on θ_a and θ_b from (K.1), the range of (K.2) is

$$\begin{aligned}\left\|\tilde{\mathbf{e}}-\tilde{\mathbf{g}}\right\|^2&\geq r_a^2+r_b^2-2r_a r_c-2r_b r_c+r_c^2+r_d^2\\ &=\left(r_a-r_c\right)^2+\left(r_b-r_d\right)^2.\end{aligned} \tag{K.3}$$

The objective function $\left\|\tilde{\mathbf{e}}-\tilde{\mathbf{g}}\right\|^2$ achieves its minimal value when when $\theta_a=\theta_c$ and $\theta_b=\theta_d$. Thus, the optimal point of θ_a and θ_b are θ_c and θ_d, respectively. The optimisation problem (4.10) can be simplified as (4.11). ■

Appendix L
Proof of Proposition 10

Proof: When setting $r_a = \sec(\theta)$, and $r_b = \tan(\theta)$, the distance from $\mathbf{r}_g$ and the hyperbola can be expressed as

$$F(\theta) = |\mathbf{r}_g - \mathbf{r}_e|^2 . \tag{L.1}$$

As $F(\theta)$ is a non-negative, periodic, and differentiable function, it must have a global minimum occurring at an angle for which the first-order derivative is zero,

$$F'(\theta) = 2(\mathbf{r}_g - \mathbf{r}_e)\mathbf{r}_g^{'}. \tag{L.2}$$

For the derivative to be zero, the vectors $\mathbf{r}_g - \mathbf{r}_e$ and $\mathbf{r}_g^{'}$ must be perpendicular. The vector $\mathbf{r}_g^{'}$ is tangent to the ellipse at $\mathbf{r}_g$. This implies that the vector from $\mathbf{r}_g$ to the closest ellipse point $\mathbf{r}_e$ is normal to the curve at $\mathbf{r}_g$. Using the implicit form of the ellipse, namely, $\lambda_1 r_a^2 + \lambda_{2M-1} r_b^2 = P_{max}$, half of its gradient is a normal vector to the ellipse at (r_a, r_b), so $(r_c, r_d) - (r_a, r_b) = t(\lambda_1 r_a, \lambda_2 r_b)$ for some scalar t, or

$$r_c = r_a(1 + \lambda_1 t),\ r_d = r_b(1 + \lambda_{2M-1} t). \tag{L.3}$$

As all signals are transmitted through the antenna elements, and $r_c > 0$, $r_d > 0$, we have

$$r_a = \frac{r_c}{1 + \lambda_1 t}, r_b = \frac{r_d}{1 + \lambda_{2M-1} t}. \tag{L.4}$$

In order to describe the constraint area, we introduce a auxiliary function $G = \lambda_1 r_a^2 + \lambda_{2M-1} r_b^2 - P_{max}$. By substitute (L.4) into it to obtain

$$G(t) = \lambda_1 \left(\frac{r_c}{1 + \lambda_1 t}\right)^2 + \lambda_{2M-1} \left(\frac{r_d}{1 + \lambda_{2M-1} t}\right)^2 - P_{max}. \tag{L.5}$$

We know that the closest point in the first quadrant requires $1+\lambda_{2M-1}t \geq 0$ and $1+\lambda_1 t \geq 0$, which implies $t \geq -\frac{1}{\lambda_{2M-1}}$ and $t \leq -\frac{1}{\lambda_1}$.

The first-order derivative of $G(t)$ are

$$G^{'}(t) = -\frac{2\lambda_1^2 r_c^2}{(1+\lambda_1 t)^3} - \frac{2\lambda_{2M-1}^2 r_d^2}{(1+\lambda_{2M-1}t)^3} < 0. \tag{L.6}$$

For $t \geq -\frac{1}{\lambda_{2M-1}}$ and $t \leq -\frac{1}{\lambda_1}$, we have the conditions $G^{'}(t) < 0$. Also observe that

$$\begin{aligned} \lim_{t \to \left(-\frac{1}{\lambda_1}\right)^+} G^{'}(t) &= -\infty, \\ \lim_{t \to \left(-\frac{1}{\lambda_{2M-1}}\right)^-} G^{'}(t) &= +\infty. \end{aligned} \tag{L.7}$$

These two expressions are one-sided limits where t approaches $-\frac{1}{\lambda_{2M-1}}$ through values larger than $-\frac{1}{\lambda_1}$. We have shown that $F(t)$ is a strictly decreasing function for $t \in (-\frac{1}{\lambda_{2M-1}}, -\frac{1}{\lambda_1})$ that is initially positive, then becomes negative. Consequently it has a unique root on the specified domain. ■

Appendix M
List of Publications

This Appendix contains a list of published papers.

M.1 Accepted Journal Publications

- **L. Zhou**, F. Khan, T. Ratnarajah, and C. B. Papadias, "Single-RF Multi-antenna Transmission with Peak Power Constraint," *IEEE Trans. on Communications*, Vol. 65, Issue 12, pp. 5197-5208, Dec. 2017.
- **L. Zhou**, F. Khan, T. Ratnarajah, and C. B. Papadias, " Achieving Arbitrary Signals Transmission Using a Single Radio Frequency Chain," *IEEE Trans. on Communications*, vol. PP, no.99, 2015.
- A. Cirik, **L. Zhou** and T. Ratnarajah, " Linear Transceiver Design With Per-Antenna Power Constraints in Full-Duplex Multi-User MIMO Systems," *IEEE Wireless Communications Letters*, vol. 5, no. 4, pp. 412-415, Aug. 2016.
- M. Artuso, D. Boviz, A. Checko, H. L. Christiansen, B. Clerckx, L. Cottatellucci, D. Gesbert, B. Gizas, A. Gopalasingham, F. Khan, J. M. Kelif, R. Muller, D. Ntaikos, K. Ntougias, C. B. Papadias, B. Rassouli, M. A. Sedaghat, T. Ratnarajah, L. Roullet, S. Senecal, H. Yin and **L. Zhou**, " Enhancing LTE with Cloud-RAN and Load-Controlled Parasitic Antenna Arrays," *IEEE Communications Magazine*, pp183-191, Dec. 2016.

M.2 Accepted Conference Publications

- **L. Zhou**, F. H. Khan, T. Ratnarajah and C. B. Papadias, " Multi-Antenna Transmission Using ESPAR with Peak Power Constraints," In Proc. 25th European Signal Processing Conference, Kos island, Greece, Aug. 28-Sep. 2, 2017.

- **L. Zhou**, T. Ratnarajah, J. Xue, and F. A. Khan, " Energy Efficient Cloud Radio Access Network with a Single RF Antenna," *In Proc. the IEEE International Conference on Communications (ICC)*, Kuala Lumpur, Malaysia, May 23-27, 2016.

- **L. Zhou**, F. Khan, and T. Ratnarajah, " Arbitrary Signal Transmission Using An ES-PAR Antenna," *in Proc. IEEE International Conference on Communications (ICC)*, pp. 4919-4924. London, June 9-12, 2015.

- **L. Zhou**, T. Ratnarajah and J. Xue, " Channel estimation and performance analysis of beamspace MIMO systems," *In Proc. Networks and Communications (EuCNC)*, pp. 1-5, 2014 European Conference on, Bologna, 2014.

References

[1] D. P. Bertsekas and J. N. Tsitsiklis, *Parallel and distributed computation: numerical methods*, vol. 23. Prentice hall Englewood Cliffs, NJ, 1989.

[2] S. Boyd, N. Parikh, E. Chu, B. Peleato, and J. Eckstein, *Distributed optimization and statistical learning via the alternating direction method of multipliers*, vol. 3. Now Publishers Inc., 2011.

[3] M. Duarte, C. Dick, and A. Sabharwal, "Experiment-driven characterization of full-duplex wireless systems," *IEEE Trans. Wireless Commun.*, vol. 11, no. 12, pp. 4296–4307, 2012.

[4] A. C. Cirik, R. Wang, Y. Hua, and M. Latva-aho, "Weighted sum-rate maximization for full-duplex mimo interference channels," *IEEE Trans. Commun.*, vol. 63, no. 3, pp. 801–815, 2015.

[5] D. Bharadia and S. Katti, "Full duplex mimo radios," pp. 359–372, 2014.

[6] Y. Fei, *Compact MIMO terminals with matching networks*. PhD thesis, The University of Edinburgh, 2008.

[7] A. Checko, H. L. Christiansen, Y. Yan, L. Scolari, G. Kardaras, M. S. Berger, and L. Dittmann, "Cloud ran for mobile networks;a technology overview," *IEEE Communications Surveys Tutorials*, vol. 17, no. 1, pp. 405–426, 2015.

[8] M. A. Sedaghat, V. I. Barousis, C. Papadias, *et al.*, "Load modulated arrays: a low-complexity antenna," *IEEE Communications Magazine*, vol. 54, no. 3, pp. 46–52, 2016.

[9] O. Onireti, F. Heliot, and M. Imran, "On the energy efficiency-spectral efficiency trade-off of distributed MIMO systems," *IEEE Trans. Commun.*, vol. 61, pp. 3741–3753, September 2013.

[10] J. Joung, Y. K. Chia, and S. Sun, "Energy-efficient, large-scale distributed-antenna system (l-das) for multiple users," *IEEE J. Sel. Areas Commun.*, vol. 8, pp. 954–965, Oct 2014.

[11] E. Björnson, L. Sanguinetti, J. Hoydis, and M. Debbah, "Optimal design of energy-efficient multi-user MIMO systems: Is massive MIMO the answer?," *arXiv preprint arXiv:1403.6150*, 2014.

[12] A. Kalis, A. Kanatas, and C. Papadias, "A novel approach to MIMO transmission using a single RF front end," *IEEE J. Sel. Areas Commun.*, vol. 26, no. 6, pp. 972–980, 2008.

[13] V. Barousis and A. G. Kanatas, "Aerial degrees of freedom of parasitic arrays for single RF front-end MIMO transceivers," 2011.

[14] O. Alrabadi, J. Perruisseau-Carrier, and A. Kalis, "MIMO transmission using a single RF source: Theory and antenna design," *IEEE Trans. Antennas Propag.*, vol. 60, no. 2, pp. 654–664, 2012.

[15] T. Ohira and K. Iigusa, "Electronically steerable parasitic array radiator antenna," *Electronics and Communications in Japan (Part II: Electronics)*, vol. 87, no. 10, pp. 25–45, 2004.

[16] V. Barousis and C. Papadias, "Arbitrary precoding with single-fed parasitic arrays: Closed-form expressions and design guidelines," *IEEE Wireless Communications Lett.*, vol. PP, no. 99, pp. 1–4, 2014.

[17] C. A. Balanis, *Antenna theory: analysis and design*. John Wiley & Sons, 2012.

[18] D. M. Pozar, *Microwave engineering*. Wiley, 2012.

[19] L. Zhou, F. A. Khan, T. Ratnarajah, and C. B. Papadias, "Achieving arbitrary signals transmission using a single radio frequency chain," *IEEE Trans. Commun.*, vol. 63, no. 12, pp. 4865–4878, 2015.

[20] D. Tse and P. Viswanath, *Fundamentals of wireless communication*. Cambridge university press, 2005.

[21] L. Zhengand D. Tse . " Diversity and multiplexing: A fundamental tradeoff in multiple-antenna channels. " *IEEE Transactions on information theory.*, 49(5), pp.1073–1096, 2003.

[22] Y. Okumura, E. Ohmori, T. Kawano, and K. Fukuda, "Field strength and its variability in vhf and uhf land-mobile radio service," *Rev. Elec. Commun. Lab*, vol. 16, no. 9, pp. 825–73, 1968.

[23] V. Erceg, L. J. Greenstein, S. Y. Tjandra, S. R. Parkoff, A. Gupta, B. Kulic, A. A. Julius, and R. Bianchi, "An empirically based path loss model for wireless channels in suburban environments," *IEEE Journal on Selected Areas in Communications*, vol. 17, no. 7, pp. 1205–1211, 1999.

[24] M. Hata and T. Nagatsu, "Mobile location using signal strength measurements in a cellular system," *IEEE Transactions on Vehicular Technology*, vol. 29, no. 2, pp. 245–252, 1980.

[25] B. Sklar, "Rayleigh fading channels in mobile digital communication systems. i. characterization," *IEEE Communications Magazine*, vol. 35, no. 9, pp. 136–146, 1997.

[26] E. Biglieri, MIMO *wireless communications*. Cambridge University Press, 2007.

[27] A. Goldsmith, *Wireless communications*. Cambridge university press, 2005.

[28] S. Bernard, *Digital communications fundamentals and applications*. 2001.

[29] A. Paulraj, R. Nabar, and D. Gore, *Introduction to space-time wireless communications*. Cambridge university press, 2003.

[30] M. Steinbauer, A. F. Molisch, and E. Bonek, "The double-directional radio channel," *IEEE Antennas and Propagation Magazine*, vol. 43, pp. 51–63, Aug 2001.

[31] A. G. Burr, "Capacity bounds and estimates for the finite scatterers mimo wireless channel," *IEEE Journal on Selected Areas in Communications*, vol. 21, pp. 812–818, June 2003.

[32] C. Oestges and B. Clerckx, MIMO *Wireless Communication, From Real-World Propagation to Space-Time Code Design*. 2007.

[33] A. Kalis, A. G. Kanatas, and C. B. Papadias, *Parasitic Antenna Arrays for Wireless* MIMO *Systems*. Springer, 2014.

[34] A. C. Cirik, *On Duality of MIMO Relays and Performance Limits of Full-Duplex MIMO Radios*. PhD thesis, 2014.

[35] P. Rost, C. J. Bernardos, A. Domenico, M. Girolamo, M. Lalam, A. Maeder, D. Sabella, *et al.*, "Cloud technologies for flexible 5g radio access networks," *IEEE Commun. Mag.*, vol. 52, no. 5, pp. 68–76, 2014.

[36] E. Dahlman, S. Parkvall, J. Skold, and P. Beming, *3G evolution: HSPA and LTE for mobile broadband*.

[37] G. Kardaras and C. Lanzani, *Advanced multimode radio for wireless & mobile broadband communication*.

[38] Y. Lin, L. Shao, Z. Zhu, Q. Wang, and R. K. Sabhikhi, "Wireless network cloud: Architecture and system requirements," *IBM Journal of Research and Development*, vol. 54, pp. 4:1–4:12, January 2010.

[39] C. Mobile, "C-ran: the road towards green ran," *White Paper, ver*, vol. 2, 2011.

[40] M. Ozdemir, H. Arslan, and E. Arvas, "A mutual coupling model for mimo systems," in *Wireless Communication Technology, 2003. IEEE Topical Conference on*, pp. 306–307, Oct 2003.

[41] M. Ozdemir, E. Arvas, and H. Arslan, "Dynamics of spatial correlation and implications on mimo systems," *Communications Magazine, IEEE*, vol. 42, pp. S14–S19, June 2004.

[42] B. Clerckx, C. Craeye, D. Vanhoenacker-Janvier, and C. Oestges, "Impact of antenna coupling on 2 times; 2 MIMO communications," *IEEE Trans. Veh. Technol.*, vol. 56, pp. 1009–1018, May 2007.

[43] J. Wallace and M. Jensen, "Mutual coupling in MIMO wireless systems: a rigorous network theory analysis," *IEEE Trans. Wireless Commun.*, vol. 3, no. 4, pp. 1317–1325, 2004.

[44] J. Wallace and M. Jensen, "Termination-dependent diversity performance of coupled antennas: network theory analysis," *IEEE Trans. Antennas Propag.*, vol. 52, pp. 98–105, Jan 2004.

[45] Y. Fei, Y. Fan, B. K. Lau, and J. Thompson, "Optimal single-port matching impedance for capacity maximization in compact MIMO arrays," *IEEE Trans. Antennas Propag.*, vol. 56, no. 11, pp. 3566–3575, 2008.

[46] "http://www.feko.info/product-detail/overview-of-feko."

[47] "http://www.sonnetsoftware.com/products/sonnet-suites/how-em-works.html."

[48] Y. Hao and R. Mittra, *FDTD modeling of metamaterials: Theory and applications*. Artech house, 2008.

[49] "http://www.semcad.com."

[50] H. Kawakami and T. Ohira, "Electrically steerable passive array radiator (ESPAR) antennas," *IEEE Antennas Propag. Mag.*, vol. 47, no. 2, pp. 43–50, 2005.

[51] O. Alrabadi, C. Papadias, A. Kalis, and R. Prasad, "A universal encoding scheme for MIMO transmission using a single active element for PSK modulation schemes," *IEEE Trans. Wireless Commun.*, vol. 8, no. 10, pp. 5133–5142, 2009.

[52] V. Barousis, A. Kanatas, and A. Kalis, "Beamspace-domain analysis of single-RF front-end MIMO systems," *IEEE Trans. Veh. Technol.*, vol. 60, no. 3, pp. 1195–1199, 2011.

[53] O. N. Alrabadi, C. Divarathne, P. Tragas, A. Kalis, N. Marchetti, C. B. Papadias, and R. Prasad, "Spatial multiplexing with a single radio: Proof-of-concept experiments in an indoor environment with a 2.6-ghz prototype," *Communications Letters, IEEE*, vol. 15, no. 2, pp. 178–180, 2011.

[54] C. B. Papadias, "An emerging technology: load-modulated arrays for small and large scale mimo systems," in *Presentation given in the Smart Antennas Workshop, Stanford, USA*, 2014.

[55] V. Barousis, C. Papadias, and R. Muller, "A new signal model for MIMO communication with compact parasitic arrays," in *Communications, Control and Signal Processing (ISCCSP), 2014 6th International Symposium on*, pp. 109–113, 2014.

[56] M. T. Ivrlac and J. A. Nossek, "Toward a circuit theory of communication," *IEEE Trans. Circuits Syst.*, vol. 57, no. 7, pp. 1663–1683, 2010.

[57] R. Harrington, "Reactively controlled directive arrays," *IEEE Trans. Antennas Propag.*, vol. 26, pp. 390–395, May 1978.

[58] R. R. Müller, M. Sedaghat, G. Fischer, *et al.*, "Load modulated massive mimo," in *Signal and Information Processing (GlobalSIP), 2014 IEEE Global Conference on*, pp. 622–626, IEEE, 2014.

[59] M. A. Sedaghat, R. R. Müller, and G. Fischer, "Broadcast precoding for massive MIMO subject to an instantaneous total power constraint," in *Global Telecommunications Conference (GLOBECOM 2014), 2014 IEEE*, pp. 1–5, Dec 2014.

[60] M. A. Sedaghat, R. R. Müeller, and G. Fischer, "A novel single-rf transmitter for massive mimo," in *Smart Antennas (WSA), 2014 18th International ITG Workshop on*, pp. 1–8, March 2014.

[61] M. Ivrlac and J. Nossek, "A multiport theory of communications," in *Source and Channel Coding (SCC), 2010 International ITG Conference on*, pp. 1–5, 2010.

[62] V. Barousis, M. A. Sedaghat, R. R. Müller, and C. B. Papadias, "Massive antenna arrays with low front-end hardware complexity: An enabling technology for the emerging small cell and distributed network architectures," *CoRR*, vol. abs/1407.7733, 2014.

[63] E. Tsakalaki, O. Alrabadi, C. B. Papadias, and R. Prasad, "Adaptive reactance-controlled antenna systems for multi-input multi-output applications," *IET microwaves, antennas & propagation*, vol. 5, no. 8, pp. 975–984, 2011.

[64] G. Alexandropoulos, V. Barousis, and C. Papadias, "Precoding for multiuser mimo systems with single-fed parasitic antenna arrays," in *Global Communications Conference (GLOBECOM), 2014 IEEE*, pp. 3897–3902, Dec 2014.

[65] D. F. Kelley and W. L. Stutzman, "Array antenna pattern modeling methods that include mutual coupling effects," *IEEE Trans. Antennas Propag.*, vol. 41, no. 12, pp. 1625–1632, 1993.

[66] S. Boyd and L. Vandenberghe, *Convex optimization*. Cambridge university press, 2009.

[67] R. Hunger, *Floating point operations in matrix-vector calculus*. Munich University of Technology, Inst. for Circuit Theory and Signal Processing Munich, 2005.

[68] V. I. Barousis, A. G. Kanatas, A. Kalis, and J. Perruisseau-Carrier, "Reconfigurable parasitic antennas for compact mobile terminals in multiuser wireless systems," EURASIP Journal on Wireless Communications and Networking, vol. 2012, no. 1, pp. 1-10, 2012

[69] G. H. Golub and C. F. Van Loan, *Matrix computations*, vol. 3. JHU Press, 2012.

[70] B. Han, V. Barousis, A. Kalis, and A. Kanatas, "Active parasitic arrays for low cost compact MIMO transmitters," in *Antennas and Propagation (EUCAP), Proceedings of the 5th European Conference on*, pp. 3663–3667, IEEE, 2011.

[71] B. Han, V. I. Barousis, A. Kalis, C. B. Papadias, A. G. Kanatas, and R. Prasad, "A single rf mimo loading network for high-order modulation schemes," *International Journal of Antennas and Propagation*, vol. 2014, 2014.

[72] B. Han, V. Barousis, C. Papadias, A. Kalis, and R. Prasad, "MIMO over ESPAR with 16-QAM modulation," *IEEE Wireless Communications Lett.*, vol. 2, pp. 687–690, December 2013.

[73] W. L. Stutzman and W. A. Davis, *Antenna theory*. Wiley Online Library, 1998.

[74] T. K. Y. Lo, "Maximum ratio transmission," *IEEE Trans. Veh. Commun.*, vol. 47, pp. 1458–1461, Oct 1999.

[75] R. Baxley, B. Walkenhorst, and G. Acosta-Marum, "Complex gaussian ratio distribution with applications for error rate calculation in fading channels with imperfect CSI," in *Global Telecommunications Conference (GLOBECOM 2010), 2010 IEEE*, pp. 1–5, Dec 2010.

[76] P. Demestichas, A. Georgakopoulos, D. Karvounas, K. Tsagkaris, V. Stavroulaki, J. Lu, C. Xiong, and J. Yao, "5G on the horizon: key challenges for the radio-access network," *IEEE Veh. Technol. Mag.*, vol. 8, no. 3, pp. 47–53, 2013.

[77] F. Khan, H. He, J. Xue, and T. Ratnarajah, "Performance analysis of cloud radio access networks with distributed multiple antenna remote radio heads," *IEEE Trans. Signal Process.*, 2015.

[78] M. Hadzialic, B. Dosenovic, M. Dzaferagic, and J. Musovic, "Cloud-RAN: innovative radio access network architecture," in *ELMAR, 2013 55th International Symposium*, pp. 115–120, IEEE, 2013.

[79] A. Chakrabarti, C. Lott, D. Ghosh, and R. Attar, "Repeaters and remote radioheads in EVDO networks," in *Vehicular Technology Conference Fall (VTC 2010-Fall), 2010 IEEE 72nd*, pp. 1–6, Sept 2010.

[80] P. Rost, C. J. Bernardos, A. Domenico, M. Girolamo, M. Lalam, A. Maeder, D. Sabella, *et al.*, "Cloud technologies for flexible 5G radio access networks," *IEEE Commun. Mag.*, vol. 52, no. 5, pp. 68–76, 2014.

[81] C. He, B. Sheng, P. Zhu, X. You, and G. Li, "Energy- and spectral-efficiency tradeoff for distributed antenna systems with proportional fairness," *IEEE J. Sel. Areas Commun.*, vol. 31, pp. 894–902, May 2013.

[82] S.-R. Lee, S.-H. Moon, H.-B. Kong, and I. Lee, "Optimal beamforming schemes and its capacity behavior for downlink distributed antenna systems," *IEEE Trans. Wireless Commun.*, vol. 12, pp. 2578–2587, June 2013.

[83] H. Kim, S.-R. Lee, C. Song, and I. Lee, "Optimal power allocation for energy efficiency maximization in distributed antenna systems," in *Communications (ICC), 2013 IEEE International Conference on*, pp. 5769–5773, June 2013.

[84] W. Choi and J. Andrews, "Downlink performance and capacity of distributed antenna systems in a multicell environment," *IEEE Trans. Wireless Commun.*, vol. 6, pp. 69–73, Jan 2007.

[85] Y. Chen, S. Zhang, S. Xu, and G. Li, "Fundamental trade-offs on green wireless networks," *IEEE Commun. Mag.*, vol. 49, pp. 30–37, June 2011.

[86] Z. Xu, C. Yang, G. Y. Li, Y. Liu, and S. Xu, "Energy-efficient comp precoding in heterogeneous networks," *IEEE Trans. Signal Process.*, vol. 62, no. 4, pp. 1005–1017, 2014.

[87] 3GPP Technical Specification TR 36: V2, "Further advancements for E-UTRA physical layer aspects." 2010.

[88] 3GPP, TR 36.828, "Further enhancements to LTE time division duplex (TDD) for downlink-uplink (DL-UL) interference management and traffic adaptation (Release 11)," June 2012.

[89] "LTE; E-UTRA; RF Requirements for LTE Pico Node B¿‘ 2011, [online] Available: http://www.etsi.org/deliver/.

[90] R. Qian and M. Sellathurai, "On the implementation of blind interference alignment with single-radio parasitic antennas," *IEEE Transactions on Vehicular Technology*, vol. 65, no. 12, pp. 10180–10184, 2016.

[91] R. Bains, A. Kalis, and R. Muller, "On the link performance of a proposed compact antenna system," *IEEE Commun. Lett.*, vol. 12, no. 10, pp. 711–713, 2008.

[92] R. Bains, R. R. Müller, and A. Kalis, "Link performance of an espar-antenna array in rich scattering and clustered channels," *Wireless personal communications*, vol. 50, no. 1, pp. 45–56, 2009.

[93] D. Eberly, "Distance from a point to an ellipse, an ellipsoid, or a hyperellipsoid,"

[94] D. H. Eberly, *3D game engine design: a practical approach to real-time computer graphics*. CRC Press, 2006.

[95] L. Petit, L. Dussopt, and J.-M. Laheurte, "MEMS-switched parasitic-antenna array for radiation pattern diversity," *IEEE Trans. Antennas Propag.*, vol. 54, no. 9, pp. 2624–2631, 2006.

[96] S. Li, R. D. Murch, and V. K. N. Lau, "Linear transceiver design for full-duplex multi-user mimo system," in *2014 IEEE International Conference on Communications (ICC)*, pp. 4921–4926, 2014.

[97] T. M. Kim, F. Sun, and A. J. Paulraj, "Low-complexity mmse precoding for coordinated multipoint with per-antenna power constraint," *IEEE Signal Processing Letters*, vol. 20, no. 4, pp. 395–398, 2013.

[98] W. Yu and T. Lan, "Transmitter optimization for the multi-antenna downlink with per-antenna power constraints," *IEEE Trans. Signal Process.*, vol. 55, no. 6, pp. 2646–2660, 2007.

[99] B. P. Day, A. R. Margetts, D. W. Bliss, and P. Schniter, "Full-duplex bidirectional mimo: Achievable rates under limited dynamic range," *IEEE Trans. Signal Process.*, vol. 60, no. 7, pp. 3702–3713, 2012.

[100] H. Suzuki, T. V. A. Tran, I. B. Collings, G. Daniels, and M. Hedley, "Transmitter noise effect on the performance of a mimo-ofdm hardware implementation achieving improved coverage," *IEEE J. Sel. Areas Commun.*, vol. 26, no. 6, pp. 867–876, 2008.

[101] W. Namgoong, "Modeling and analysis of nonlinearities and mismatches in ac-coupled direct-conversion receiver," *IEEE Transactions on Wireless Communications*, vol. 4, no. 1, pp. 163–173, 2005.

[102] D. P. Palomar and M. Chiang, "A tutorial on decomposition methods for network utility maximization," *IEEE J. Sel. Areas Commun.*, vol. 24, no. 8, pp. 1439–1451, 2006.

[103] R. Hunger, *Floating point operations in matrix-vector calculus*. Munich University of Technology, Inst. for Circuit Theory and Signal Processing Munich, 2005.

[104] D. Coppersmith and S. Winograd, "Matrix multiplication via arithmetic progressions," pp. 1–6, 1987.

[105] E. U. T. R. Access, "Further enhancements to lte time division duplex (tdd) for downlink-uplink (dl-ul) interference management and traffic adaptation," 2012.

[106] B. Alshami, H. Aboulnour, and M. Dib, "Design of a broadband espar antenna," in *Microwave Symposium (MMS), 2009 Mediterrannean*, pp. 1–6, Nov 2009.

[107] B. Alshami, H. Aboulnour, and M. Dib, "Implementation and field test of a broadband espar antenna," in *Microwave Symposium (MMS), 2010 Mediterranean*, pp. 139–143, IEEE, 2010.

[108] C. Gu, S. Gao, M. Zhang, L. Xu, B. Sanz-Izquierdo, and M. Sobhy, "Design of broadband espar antenna using inverted f monopoles," in *Antennas and Propagation (EuCAP), 2014 8th European Conference on*, pp. 1814–1817, April 2014.

[109] R. Mohammadkhani and J. Thompson, "Adaptive uncoupled termination for coupled arrays in mimo systems," *IEEE Trans. Antennas Propag.*, vol. 61, pp. 4284–4295, Aug 2013.

[110] R. Mohammadkhani, *Adaptive Impedance Matching to Compensate Mutual Coupling Effects on Compact MIMO Systems*. PhD thesis, The University of Edinburgh, June 2012.

[111] N. Honma, "Method of mimo channel estimation between parasitic antenna arrays," *IEEE Trans. Antennas Propag.*, vol. 61, pp. 2792–2800, May 2013.

[112] A. C. Cirik, S. Biswas, O. Taghizadeh, A. Liu, and T. Ratnarajah, "Robust transceiver design in full-duplex mimo cognitive radios," pp. 1–7, 2016.

[113] A. C. Cirik, S. Biswas, S. Vuppala, and T. Ratnarajah *IEEE Transactions on Communications*, no. 11, pp. 4635–4651.

[114] A. Jeffrey and D. Zwillinger, *Table of integrals, series, and products*. Academic Press, 2007.

[115] M. Vu, "MISO capacity with per-antenna power constraint," *IEEE Trans. Commun.*, vol. 59, pp. 1268–1274, May 2011.

[116] S. Sesia, M. Baker, and I. Toufik, *LTE-the UMTS long term evolution: from theory to practice*. John Wiley & Sons, 2011.

[117] Luo, Zhi-Quan, et al."Semidefinite relaxation of quadratic optimization problems." IEEE Signal Processing Magazine 27.3 (2010): 20-34.

[118] S. Wolfram, "The mathematica® book, version 4," 1999.

[119] L. Zhou, F. A. Khan, and T. Ratnarajah, "Arbitrary signal transmission using an espar antenna," in *Communications (ICC), 2015 IEEE International Conference on*, pp. 4919–4924, IEEE, 2015.